Localization of the Human Malaria Parasite's Dihydrofolate Reductase-Thymidylate Synthase and Examining Its Role in Proguanil and Atovaquone Drug Synergy

Joseph William Fowble

A dissertation

submitted in partial fulfillment of the

requirements for the degree of

Doctorate of Philosophy

University of Washington

2014

Reading Committee:

Pradipsinh K. Rathod, Chair

Tomikazu Sasaki

Robert E. Synovec

Program Authorized to Offer Degree:

Chemistry

University of Washington

Abstract

Localization of the Human Malaria Parasite's Dihydrofolate Reductase-Thymidylate Synthase and Examining Its Role in Proguanil and Atovaquone Drug Synergy

Joseph W. Fowble

Chair of the Supervisory Committee:
Professor Pradipsinh K. Rathod
Departments of Chemistry and Global Health

Malaria is the common name for a disease caused by *Plasmodium* parasites. Malaria kills an estimated 1 million people out of approximately 200 to 500 million cases annually. The incredible number of cases of the disease, high numbers of parasites present in an infected individual, and sometimes rapid ability of the parasite to acquire drug resistance emphasizes the need to find new drugs to treat individuals and prevent infection. In the race to develop new drugs, elucidation of the exact mechanisms of older drugs and their targets is sometimes left unresolved.

Dihydrofolate reductase (DHFR) has been an antimalarial drug target since the late 1940s, well before the rise of modern biochemistry and genetic analysis methods. Antimalarials targeting DHFR have been used for so long that resistant populations of parasites have rendered these antimalarials ineffective in many countries. While DHFR

is among the oldest antimalarial drug targets identified, significant gaps remain in our understanding of the enzyme. Low levels of expression and essentiality in a haploid genome have made biochemical investigations of malarial DHFR and genetic manipulation particularly difficult.

A few of the proteins proteins involved in pyrimidine biosynthesis and the folate cycle (dihydroorotate dehydrogenase (DHODH) and an isoform of serine hydroxymethyltransferase (SHMT)) have experimentally identified localizations that are mitochondrial. However, the localization of the malaria parasite's conjoined dihydrofolate reductase and thymidylate synthase enzymes (DHFR-TS) has not been either investigated or reported. We pursued a theory that DHFR-TS is localized in the malaria parasite and that the observed in vitro synergy of Malarone®, combining an inhibitor of the mitochondrial electron transport chain and a pro-drug for a DHFR inhibitor, was influenced by DHFR inhibition and disruption of localization. The subcellular localization of the endogenous form of the DHFR-TS enzyme was investigated using the latest design techniques for peptide antigen-derived polyclonal antibodies, laser-scanning confocal microscopy, and advanced image analysis techniques interrogate the patterned DHFR-TS signal in relation to the organelles of the parasite. Comparisons between DHFR-TS and mitochondria-marking dyes, an engineered mitochondrial protein (HProtein-GFP), and native DHODH enzyme all indicate mitochondrial localization of this important drug target, DHFR-TS. Digitonin

based selective permeabilization of cell membranes further illustrated that DHFR-TS is not cytosolic but localized and released alongside known mitochondrial protein.

Proguanil and atovaquone drug synergy was evaluated with added consideration of DHFR localization involvement. Even with widespread resistance to antimalarials based on DHFR inhibitors, the modern antimalarial drug Malarone® combines atovaquone-based inhibition of the electron transport chain pathway with proguanil/cycloguanil-based inhibition of DHFR and the folate cycle. Atovaquone's clinical trials were initially halted when it could not reliably cure patients due to the rapid acquisition of resistance to atovaquone. After proguanil was added to atovaquone a 98.7% cure rate was achieved, even in regions where DHFR-based drug resistance phenotypes were well established.

We evaluated parasite strains with known DHFR mutations and observed Malarone® susceptibility in flasks largely matched the EC_{50} patterns predicted for DHFR-based inhibition by cycloguanil. We also identified parasite strains that displayed no synergistic interactions between proguanil and atovaquone. We analyzed parasite cultures treated with proguanil and atovaquone and, against the dogma of a human liver being necessary to create cycloguanil, observed low quantities of cycloguanil. In order to pursue a cycloguanil connection with minimal background genetic changes, a strain of parasites expressing a cycloguanil-resistant *Plasmodium vivax* DHFR-TS enzyme was created. The cycloguanil resistance conferred by the rescue plasmid did not translate into resistance to proguanil and atovaquone treatment with a transfection

construct that did not localize as the native DHFR-TS. We concluded that the rescue construct, without proper localization, was unable to fully replicate the function of the native *falciparum* DHFR-TS enzyme.

Prior Publications

Rathod Lab

Narayanasamy K, Chery L, Basu A, Duraisingh MT, Escalante A, **Fowble J**, Guler JL, Herricks T, Kumar A, Majumder P, Maki J, Mascarenhas A, Rodrigues J, Roy B, Sen S, Shastri J, Smith J, Valecha N, White J, Rathod PK. (2012). "Malaria evolution in South Asia: knowledge for control and elimination." Acta Trop **121**(3): 256-266.

Guiguemde WA, Shelat AA, Bouck D, Duffy S, Crowther GJ, Davis PH, Smithson DC, Connelly M, Clark J, Zhu F, Jiménez-Díaz MB, Martinez MS, Wilson EB, Tripathi AK, Gut J, Sharlow ER, Bathurst I, El Mazouni F, **Fowble JW**, Forquer I, McGinley PL, Castro S, Angulo-Barturen I, Ferrer S, Rosenthal PJ, Derisi JL, Sullivan DJ, Lazo JS, Roos DS, Riscoe MK, Phillips MA, Rathod PK, Van Voorhis WC, Avery VM, Guy RK. (2010). "Chemical genetics of Plasmodium falciparum." Nature **465**(7296): 311-315.

Mui EJ, Schiehser GA, Milhous WK, Hsu H, Roberts CW, Kirisits M, Muench S, Rice D, Dubey JP, **Fowble JW**, Rathod PK, Queener SF, Liu SR, Jacobus DP, McLeod R. (2008). "Novel triazine JPC-2067-B inhibits Toxoplasma gondii in vitro and in vivo." PLoS Negl Trop Dis **2**(3): e190.

Ganesan K, Ponmee N, Jiang L, **Fowble JW**, White J, Kamchonwongpaisan S, Yuthavong Y, Wilairat P, Rathod PK. (2008). "A genetically hard-wired metabolic transcriptome in Plasmodium falciparum fails to mount protective responses to lethal antifolates." PLoS Pathog **4**(11): e1000214.

Previous Labs

Lockard JV, Zink JI, Luo Y, Weaver MN, Konradsson AE, **Fowble JW**, Nelsen SF. (2006). "Excited-state mixed-valence distortions in a diisopropyl diphenyl hydrazine cation." J Am Chem Soc **128**(51): 16524-16531.

Kulp SK, Yang YT, Hung CC, Chen KF, Lai JP, Tseng PH, **Fowble JW**, Ward PJ, Chen CS. (2004). "3-phosphoinositide-dependent protein kinase-1/Akt signaling represents a major cyclooxygenase-2-independent target for celecoxib in prostate cancer cells." Cancer Res **64**(4): 1444-1451.

Zhu J, Huang JW, Tseng PH, Yang YT, **Fowble J**, Shiau CW, Shaw YJ, Kulp SK, Chen CS. (2004). "From the cyclooxygenase-2 inhibitor celecoxib to a novel class of 3-phosphoinositide-dependent protein kinase-1 inhibitors." Cancer Res **64**(12): 4309-4318.

Table of Contents

List of Abbreviations

ATO – Atovaquone
CG – Cycloguanil
DHF - 7,8-dihydrofolic Acid
DHFR/DHFR-TS – Dihydrofolate Reductase-(Thymidylate Synthase)
DHODH – Dihydroorotate Dehydrogenase
DHPS – Dihydropteroate Synthase
DTT - Dithiothreitol
EC_{50} – Effective Concentration of an inhibitor to reduce cellular effect by 50%
ETC – Electron Transport Chain (mitochondrial membrane potential source)
GFP – Green Fluorescent Protein
GST – Glutatione S-Transferase
HProtein – A component of the Glycine Cleavage System, Mitochondrial
IC_{50} – Inhibitory Concentration, concentration of inhibitor to reduce enzymatic activity by 50%
MTX – Methotrexate
mTHF - N^5,N^{10}-Methylene Tetrahydrofolic Acid
NADPH - Nicotinamide Adenine Dinucleotide Phosphate, Reduced
PG – Proguanil
SHMT – Serine Hydroxymethyltransferase
TCA – Tricarboxylic Acid (Citric Acid Cycle/Krebs Cycle)
THF - 5,6,7,8-Tetrahydrofolic Acid
TS – Thymidylate Synthase

Chapter 1 - Background

Malaria

Global Burden of Malaria

Malaria is a tropical disease caused by *Plasmodium* parasites. Approximately 48% of the world's population lives in regions where malaria is endemic [1, 2]. The global impact to humans is estimated to be hundreds of millions of malaria infections each year and around one million deaths annually over a wide geographic distribution (Figure 1.1). The number of cases and deaths are typically are usually reported as broad ranges, mainly due to malaria's prevalence in third-world countries and away from developed healthcare settings. Recent World Health Organization estimates for 2010 indicate around 216 million cases of malaria and attribute malaria as the cause of 655,000 deaths [3]. Other studies have resulted in significantly higher estimates of the number of deaths in 2010 at 1.24 million [4]. The 1.24 million can be further divided into the largest proportion of deaths due to malaria occurring in children of age five or younger (approximately 714,000 deaths) while all ages greater than 5 years old represented approximately 524,000 deaths.

The inability to conclusively diagnose a case of malaria and, even when properly assessed, obtain a full treatment with the most effective drugs has made malaria a difficult disease to control. Even with a low likelihood of adult death due to malaria infections, the general effects of the illness result in widespread economic impairment.

The most direct cause of economic impairment is due to illness affecting the ability to work and the need for medicines that may come at locally significant expense. Beyond being those most likely to die from episodes of malaria, the lives of young children can be put at a severe disadvantage by living in malaria-endemic regions. Studies have found that malaria is responsible for primary school children in Kenya missing 11% of school days resulting in long-lasting educational disadvantages [5]. The malaria-attributed economic losses in Africa alone are estimated at $12 billion annually [6]. Increased public awareness and support from organizations like the Bill and Melinda Gates Foundation, the President's Malaria Initiative, and the Roll Back Malaria Partnership have focused efforts to combat the disease but has also resulted in added pressure to show marked progress [6-8].

History of Malaria

Malaria has sickened and killed humans for many thousands of years. Genetically, the human-lethal malaria parasite species *Plasmodium falciparum* is an evolutionarily recent zoonotic offshoot of the reasonably well tolerated western gorilla malaria parasite [9]. Finding a recent species hop from gorillas to humans suggests some species of malaria parasites that are reasonably tolerated in humans might have co-evolved while more lethal forms are recent crossover events. The pathology of malaria is marked by the fevers that occur, often in two day cycles. Cyclical fevers, headaches, and chill symptoms associated with malaria infections and stagnant marshland appear in writings from over 4,000 years ago detailing the history of Egypt,

Samaria, and India. The association between the disease and causative protozoan parasites was first recorded by Charles Louis Alphonse Laveran, the Chair of Military Diseases and Epidemics at Ecole du Val de Grace while in Algeria in 1880 [10, 11]. The full life-cycle of the malaria parasite (from host to mosquito to host) was subsequently observed in Indian birds by Patrick Manson and Ronald Ross in 1897 and in Roman humans by Giovanni Battista Grassi in 1898 [12]. In temperate climates, as found in much of the United States, where freezing winters knock down the mosquito population, malaria eradication was achieved through widespread insecticide spraying, land reformation, and the use of natural products and early synthetic drugs. Natural products like quinine and artemisinin have a long history treating malaria. Many years would pass before Western medicine had advanced to the point of developing new synthetic drugs to combat malaria. Both quinine and artemisinin are still used to treat malaria, with differing scopes of use.

Species Differences/Distribution

The parasite that causes malaria belongs to the *Plasmodium* genus. *Plasmodium* parasites have a life cycle involving two hosts, a mosquito and a vertebrate. There are five species of malaria parasites that are known to infect humans – *Plasmodium falciparum, Plasmodium vivax, Plasmodium ovale, Plasmodium malariae*, and *Plasmodium knowlesi* [13-15].

Of the less prevalent species, *Plasmodium ovale* and the morphologically nearly-identical *Plasmodium malariae* take on an oval shape. *Plasmodium ovale* is able to

produce hypnozoites during infections [16]. *Plasmodium malariae* has a longer, 72 hour erythrocytic life cycle, lacks a hypnozoite stage, and has a geographical distribution similar to that of *falciparum* [17]. *Plasmodium knowlesi* is restricted to areas of southeast Asia, where it can infects both macaques and humans, and has a rapid, 24 hour erythrocytic life cycle [18].

The two most studied and most prevalent species of human malaria-causing parasites are *Plasmodium vivax* and *Plasmodium falciparum*. Malaria caused by *Plasmodium falciparum* is implicated in half of all clinical cases and accounts for 95% of all malaria-related deaths. Malaria caused by *Plasmodium vivax* accounts for 45% of all clinical cases but is rarely implicated in malaria fatalities [19]. *Plasmodium falciparum* and *vivax* are typically diagnosed by morphological differences observed using light microscopy of blood smears or rapid diagnostic tests. *Plasmodium vivax* and *falciparum*, under ideal conditions, each require different antimalarial drug treatments to address unique features of the parasite's life. *Plasmodium vivax* parasites are able to enter a dormant state in the human liver (hypnozoites) where they do not divide and have minimal metabolic activities for months or years before parasites re-emerge and the infection resumes. The *falciparum* form of malaria does not differentiate into hypnozoites, but the life cycles are otherwise very similar.

The Parasite Life Cycle

The life cycle of *Plasmodium* parasites is complex and, with the human infecting forms *falciparum* and *vivax*, takes place in two different hosts. We will first examine the

overall pathway from infected mosquito to naïve human to naïve mosquito and then we will more thoroughly examine how parasites develop and mature in the circulatory, human blood stages (Figure 1.2) [20]. A malaria-infected female mosquito that feeds on human blood will inject malaria parasite-containing saliva during the feeding process. The parasites transferred during the bite are in the sporozoite life-stage. The motile sporozoites make their way into circulatory blood until they sequester in the human liver. Rapid replication and cell division creates massive groups of individual parasites (merozoites) inside the liver hepatocytes. Upon release of the thousands of individual merozoites into the circulating blood, the malaria parasite invades the red blood cell (erythrocyte) and most continue in an erythrocyte-based replication cycle with ten-fold or greater multiplication in each cycle. The erythrocytic, asexual replication cycle will be detailed more thoroughly in the next paragraph. A small fraction of merozoites that invade erythrocytes differentiate into sexual-stage parasites called the gametocytes. When a naïve mosquito bite results in the uptake of blood containing gametocytes, the sexual parasites develop into gametes which merge and fertilize to create zygotes. The zygotes sequester in the mosquito gut to form oocysts. The parasite rapidly replicates and divides into thousands of sporozoites which then migrate to the mosquito salivary glands. An infected mosquito can thus bite a new human host and another life cycle begins [21].

During the erythrocytic, asexual replication cycle the parasite starts from a haploid genome and amasses materials sufficient for the individual parasite to divide

into ten to twenty daughter parasites over a two day period. Those daughter parasites then rupture the red blood cell and invade new erythrocytes. The erythrocytic, asexual replication cycle can be viewed as starting when the merozoite invades a red blood cell. During invasion the merozoite pushes into the erythrocyte membrane via an apical structure that uses actin-myosin motors inside the parasite to pull the parasite into the membrane [22]. The parasite does not traverse the erythrocyte membrane, instead wrapping itself with the membrane. The parasite ends up with a fluid bubble (parasitophorous vacuole) that separates it from the red blood cell contents [23]. The merozoite then develops into a ring-stage (early trophozoite) parasite where certain organelles like the mitochondria expand and the parasite assembles many of the substrates needed for further replication. The ring-state parasite develops into a large, late stage trophozoite and then a schizont. As the trophozoite matures into a schizont, the parasite replicates its genome and organelles like the mitochondria bud off until the parasite has fully divided into a cluster of pre-merozoites encapsulated in the same parasitophorous vacuole. The schizont then degrades the erythrocyte membranes and allows mature merozoites to egress and find new erythrocytes to invade [22].

Established Antimalarial Drug Targets

Management of the malaria disease has depended upon chemoprophylaxis and chemotherapy. Over time, the drugs used to treat malaria have changed significantly. Early treatments based on natural products (e.g. quinine originally isolated from tree

bark and artemisinin once isolated from wormwood) are still used to treat malaria while some of the synthetic antimalarial agents that have been mass-produced for decades have fallen from favor due to widespread drug resistance. Following is a brief overview of some of the most common antimalarial drug targets and the key differences between the malaria parasite and the human host that are routinely exploited.

Pyrimidine Biosynthesis and the Folate Cycle

Reproduction of the parasite genome, a necessary step for cells to grow and multiply, requires a sufficient supply of component DNA bases. The malaria parasite can salvage purinic DNA bases (adenine and guanine) from the human host but lacks components of the pyrimidine salvage pathway such that it can't utilize the host's pyrimidine bases (thymine and cytosine) [24]. The only way for the malaria parasite to obtain new pyrimidine bases for making DNA is through *de novo* biosynthesis, which also depends on the folate recycling pathway (Figure 1.3) [25, 26]. During growth, the human host is able to both make new pyrimidine DNA bases and recycle existing pyrimidine bases. The net result of these nucleotide salvage differences is that malaria parasites are more sensitive to DNA nucleotide supplies and imbalances than the human host.

A number of antimalarial drugs have come from larger scale efforts to create folate analogs to treat human cancer. The dihydrofolate reductase (DHFR) enzyme has been a drug target since the 1940s with the introduction of aminopterin to treat human cancer [27-30]. Further refining of aminopterin via analogs yielded methotrexate (MTX),

a drug still used to treat leukemia, breast/head and neck cancers, and rheumatoid arthritis [31]. Additional folate analogs have been created to perturb the balance of DNA nucleotides in a way that is lethal for the malaria parasite but not to the host. During massive war-effort screening to find new antimalarials, aminopterin analogs were identified with antimalarial activity and eventually lead to the antifolate proguanil being the earliest DHFR-inhibiting antimalarial [32-35].

The pyrimidine biosynthesis pathway, as well as many other cellular processes, requires a pool of one-carbon (C1) donors and acceptors to function. The folate pathway (Figure 1.3) is one way that the cell maintains the supply of the C1 donors and acceptors. The folate pathway can be viewed as having five steps to make the base folate, 7,8-dihydrofolic acid (DHF) and three enzymatic steps that cycle the base folate into other folate derivatives (THF, mTHF) which then can be converted back to DHF [26]. The folate cycle can be viewed as 7,8-dihydrofolic acid's reduction to 5,6,7,8-tetrahydrofolic acid via dihydrofolate reductase (DHFR) enzyme, the conversion of 5,6,7,8-tetrahydrofolic acid to N^5,N^{10}-methylene tetrahydrofolic acid via serine hydroxymethyltransferase (SHMT) enzyme, and the conversion of N^5,N^{10}-methylene tetrahydrofolic acid back into 7,8-dihydrofolic acid via thymidylate synthase (TS) enzyme [36]. The folate cycle is an important process, providing multiple drug targets, because proper one-carbon donor flux is essential to maintaining the synthesis of pyrimidine nucleotides [37].

The antimalarial drugs that target the core components of the folate cycle target the malarial DHFR. Malarial DHFR is significantly divergent from the human version of the enzyme, differing both in sequence as well as structure by having a second enzyme, thymidylate synthase, conjoined to it [38, 39]. The sequences of the human and malarial DHFR enzymes align at 33% of the residues and are only 20% similar, however both enzymes still perform the same reaction using identical substrates. While some drugs that inhibit DHFR, like methotrexate, are cross reactive with malarial and human DHFR, the divergent sequence and regulation of the two enzymes creates opportunities for drug selectivity [40]. Optimizations to folate analogs have created proguanil (via its active form cycloguanil) and pyrimethamine, which are much stronger inhibitors of the *Plasmodium* DHFR enzyme, the folate cycle, and, thus, the parasite's DNA synthesis [41]. Point mutations in the DHFR enzyme sequences are the most commonly observed method that malaria parasites gain resistance to DHFR-targeting drugs [22, 30, 34, 42-44].

The dihydropteroate-synthase (DHPS) enzyme is used by malaria parasites to create the folic acid (Vitamin B_9) substrate of the folate cycle. The parasite must perform *de novo* synthesis of folates but the human relies on folate salvage mechanisms and has no ability to perform *de novo* folate biosynthesis, providing a great deal of selectivity. Sulfonamides such as sulfadoxine and sulfamethoxypyridazine target the dihydropteroate synthase enzyme and reduce the malaria parasite's ability to make

DNA, leading to parasite death. Resistance for DHPS-targeting drugs is typically due to amino acid mutations in the enzyme [45-47].

Electron Transport Chain/Mitochondrial Function

Coenzyme Q is a central, membrane bound substrate involved in transferring electrons between components of the electron transport chain in eukaryotes (Figure 1.4). Libraries of coenzyme Q analogs have, thus far, yielded one antimalarial drug. The clinically used antimalarial/ETC inhibitor atovaquone targets the cytochrome b subunit of cytochrome b/c1 component (Complex III) in the electron transport chain [48]. While the intra-erythrocytic malaria parasite does not derive significant energy from the mitochondria, it does use that organelle to perform specific tasks such as TCA substrate conversion, iron-sulphur cluster biogenesis, ubiquinone synthesis, and some aspects of heme synthesis [49, 50]. Inhibition of the electron transport chain can disrupt several of these important functions. Electron transport chain inhibition by atovaquone has long been expected to inhibit pyrimidine biosynthesis via dihydroorotate dehydrogenase (DHODH), which also utilizes the substrate coenzyme Q [51]. The experiments performed by Painter indicated that, at least in the red blood cell stages, the malaria parasite's electron transport chain's most critical role is to recycle the DHODH substrate coenzyme Q [52].

Unfortunately, malaria patients treated with atovaquone alone were able to develop resistance readily, even during initial and follow up clinical trials [53-55]. For this reason, atovaquone is not recommended for use as a prophylactic or single agent

antimalarial drug [54]. Atovaquone is sometimes used in advanced clinical settings as a single anti-parasitic agent administered intravenously to treat pneumonia or parasitic diseases such as toxoplasmosis or babesiosis [56-58]. With malaria, atovaquone is generally combined with a secondary agent like proguanil with synergistic effect [59].

Beyond atovaquone, electron transport chain inhibition to treat malaria is still at the development stage. The acridones are a family of inhibitors that have been explored for their ability to act like atovaquone and inhibit mitochondrial function but they also can be tuned to target heme processing [60, 61]. As a poly-aromatic compound, there are good arguments for both functions being effective targets. The acridone family resembles coenzyme Q and the pi-pi stacking can result in the acridone binding to heme and inhibiting polymerization. The coenzyme Q-like structure has been successful for many inhibitors and projects are actively working on advancing acridone-based antimalarials that inhibit complex III of the electron transport chain [62].

Malaria parasites also possess somewhat unusual, non-canonical enzymes that are coupled to the electron transport chain. One such enzyme, an alternate type II NADH:dehydrogenase (alternate complex I, PfNDH2) has also produced interesting experimental inhibitors based on coenzyme Q analogs, although it's uncertain if those inhibitors are also acting through DHODH inhibition directly [61, 63].

Heme Polymerization and Waste Disposal

A major source of materials for the intra-erythrocytic malaria parasite is human hemoglobin contained in the red blood cells. The parasites produces proteases which

break down hemoglobin in an organelle compartment called the food vacuole. The breakdown process generates a number of cellular substrates and results in the production of a reactive and toxic byproduct, heme. The parasite minimizes heme toxicity by polymerizing the heme into a crystalline form called hemozoin [64]. The unique heme digestion and storage process is ripe with potential antimalarial drug targets. Several antimalarial agents (quinine, chloroquine, mefloquine, halofantrine) inhibit heme polymerization and perturb the digestive vacuole's function [65-67]. The buildup of quinine derivatives in the food vacuole generally inhibits polymerization, changes the local pH, and kills the parasite via mechanisms involving the toxicity of the heme. Resistance to this class of drugs is associated with mutated transporter genes such as the chloroquine resistance transporter (CRT) or the ABC transporter "multi-drug resistance gene" (MDR1) [68, 69].

Unclear Target – Artemisinin Family

Drugs based on the artemisinin core are derived from ancient Eastern medicine's use of the herb *qing-hao*. The natural product was isolated in the 1970s and derivatives which improve bioavailability created the artemisinin-family drugs. Artemisinins were long thought to inhibit the heme metabolic pathway via a radical-mechanism but the "evidence" is not yet conclusive. Other targets like a calcium ATPase or depolarization of the plasma membrane potential have also been implicated in artemisinin's mechanism of action [70-73]. Artemisinin-derived drugs are frequently used with a partner drug because earlier use of poorly bioavailable derivatives was associated with

recrudescence and a second drug may help ward off the generation of drug resistance [74]. Unfortunately, recent field reports indicate that some parasite populations along the Thai border have acquired resistance to artemisinin as evidenced by delayed parasite clearance [75, 76].

The Mitochondrion

The malarial mitochondria functions differently from canonical eukaryotic mitochondria. In most eukaryotes, the mitochondrially located tricarboxylic acid (TCA) cycle is the main source of ATP and energy for the cell. During TCA-cycle derived ATP production, glycolysis is used to pump protons into the mitochondrial matrix and to create an electrochemical gradient to drive the ATP synthase complex. Other functions of the typical eukaryote mitochondria include heme and steroid synthesis, calcium storage, apoptosis, producing warmth, and cell cycle control [77].

The malaria parasite's mitochondria are used in an atypical manner, with significant changes during the cell cycle [78]. In blood-stage malaria parasites the mitochondria is far less active in energy production [79]. The morphological and physiological conditions change significantly during the parasite life cycle, particularly the oxygen levels that are needed for aerobic energy production. The oxygen available in the human liver is reduced compared to circulating blood or that available in the mosquito midgut. During the intraereythrocytic stages the malaria mitochondrion

progresses from a small, punctate organelle during the merozoite stage into a branched structure in later stages. During maturation and growth of the mitochondria it greatly reduces the number of cristate, indicating a reduction in even the ability for the mitochondria to perform standard metabolic activity [79]. Energy production by blood-stage malaria parasites occurs largely through anaerobic glycolysis, with the malaria parasite's TCA-cycle enzymes not actively producing energy [80, 81].

The malaria parasite's unusually small mitochondrial genome has also led to speculation that the mitochondrion of the parasite is trimmed to minimal function. The mitochondrial genome of *Plasmodium falciparum* is only 6 kb and encodes the Cox I, cytochrome b, and Cox III subunits of the electron transport chain [39, 82]. Most known mitochondrial proteins are encoded by the nucleus to be imported post-translationally. The mitochondria of the intraerythrocytic parasite are viewed as near-vestigial and have only essential mitochondrial functions retained. One such function is the conversion of various substrates using classically mitochondrial enzymes, such as those involved in the citric acid cycle or turnover of coenzyme Q [49, 52].

Mitochondrial Localization Processes

Eukaryotic cells have organelles and internal compartmentalization of substances into organelles like the nucleus, chloroplast, lysosome, mitochondria, and others. The compartmentalization creates micro-environs and localized concentration gradients which can make enzymatic processes more efficient. The *Plasmodium* mitochondrion has two primary avenues for protein import to deposit proteins into

different compartments of the mitochondria, the TOM (translocator outer membrane) and TIM (translocator inner membrane) complexes [50].

The understanding of localization signals in malaria parasites is still incomplete. Predictive algorithms have been created based on similarity to proteins in more frequently studied organisms [83, 84]. The most common algorithms have determined that proteins targeted to *Plasmodium* mitochondria tend to contain N-terminal mitochondrial targeting signals with positive charges and few negatively charged amino acids [84]. The leading N-terminal region, sometimes found as excisable transit peptides, interact with the translocase complexes and use the electron transport chain's resulting gradient to drive the translocase. The bias of N-terminal residues is not entirely predictive of mitochondrial localization in the plasmodium parasite as some transmembrane domains, C-terminal, and internal targeting motifs have been demonstrated to control localization [85, 86].

Mitochondrial Localization Prediction Methods

There are many shortfalls in our ability to predict the localization of proteins based on raw genetic sequence. Large-scale gene sequencing vastly expanded the data available to determine localization signatures. Most efforts have gone into the study of model organisms or those with the greatest payoff (humans), with little attention paid to apicomplexa like *Plasmodium*. After the malaria parasite genome was published, the inability of common eukaryote genomic prediction methods to appropriately interpret the *Plasmodium* genome became evident and required further algorithm development.

Despite efforts to design good algorithms, protein localization still requires biological verification. An example of algorithms falling short is illustrated by the lipoic acid scavenging enzyme LipL1 which has been GFP tagged and found to localize to the mitochondria while it is predicted by MitoProt II algorithm to be mitochondrially targeted with a probability of 0.93, apicomplexa-targeted PlasMit predicts a cytosolic localization with a 99% confidence [87].

MitoProt II

Efforts to predict mitochondrial localization have resulted in computer algorithms that are trained with data sets of proteins expected or known to be localized. The predictive ability of the resulting algorithms can be cautiously useful. MitoProt II is an early algorithm developed for predicting mitochondrial localization in eukaryotes based on the N-terminal sequence [88]. The authors of the program developed 47 parameters that were evaluated against the 40 N-terminal residues. Claros *et al* claim a 75-97% prediction rate for proteins that have been studied, although the method was developed using a limited base of only 61 known mitochondrial proteins (an additional 49 were putative)[88].

TargetP

With further refinement, the prediction algorithm for eukaryotic localization TargetP was released in 2000 [89, 90]. TargetP 1.1 is a neural-network based tool designed to take the N-terminal protein sequence of eukaryotic genes and predict the

localization to mitochondria, chloroplasts, the secretory pathway (ER, Golgi), or some "other" location. The designers claim a 90% success rate for non-plant genes in redundancy-reduced test sets [89].

PlasMit

In order to address shortfalls in the general eukaryote predictions when applied to apicomplexans, a *Plasmodium*-specific neural network-based algorithm called PlasMit was developed in 2002. The PlasMit algorithm analyzes 19 physiochemical properties as well as amino acid frequencies of the first 24 N-terminal amino acids. The algorithm predicted that N-terminal sequences more abundant in isoleucine, tyrosine, asparagine, and lysine are more likely to be localized to the mitochondria [84]. The designers of the PlasMit algorithm reported 84% correct prediction in a 10-fold cross-validation study. The algorithm has been cited as predicting 381 mitochondrial genes out of 5,334 annotated genes in the *Plasmodium falciparum* genome [85]. Experimentally, others have found mitochondrial localization signals of folate cycle proteins are much more involved than just the first 24 amino acids [85, 91, 92].

Resident Mitochondrial Folate-Utilizing Enzymes

Organisms require folic acid for many of their one-carbon metabolic activities. Certain plants, like carrots, peas, potatoes, mosses, and pines, have been found to sequester their folate-recycling enzymes in organelles like mitochondria or chloroplasts

in a way that may make the folate cycle more efficient [93-95]. Most plants also possess a bifunctional DHFR-TS enzyme (e.g. carrots, *Arabidopsis thaliana,* soybeans, and corn) [96-100]. Beyond plants, the bifunctional DHFR-TS motif is also observed in the DHFR and TS genes of protozoa like *Leishmania, Trypanosoma*, and *Plasmodia* [101, 102].

Advances in tools and genetic manipulation have made it possible to identify the cellular distribution of many enzymes, including those of the malaria parasite. Recent papers have examined the localization of several enzymes related to the folate cycle. Some have found HProtein, a component of the glycine cleavage system, which is coupled to SHMT, to be localized to the mitochondria [103]. A more complicated pattern has been observed for both the cytoplasmic and mitochondrial SHMT isoforms [91, 92]. Read *et al* suggests that the cytoplasmic SHMT is not excluded from organelles like the mitochondria and apicoplast [91]. Read *et al* also found the mitochondrial SHMT is well distributed throughout the cell but has some bias for the mitochondria as well as the tips of apicoplast. Curiously, transfection with a truncated version of the mitochondrial SHMT with only one hundred N-terminal amino acids and a GFP domain resulted in a solely mitochondrial localization [91]. Supporting the theory of large domains determining mitochondrial localization, the mitochondrial SHMT's first 80 amino acids fused to GFP resulted in a mixed localization of mitochondrial and cytosolic signal [92]. Additionally, fusions with segmented 40 amino acid domains walking down the N-terminal 120 amino acids of mitochondrial SHMT were all cytoplasmic and only

full length SHMT sequence (or that with the first 24 amino acids deleted) was exclusively mitochondrial [92].

Our investigation concerns the localization of DHFR-TS, which performs two of the three catalytic functions involved in the folate cycle. The localization prediction methods TargetP and PlasMit fail to identify any transit peptides and are unable to predict any localization for DHFR-TS. As highlighted by SHMT, the third component of the folate cycle, prediction algorithms may provide an initial hypothesis for localization but the diverse and uncertain determinants require follow-up with biologically relevant studies to demonstrate localization.

Malarone® Development

Proguanil

The prevailing theory of proguanil's activation to cycloguanil requires specific cytochrome P450s enzymes that are most abundant in the human liver (CYP2C19, CYP3A4, and CYP2D6) [59, 104, 105]. Proguanil was developed in the western world where CYP2C19 deficiency is rare but as many as 13-23% of Asian and other ethnic populations are deficient in CYP2C19 activity. When proguanil was developed as an alternative for Ally soldiers unable to acquire quinine, the lack of attention to poor metabolizer phenotypes was not a great concern. After wartime usage, the high

prevalence of these deficiencies in locations with endemic malaria led to studies of drug's efficacy amongst populations where CYP2C19 poor metabolizer phenotypes are common. Unfortunately, people in the Philippines and Vietnam, where the phenotype for CYP2C19 activity is low, were the same populations that would most benefit from an affordable antimalarial like proguanil. Over time, larger studies with have shown that people with CYP2C19 deficiencies and reduced abilities to convert proguanil to cycloguanil have proguanil-based cure rates statistically equal to normal metabolizers, a very unexpected result [106-108]. While most people have the ability to convert proguanil into cycloguanil, the seeming lack of correlation between cure rates and conversion has not been explained.

Additional studies have found direct administration of proguanil more effective at treating malaria than cycloguanil, leading to hypotheses about a direct proguanil activity which never developed beyond speculation [109-112]. Adding to possible alternate targets, it has been suggested cycloguanil metabolites have their own targets as the susceptibility to cycloguanil can vary significantly between parasite isolates with identical DHFR sequences [113, 114]. The mechanism by which *in vitro* cultures of parasites, where no liver-based CYP450 metabolism is occurring, are killed by proguanil is not yet known [115]. In 1998, David Fidock bypassed malarial DHFR inhibition by transfecting human DHFR into malaria parasites [112]. The presence of human DHFR generated 1,000 fold shifts in the nanomolar levels of cycloguanil potency but no change in the high micromolar proguanil potency. The lack of a proguanil EC_{50} shift was cited as

evidence for a non-DHFR target for proguanil, but no candidate was proposed [112]. There have been no other proguanil targets identified beyond the cycloguanil-based target enzyme DHFR.

Atovaquone

Atovaquone was created as an analog to ubiquinone, a substrate known to be important in the electron transport chain as well as other processes. Atovaquone's development as a treatment for malaria hit a stumbling block when resistance emerged in patients during clinical trials [53, 54, 116]. Following drug treatment and an initial reduction in parasitemia, parasites frequently recrudesced after developing mutations in the cytochrome b component of the electron transport chain [117-119]. The resulting 67% cure rate at 28 days was considered too low for further development of atovaquone as a monotherapy [120]. Already approved drugs with antimalarial activity were investigated for use as partner drugs (tetracycline, doxycycline, pyrimethamine, and proguanil) and acceptable performance reported with doxycycline, tetracycline, and proguanil [54]. Tetracycline was a strong candidate, but fast elimination and tooth enamel staining were concerns. The tetracycline analog, doxycycline, had a longer half-life, but adverse reactions in young children made it less desirable [116, 121]. The slightly improved performance of atovaquone with proguanil, combined with the relatively impermanent side effect of stomach upset, low cost, and atovaquone-compatible dosing schedule, made proguanil the better partner choice. Atovaquone

drug development was rescued by combining with proguanil and the resulting treatment consists of both proguanil and atovaquone [59].

Malarone®

The first characterization of the combination of proguanil and atovaquone as synergistic was reported in 1995, although atovaquone and the proguanil-like PS-15 (a prodrug of WR99210) synergy was reported in 1993 [59, 122]. In a synergistic drug combination, multiple drugs combine to give a response beyond what would be predicted by simple addition of single drugs. In the case of Malarone®, as shown in Table 3.1 and 3.2 B, the EC_{50} of proguanil was found to be 13 µM and atovaquone measured at 4.6 nM in 3d7 parasites. When only 1 nM atovaquone was combined with proguanil, the measured EC_{50} of the proguanil with 1 nM atovaquone was shifted 81 fold to 0.16 µM.

Theories to explain the synergy between proguanil and atovaquone have been proposed and updated over the years, but none have been biochemically verified. Initially, it was assumed that the synergy between antifolates and atovaquone came from the ubiquinone link (Figure 1.5) between the electron transport chain and pyrimidine biosynthesis (both DHODH's need for ubiquinone and DHFR inhibition by cycloguanil) [116]. Experiments in culture flasks also displayed synergy between proguanil and atovaquone, contradicting the presumed mechanism which required metabolic activation of proguanil to cycloguanil by liver-based cytochrome P450s [59]. When populations deficient in the P450s responsible for creating cycloguanil were

investigated, the combination of proguanil with atovaquone was still sufficiently effective to avoid changing the proguanil component of the formulation and supported ideas of alternate mechanisms of action [123]. One lab has offered multiple theories, including one where proguanil, as a biguanide, was responsible for causing the gradient of the electron transport chain to become "leaky" but only with atovaquone and no other ETC inhibitors [124]. In additional studies, Painter *et al* transfected parasites with yeast-derived DHODH that would bypass the need for ubiquinone recycling to function. The parasites were highly resistant to ETC inhibitors but the combination of proguanil with atovaquone was still lethal. Painter *et al* proposed an alternate theory that proguanil's alternate target was something used to create a mitochondrial membrane potential after the main driver of that potential, the electron transport chain, was inhibited [52]. Despite never resolving the synergy or alternate target for proguanil, the drug combination has been sufficiently effective that its use has continued and it is now the most prescribed antimalarial in the US [125].

The product of combining proguanil and atovaquone is a single pill called Malarone®. A Malarone® tablet contains 250 mg of atovaquone and 100 mg of proguanil hydrochloride and the dosage schedule is once a day for prophylactic use and four pills at a time as a treatment dose [123]. The Malarone® combination achieved an average 98.7% cure rate against *Plasmodium falciparum* over ten studies involving five hundred patients where patients were given treatment for three days, including those living in areas where proguanil resistance was widespread [116]. The steady state

concentrations of proguanil and cycloguanil have been reported at 131 - 473 nM and 57 - 154 nM, respectively [126, 127]. The elimination half-lives of the compounds are a bit more imbalanced, with proguanil's half-life of 14 hours and atovaquone's half-life measuring just under six days [107, 128, 129]. Physiologically, the Malarone® combination results in proguanil/cycloguanil as the fast acting agent and atovaquone acting as the long-lasting agent to clear any lingering parasites. The still-great mystery surrounding how the two components of Malarone® interact is how patients with a reduced ability to convert proguanil into cycloguanil differ so significantly in cycloguanil exposure, with a 3 hr post-dosage cycloguanil plasma concentration of 71 nM in poor metabolizers but 171 nM in normal/extensive metabolizers (proguanil was 4,030 nM and 3,721 nM), yet clinical trials of the combination indicate similar cure rates even where parasites are largely resistant to antifolates [107, 116].

Chapter 1 Figures

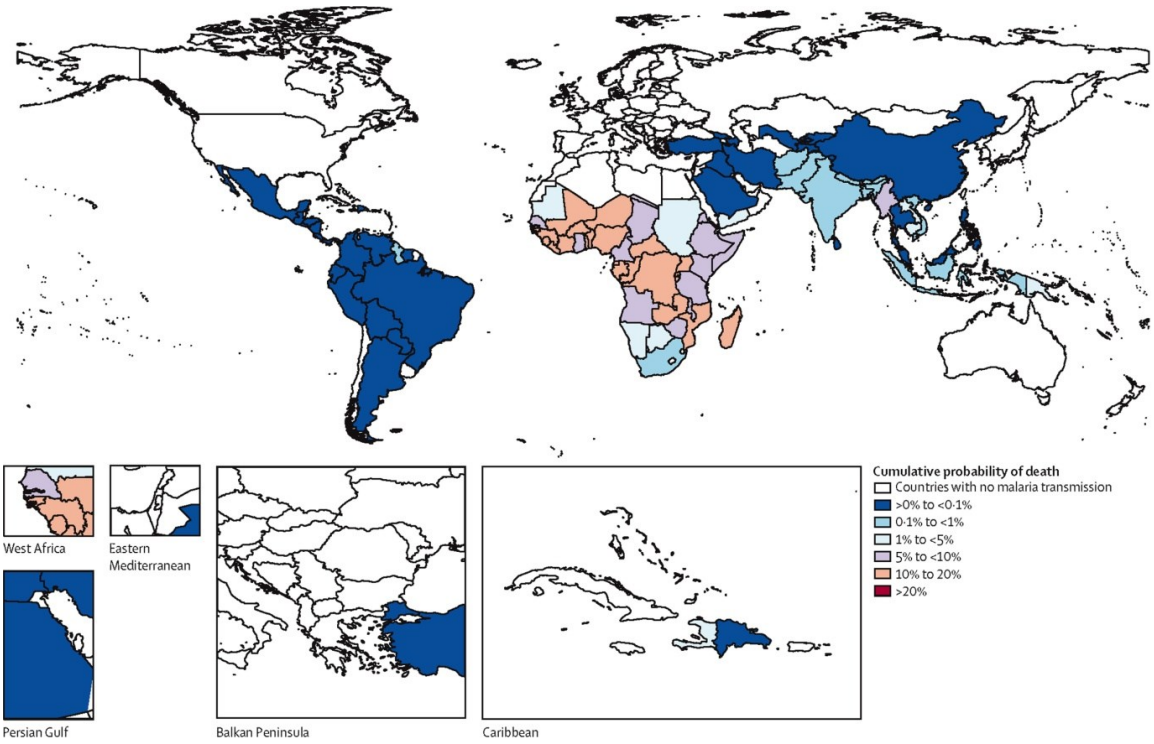

Figure 1.1 – Cumulative Probability of Death Caused by Malaria (2010)

The likelihood of an individual's death to be caused by malaria infection at any point in an individual's life, from ages 0-80, is grouped into color coded countries. Countries in Africa and parts of Southeast Asia have particularly high likelihoods of death caused by malaria. Figure used with permission from Murray 2012.

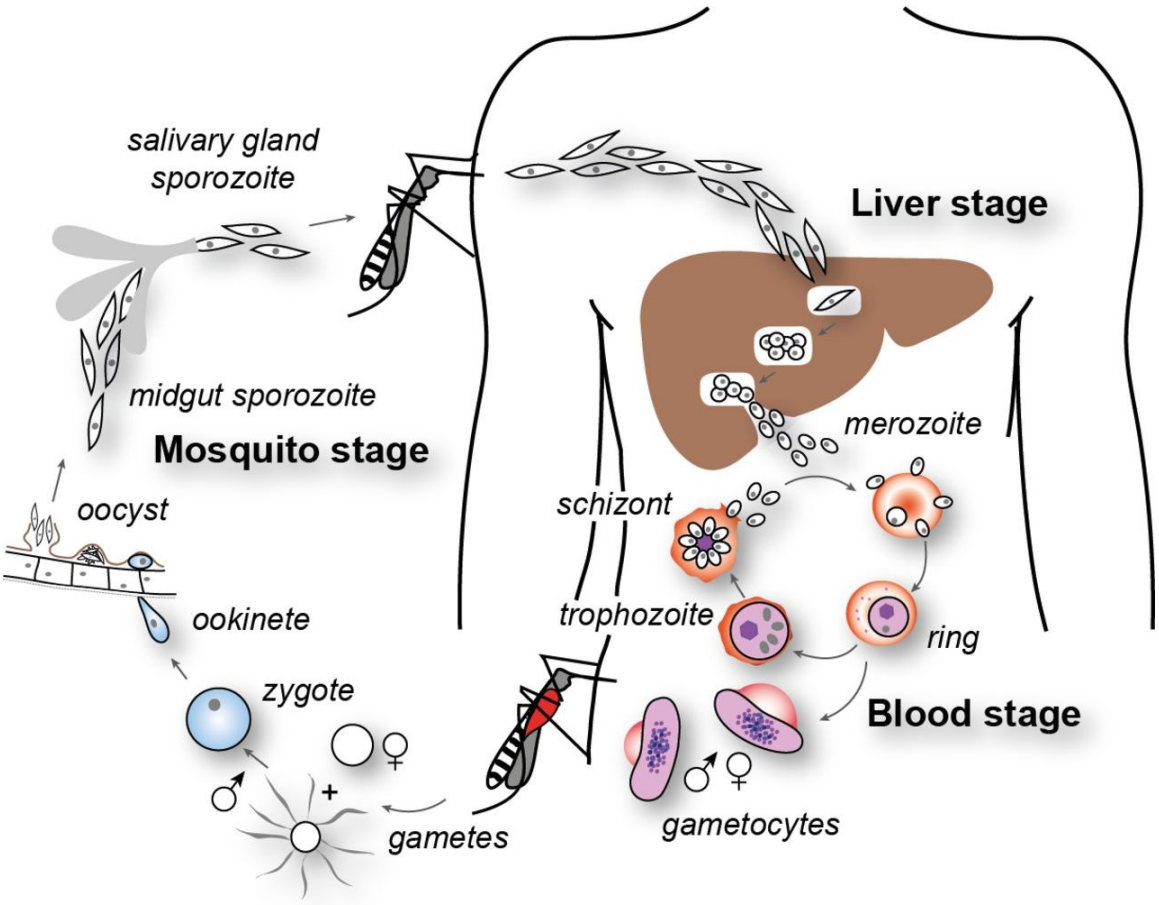

Figure 1.2 – The Malaria Parasite Life Cycle Spans Two Hosts

The human-infecting malaria parasite's life cycle is complex and involves two hosts. The sequence depicted most closely resembles the life cycle of *Plasmodium falciparum*. Starting the malaria life cycle from the initial infection, a malaria-infected *Anopheles* mosquito injects sporozoites during a blood meal. Sporozoites then make their way into liver hepatocytes. Upon infecting hepatocytes, the parasites undergo several rounds of replication before maturing into exo-erythrocytic merozoites released into the blood stream. Merozoites invade erythrocytes and grow through ring stages into trophozoites and mature schizonts. A fully matured schizont then ruptures the cell and releases merozoites that invade new erythrocytes. A small fraction of asexual, blood stage malaria parasites differentiate into sexual-stage parasites called gametocytes that can be taken up with circulating blood to infect mosquitoes. Once entering the mosquito gut, maturation of the male and female gametes occurs. Upon sexual recombination, a fertilized zygote develops into ookinetes and oocysts, eventually releasing sporozoites that can infect another human. Figure used with permission from Cowman et al., 2012. Originally published in JCB. doi: 10.1083

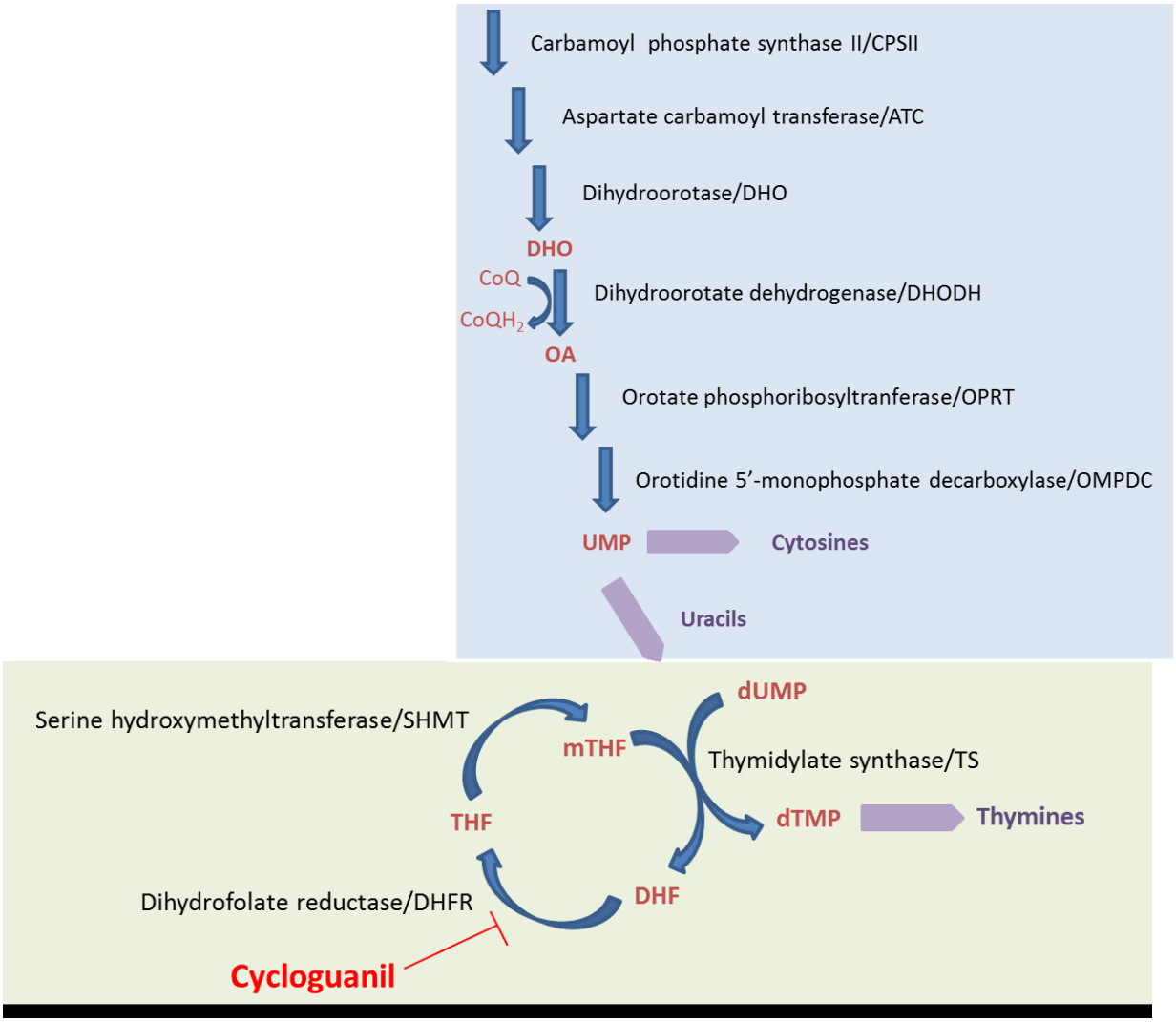

Figure 1.3 – Pyrimidine Biosynthesis and the Folate Cycle

The pyrimidine biosynthesis pathway (blue) has a number of components that are targeted with antimalarial drugs. The dihydrofolate reductase (DHFR) enzyme of the folate cycle (lavender), necessary for methyl transfer in a number of processes, is targeted by drugs like cycloguanil and pyrimethamine. Dihydropteroate synthase (DHPS) is involved in folate biosynthesis, prior to the depicted folate cycle, and was often targeted alongside DHFR in combination drugs like sulfadoxine-pyrimethamine.

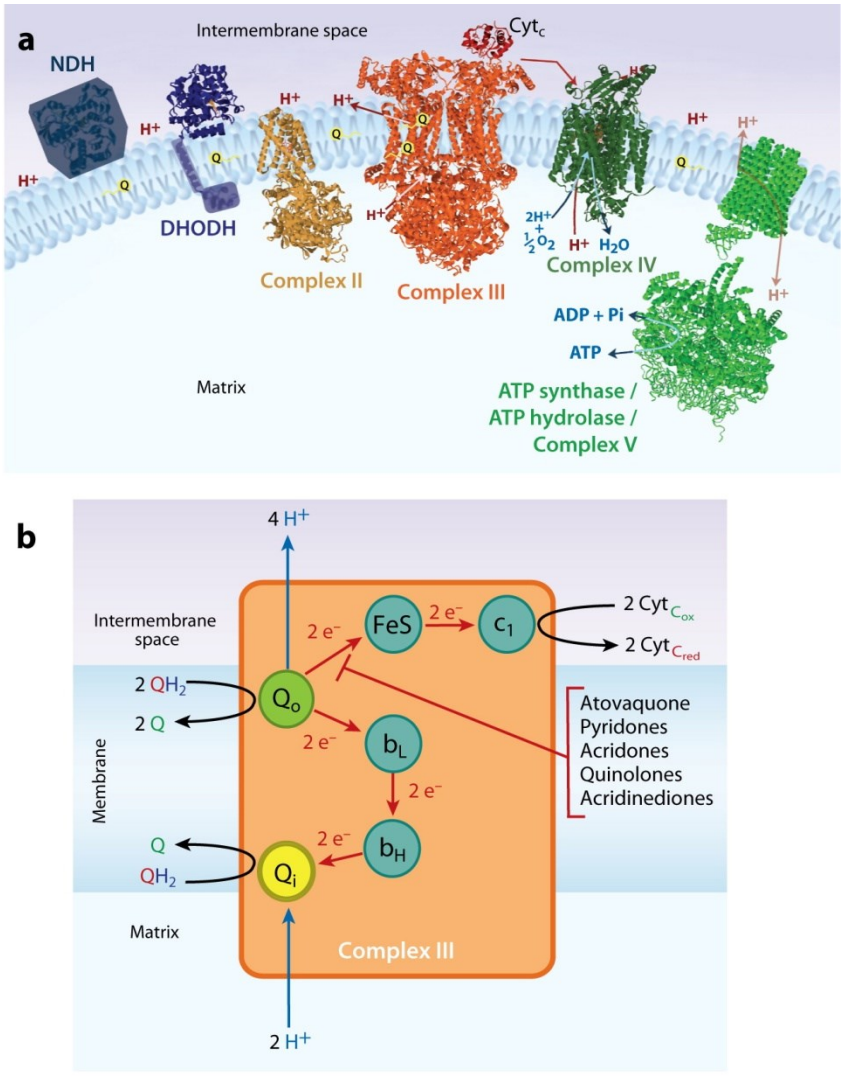

Figure 1.4 - Major Components of the *Plasmodium* Electron Transport Chain

The main components of the malarial electron transport chain and dihydroorotate dehydrogenase (DHODH) are depicted in (a). Compared to most eukaryotes, the parasite no longer posesses a canonical Complex I and, instead, has a non-proton pumping NDH (NADH dehydrogenase or NADH:ubiquinone oxidoreductase) that reduces ubiquinone. The malarial Complex II is called succinate dehydrogenase. Complex III is comprised of two subunits (cytochrome b and cytochrome c1) and is called the ubiquinol:cytochrome c reductase complex. Complex IV is called the cytochrome b oxidase complex. DHODH is membrane-associated and utilizes the membrane associated coenzyme Q substrate which is regenerated by Complex III. (b) contains a diagram of the reaction sites of Complex III. Atovaquone, myxothiazol, and several other coenzyme Q analogs inhibit at the Q_0 site of Complex III. Antimycin A inhibits at the Q_i site of Complex III. Inhibition of Complex III disrupts the membrane potential gradient and results in a buildup of reduced coenzyme Q, eventually leading to reduced DHODH activity. Figure used with permission from Vaidya 2009.

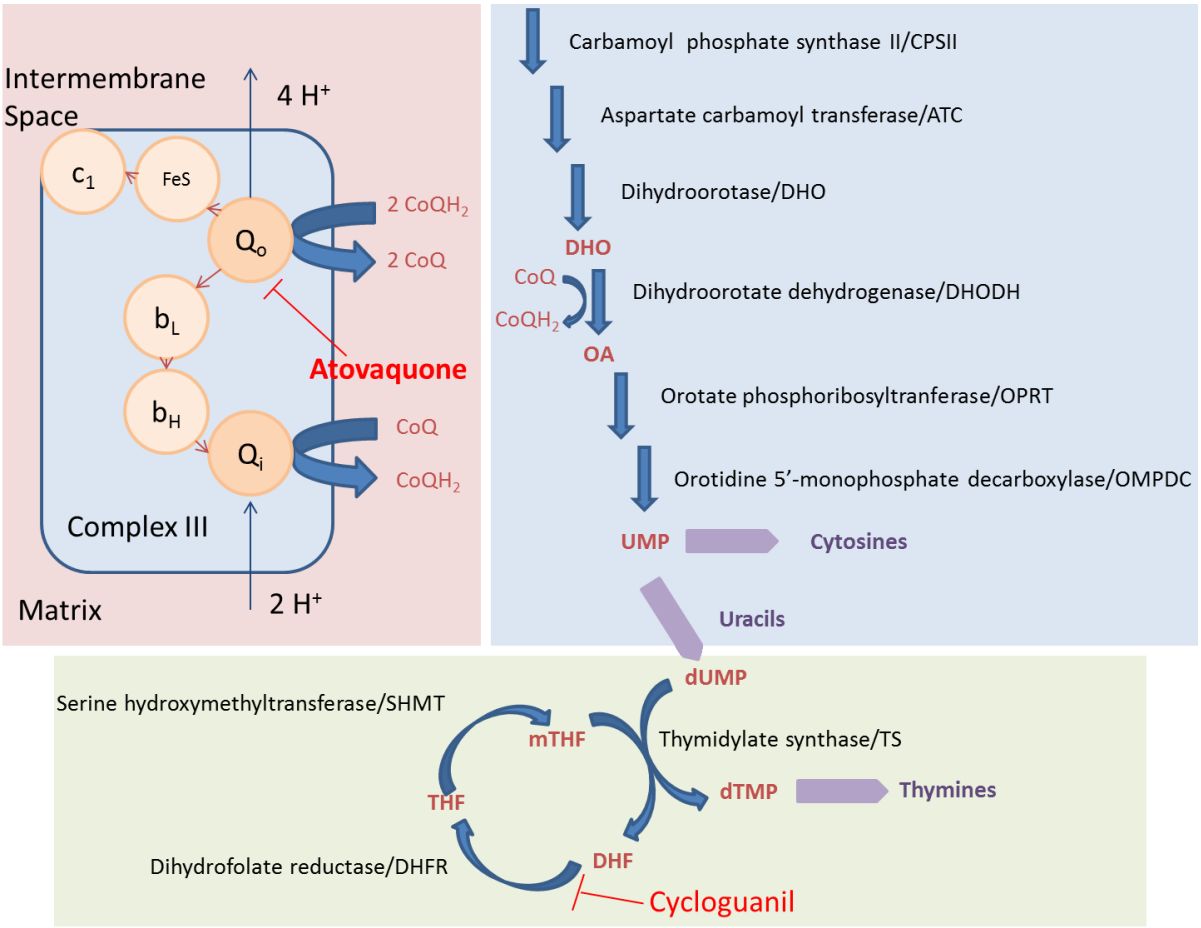

Figure 1.5 – Potential Synergistic Coenzyme Q-based Link between Pyrimidine Biosynthesis Pathway, Electron Transport Chain, and the Folate Cycle

Coenzyme Q flux has been viewed as the source of synergy that links the electron transport chain (Complex III is in the red box) to pyrimidine biosynthesis (blue box) and the folate cycle (lavender box). Atovaquone inhibits the Q_0 site and reduces the amount of oxidized coenzyme Q present. The pyrimidine biosynthesis pathway (blue box) requires DHODH activity, which requires oxidized coenzyme Q as a substrate. The folate cycle (lavender) is also necessary for pyrimidine biosynthesis and the DHFR enzyme is targeted by cycloguanil, the active form of proguanil. Multiple enzymatic targets in the same pathway may lead to drug synergy, although localization of enzymes and their targets may also lead to synergy.

Chapter 2 – Plasmodium Dihydrofolate Reductase – Thymidylate Synthase Localization

Introduction

The malaria parasite's dihydrofolate reductase (DHFR) enzyme was the first target that synthetic antimalarial drugs were specifically designed to inhibit. The DHFR enzyme catalyzes an obligate step in the folate cycle, a cycle that regenerates folate-derived C1 carriers used by the pyrimidine biosynthetic pathway. Malaria parasites are required to perform their own pyrimidine biosynthesis and maintain a balanced supply of nucleobases to survive and replicate.

Although single antimalarial drugs targeting DHFR have fallen out of favor due to established drug resistance, several actively used antimalarial drug combinations mix a DHFR inhibitor with another drug, often targeting other components in the pyrimidine pathway. The drug combination sulfadoxine and pyrimethamine inhibits folate synthesis via the dihydropteroate synthase (DHPS) enzyme and the folate cycle via the DHFR enzyme. Malarone®'s mode of action is slightly more complex, but it combines an electron transport chain inhibitor, atovaquone, with a pro-drug for a DHFR inhibitor (proguanil as the pro-drug for cycloguanil). The electron transport chain generates a proton gradient in the mitochondria. That proton gradient is utilized for several purposes, including the import of proteins to the mitochondria. The bifunctional DHFR-TS motif of malaria parasites is something also observed in plants. Plants are known to sequester folate-recycling enzymes in organelles. Further implicating the pyrimidine

biosynthesis pathway with the mitochondria, dihydroorotate dehydrogenase (DHODH) is mitochondrial, requiring a mitochondrial membrane-bound substrate, and the malaria parasite's folate cycle enzyme serine hydroxymethyltransferase (SHMT) has an isoform with a mitochondrial localization signal.

We set out to determine the localization of malarial DHFR, a drug target with a long history but also a challenging enzyme with low expression levels [40]. Knowing the localization of the drug target will help explain how current drugs work and multiple drugs interact. We applied laser-scanning confocal microscopy to compare DHFR localization patterns observed to various organelles. An algorithmic assessment of the colocalization between organelles and DHFR was employed to help compensate for low amounts of fluorescent signal while not biasing our interpretation. In total, signals from mitochondrial dye, a native mitochondrial protein, and a GFP tagged mitochondrial protein were all compared to the DHFR signal. Pushing beyond what is common for biological studies of localization, we also employed a non-microscopy-based method of cell fractionation to assess the localization of DHFR to the mitochondria.

Experimental Procedures

Materials

Antibodies to DHFR-TS

Custom polyclonal *Plasmodium falciparum* and *Plasmodium vivax* DHFR-TS antibodies were generated in rabbits. The supplier, GenScript, was provided with lab-generated reference standards of crude, recombinant target protein expressed in the wheat germ-cell free system with an N-terminal GST tag and a "background control" of wheat-germ lysate. To further evaluate reactivity and specificity, we provided lysates of 3d7 *Plasmodium falciparum* parasites and 3d7 *Plasmodium falciparum* parasites which were transformed to express *Plasmodium vivax* DHFR-TS enzyme. The peptide antigens were generated with proprietary computer algorithms and several potential antigen peptides evaluated for antigenicity in rabbits. The rabbits were immunized twice before serum was used to screen responses to the target peptide. The best candidates were further subjected to two additional booster inoculations before serum was collected and antibodies purified with antigen peptide affinity columns.

The resulting antibodies reacted with the peptides KLKWKRERYLRMEAc corresponding to *Pv*DHFR and NNDMPLKNDDKDTc corresponding to *Pf*DHFR's joining/hinge region. The results of the lalign algorithm with the antigen regions highlighted predicts the species specificity (Figure 2.1) [130]. BlastP evaluation of both

antigen sequences revealed extremely limited domains of homology to any genes in the human or *Plasmodium falciparum* genome, aside from the respective, intended targets.

Antibody specificity was assessed using parasite lysates from the major parasite strains used during the course of the thesis (3d7, PvDHFR-TS(wt) 3d7, PvDHFR-TS(cycR) 3d7, Dd2, HProtein-GFP Dd2, ACP-GFP D10) and against recombinant standards produced in a wheat germ expression system. The species specificity of the *falciparum* and *vivax* antibodies was demonstrated in Western blots against *Plasmodium falciparum* parasite lysates, including lysates created from a *Pv*DHFR-TS expressing construct in 3d7 parasites as *Plasmodium vivax* cannot be continually cultured *in vitro* (Figure 2.2).

Organelle Labels

Nucleus – DAPI/Hoechst33342

The nucleus of the malaria parasite begins as a single organelle in the early erythrocytic stage of the parasite's life cycle. Over the life cycle the genome replicates and the nucleus divides to reach approximately 14-20 nuclei in a schizont-stage parasite. Certain cationic dyes like DAPI and Hoechst 33342 bind DNA at the minor groove, with a preference for A and T nucleobases, and are able to mark the location of the nucleus where DNA concentration is highest [131-133]. The DAPI and Hoechst 33342 dyes have been utilized to mark the nucleus of malaria parasites in our lab for years. Of morphological note, in merozoite stages or late trophozoite/schizont stages the malaria

parasite's nucleus frequently appears to have a hollow, like puffed oats, due to the nucleus being squeezed aside by other organelles in a very confined cell.

Mitochondria – Mitotracker/HProtein-GFP/PfDHODH

The *Plasmodium* mitochondrion is a slightly acidic environment with lipophilic character due to the cristae that comprise its inner membrane. Dyes like mitotracker take advantage of the reduced pH and lipophilicity to be taken up into the mitochondria. Once inside the mitochondria, the mitotracker dyes react to form covalent bonds with free thiols which aid dye retention during fixation and permeabilization steps [134]. Commercially available, reduced forms of Mitotracker Orange (M-7511) and Mitotracker Red (M-7513) and non-reduced Mitotracker Deep Red (M-22426) were procured from Life Technologies/Invitrogen and utilized as appropriate at 75 - 100 nM concentrations.

A 2010 paper by Spalding *et al* has localized the HProtein subunit of the glycine cleavage complex to the *Plasmodium falciparum* mitochondria [103]. In many organisms the glycine cleavage complex (a central component of fatty acid biosynthesis) is established as mitochondrially localized [135]. The N-terminal sequence of HProtein was used to generate transfection plasmids that express HProtein with a C-terminal green fluorescent protein (GFP) fusion construct. The Prigge lab was kind enough to provide this parasite line as a reference but it should also be noted that integration of the attB mycobacteriophage targeting site to the Dd2 parasite genome has also inserted a human DHFR gene into the parasite line, additional to the intended plasmid. While

the HProtein is still useful as a marker for mitochondria, human DHFR can impart resistance to many DHFR-based antimalarial drugs and limits the drug-response studies that can be performed with H-protein^{Dd2} cells.

The HProtein-GFP containing Dd2 parasite line was also applied to digitonin-based cell fractionation experiments. The C-terminal GFP tag was probed with the monoclonal anti-GFP antibody used for immunofluorescence imaging (Santa Cruz #sc9995). HProtein-GFP containing Dd2 parasites provided a valuable, published standard for a mitochondrial protein.

Mouse sera containing polyclonal antibodies to the malarial dihydroorotate dehydrogenase enzyme were obtained from the Vaidya lab and the Phillips lab in limited quantities. Malarial DHODH has a well-established membrane anchor and requires a membrane-associated ubiquinone cofactor [136]. The native DHODH protein served as a scientifically interesting control for a mitochondrial protein that could also be probed and correlation evaluated [137].

Apicoplast – ACP-GFP

The apicoplast is an organelle common to the phylum Apicomplexa. An abundant protein localized to the *Plasmodium* apicoplast is acyl-carrier protein, an enzyme central to fatty acid biosynthesis. The McFadden lab developed a transfection plasmid to probe apicoplast protein localization and included both the signal and transit peptide domains necessary for targeting the GFP construct to the apicoplast [138].

Previously transfected D10 parasites containing the plasmid were utilized with the localized GFP signal marking the apicoplast.

Endoplasmic Reticulum – ER-Tracker Blue-White DPX

The endoplasmic reticulum (ER) of the cell is usually viewed as a center of protein translation and substrate storage. The *Plasmodium* ER tends to be associated with the nucleus and may be labeled with ER-Tracker Blue-White DPX dye (Life Technologies/Invitrogen #E-12353). The red and blue versions of the dye have been reported as effective for live *Plasmodium falciparum* parasite imaging [139, 140]. ER Tracker Blue-White DPX dye is partially retained after fixation and is able to be visualized in the UV/blue fluorescence range with 430 nm excitation maximum and emissions from 430-640 nm. Cells were treated with ER-Tracker Blue-White DPX for 30 minutes at 250 nM prior to fixation.

Digestive Vacuole – LysoTracker Red

The lysosome of the cell is an acidic environment where the cells break down proteins into smaller peptides for reuse. The parasite has one large lysosome in the digestive vacuole. The parasite also has auxiliary lysosomal bodies that may be a part of a functional endocytotic/autophagocytotic system [141-143]. Lysotracker Red dye has been shown to label the malaria parasite's digestive vacuole well [141]. Lysotracker Red DND-99 was procured from Life Technologies/Invitrogen (#L-7528) and applied directly to 100 nM concentration.

Methods

Localization Prediction Algorithms

The most frequently cited mitochondrial/apicoplast localization prediction algorithms for *Plasmodium* parasites are PlasMit and MitoProt II. For this work the PlasMit progam was used to judge mitochondrial sequence localization. The MitoProt II program was also used to help examine if DHFR-TS had any signals for localization to the mitochondria and the apicoplast. The mitochondria and apicoplast organelles develop at the same time and in proximity to each other, requiring great care in judging one from the other via microscopy.

Image Analysis Algorithms

For colocalization analysis, images were captured on a Zeiss META 510 confocal LSM system with a 63x oil immersion lens. The pinhole diameter was set to 1 airy unit for the longest wavelength light source (generally the 543 nm laser) and all other light sources had pinhole diameters set to match the optimal imaging section's depth. The z-stack slices were then captured using the "optimal" setting for the longest wavelength imaged to minimize oversampling (generally 0.41 µm and 8 to 12 slices were captured, of which approximately six capture the full depth of the parasite). The images were examined via both Zeiss LSM Image Browser v4.2 and the FiJi collection of ImageJ plug-ins.

The FiJi-ImageJ suite of programs contains several plug-ins useful to quantify colocalization of different signals in a specimen [144]. The algorithm used by the

colocalization plug-in can evaluate many different features of the image. It quantifies where each voxel (volumetric pixel) in a stack of images overlaps from one channel to another in order to assign numerical values which help compare entirely different images to one another. The parameter we used to evaluate the images was, primarily, the Pearson's correlation coefficient value [145]. The Pearson's correlation value quantifies the covariance of two signals in the image. Ideally, two signals that vary perfectly together, such that strong signals overlap each other and weak signals overlap each other, will lead to an R coloc value as high as 1. If a strong signal in one channel is never found with a signal from the other, the R coloc value has a lower limit of -1. If the algorithm determines there is no relation, a Pearson's correlation coefficient value near 0 is expected. The FiJi colocalization plugin computes a lower threshold for what is considered "signal" in the image via the Manders' thresholding algorithm and calculates a thresholded Pearson's correlation coefficient (R coloc) based only on signals exceeding the threshold [146]. Additional considerations must be given when the images captured are devoid of background signals and otherwise "dark" around the colored areas. Cells displaying low, background-type fluorescence on a slide of no signal may yield moderate values of correlation if the threshold is too low. If the image is rescaled and a more stringent threshold is set for signals, such that only the most intense signals are considered, the bar for finding covariant signals is significantly higher and moderate thresholded overlaps are significant.

One way to perform the analysis is to consider the whole image, permit the program to determine which signal levels represent background, and to allow it to output the Pearson correlation coefficient. For that method, the images were opened in FiJi (an ImageJ-based suite of tools), the color channels separated, and the image stack analyzed using the colocalization plugin. Another way to analyze the image is to crop to an infected erythrocyte, rescale the color thresholds, and only evaluate the intense, focal signals. If a stringent threshold was to be used the image was rescaled using the brightness/contrast tools to set the minimum and maximum color values of the 8 bit image. To ensure that images were of high quality, no images were analyzed where more than half of the color depth was removed unless the images were controls where low to no signal is to be expected in certain channels.

The thresholded Pearson's correlation coefficient (R coloc as labeled by FiJi's plugin) also needed to be examined with respect to the number of colocalized pixels considered for the calculation. Some images that contained very intense, localized signals gave stronger correlations but only a small number of pixels overlapped. Some images with diffuse signals showed broad swaths of the image which appeared to overlap weakly with one another. The R coloc values have difficulty comparing such vastly different signals from the background and demanded attention be given to what images are being compared. If the image had been manually thresholded to evaluate only the stronger signals (useful when mitochondrial branches are present but also contain moderate background signals) the R coloc value becomes influenced by the

manually set threshold. As a general guide, most high quality images captured contained background intensities that could be thresholded out at less than 10% of the total signal range captured.

Base Microscopy Protocol – Paraformaldehyde Fixed Cells

Sample Fixation and Permeabilization

Parasites to be imaged were grown in complete, serum supplemented RPMI-1640 media and red blood cells prior to being prepared for microscopy. Complete media was removed, the sample divided into multiple tubes or flasks, and fresh media added. In instances where fluorescent dyes were to be added less than an hour before sample preparation, the dye was added directly to media comprised of RPMI without phenol red indicator in order to minimize the conflicting fluorescent signals and lipid contents. In antibody-only sample preparations, parasites were isolated from flasks grown in standard complete media. Dye was directly added to parasites suspended in approximately 5 mL of media, the parasites put under gas, and the sample incubated at 37 °C during dye treatment.

Following dye treatment, the contents of the flasks were removed to a 50 mL centrifuge tube and spun for 3 minutes at 800 rpm/~120 rcf in a Sorvall Legend X1r swinging bucket centrifuge at 4 °C. The media was removed and the pellet resuspended in 5 mL of cold PBS. The sample was again spun for 3 minutes at 800 rpm at 4 °C. The supernatant was removed and the pellet resuspended in PBS to ~1.5 mL total volume before 4.5 mL of a freshly made 5% para-formaldehyde (PFA) in PBS solution was added

(effectively, 3.8% PFA final concentration). The sample was inverted occasionally to avoid having the parasites settle. Glutaraldehyde was added after 10 minutes to supplement the PFA to to 0.009% glutaraldehyde fixative, which helped retain the red blood cell external membrane. After 5 minutes of further fixation the parasites were spun down at 300 rpm/17 rcf for 9 minutes and the supernatant removed until the remaining contents of the tube were approximately 1 mL. With little delay, the pellets were resuspended in 4 mL of cold PBS via inversion and gentle orbital shaking. The cells were again spun down at 300 rpm for 8 minutes. Following sedimentation, the parasites were resuspended in 2 mL of cold PBS via inversion and gentle orbital shaking. Permeabilization of membranes was performed using 3 mL of PBS with 0.1% v/v Triton-X 100 for better penetration by antibodies, when appropriate. The parasites were then spun down at 300 rpm for 8 minutes. The intracellular red hemoglobin protein rapidly dissipated from this point forward. The supernatant was removed and the pellet resuspended in 3 mL of cold PBS and then 3 mL of 3% BSA (w/v) PBS was added to react with any available aldehyde groups and block reactive surfaces. The blocking mixture was allowed to react for 20 minutes before the cells were spun down at 300 rpm for 8 minutes, the supernatant removed, and 3% BSA in PBS added and the suspended cells were allowed to block for an additional hour. The cells were then spun down at 300 rpm for 8 minutes, the supernatant removed, and 3% BSA in PBS added to a total volume of approximately 0.8 mL.

The preferred method for mounting parasites for imaging was to activate the surface of a glass cover slip via brief exposure to a Bunsen burner's flame and then allow cells to settle on the cover slip. During these experiments the cover slip was flamed, the edges outlined with an ImmEdge pen (Vector Laboratories), and the cover slip placed in a humidified chamber with a lid. Cells were applied to the cover slip while suspended in blocking solution and allowed to settle for at least 30 minutes.

Immunostaining

Antibodies were added to PBS with 3% BSA at concentrations from 1:100 to 1:500 v/v dilutions for primary antibodies. 25x25mm #1 coverslips hold between 0.2 to 0.3 mL of solution during the exposure. The cells and primary antibodies were allowed to react for at least 1 hour before excess media was "poured" off the edge of the cover slip and washed with 0.35 mL portions of 3% BSA in PBS. Three rounds of combined wash/blocking were performed with a minimum incubation time of 10 minutes to allow cells to settle after manipulation. After the third wash, a solution with fluorescently tagged secondary antibody (reactive to the primary antibodies and labeled with a fluorescent Alexa Fluor tag) was applied at 1:200 to 1:500 dilutions depending on previous performance and abundance of the target. The secondary antibody was permitted to react with the cells for a minimum of 1 hour before cells were washed. The initial washes were performed with 3% BSA in PBS to extend blocking activity. After two or three BSA washes, the blocking agent was removed and the additional wash steps were performed with PBS or PBS with DAPI/Hoechst 33342 dye (10 µg/mL DAPI or

100 µg/mL for Hoechst). Background signal was minimized by washing with PBS at least three times before assembling the slide.

To assemble the slides for imaging, we poured off excess PBS from the coverslip, used a clean Kimwipe to dab excess liquid from the corner, and applied an 8 µL portion of ProLong Gold anti-fade sealant to the center of the slide. The slide was then lowered on top of the cell-coated coverslip. Generally, a small amount of excess PBS could be wicked away from the slide by tapping the slide edge to a paper towel on both long edges of the slide. The slide was then permitted to cure at room temperature overnight, in the dark prior to the imaging session. Nail polish was applied along the edges of the coverslip to ensure the coverslip was not dislodged during imaging. PBS residues could be cleaned from the top of the cured coverslip and optical clarity restored with gentle swipes of a wet Kimwipe.

Results

DHFR-TS Localization Patterns Observed

Plasmodium falciparum parasites were grown in standard 10 mL culture flasks, aliquotted, and then the parasite and red blood cells fixed using 3.8% *para*-formaldehyde (PFA) and 0.0009% glutaraldehyde solutions in phosphate buffered saline (PBS). PFA fixation for antibody use required cell permeabilization utilizing Triton-X 100 to strip away lipid layers and enable antibody penetration throughout the cell. The

antibodies used for *Plasmodium falciparum* DHFR-TS provided good localization of the DHFR-TS signal to the parasite. Upon closer examination of images obtained via confocal microscopy the appearance of localized spots of DHFR-TS signal was noted (Figure 2.3). Currently there are no known binding partners for *Pf*DHFR-TS and both the PlasMit and MitoProt II algorithms did not predict *Pf*DHFR-TS targeting to any organelles (99% non-mitochondrial by PlasMit and only a 0.2711 probability of export to the mitochondria by MitoProt II). The localized patterns observed with the DHFR antibody warranted further examination. Several organelles in the malaria parasite were systematically examined for correlation between organelle and DHFR-TS.

DHFR Antibody Localizes At Specific Organelle - Mitochondria

The availability of organelle-specific dyes and established localization of select proteins enabled their use as comparators to the localization patterns observed for the *Pf*DHFR-TS enzyme. The dyes employed successfully include ER Tracker Blue-White DPX (labeling the endoplasmic reticulum), Lysotracker Red (labeling lysosomes and the food vacuole), DAPI and Hoechst 33342 (labeling the nucleus), and Mitotracker Orange or Deep Red (labeling mitochondria). The apicoplast organelle was labeled using episomally transfected parasites containing acyl carrier protein-GFP fusions generated by Waller *et al* in 2000 [138]. Additional labels of the parasite mitochondria included a parasite line which had an integrated copy of the mitochondrial HProtein fused to GFP [103] as well as the limited use of a mouse antibody to *Pf*DHODH that was obtained from Meg Phillips and Akhil Vaidya.

Several experiments were performed to examine colocalization of *Pf*DHFR-TS signal with organelles of the parasite. Proper delineation of the signal intensity of an organelle, as opposed to the background signal observed due to nonspecific binding that is stronger in the malaria parasite, required thresholding the images using a histogram of the signal intensities. The high threshold/high stringency analysis was accomplished by isolating a single infected red blood cell from the three dimensional image, generating a histogram of pixel intensities, and setting the signal minimum above the immediately visible "bell curve" of intensities so as to remove background/the most prevalent signal of the image and adjusting the high signal intensity so no pixels were saturated. This high stringency analysis avoided the parasite membrane, with higher background signals than the red blood cell membranes, contributing large areas of low intensity overlap to the point organelle comparisons.

Comparison to Nucleus

The nucleus of the malaria parasite is a membrane-bound organelle that contains the chromosomal DNA of the parasite. Rounds of DNA replication and fission split the nucleus into 10 to 20 daughter nuclei in later stages of the parasite life cycle. The appearance of the nucleus when labeled with Hoechst 33342 or DAPI is that of an ovoid dot like a grain of rye, occasionally showing a "dimple" from the nuclear membrane being pushed aside by the digestive vacuole. The correlation coefficient for the nucleus with the *Pf*DHFR-TS was determined to have a mean and SEM of -0.038 and 0.086, respectively. There was no statistically significant correlation between DHFR-TS

and the nucleus, as evaluated by the one sample t test finding a P value of 0.68. Example images appear in Figure 2.4 and the resultant data is summarized in Figure 2.8.

Comparison to Lysosome/Digestive Vacuole

Lysotracker dye was used to examine the location of the digestive/food vacuole of the malaria parasite. The digestive vacuole of mature parasites is often observable in the DIC image due to crystallized heme causing optical interference, but the digestive vacuole is much more difficult to observe during earlier stages. Lysotracker dye targets acidic organelles and localizes to both the mature digestive vacuole and, with lower affinity, to the earlier stage parasite's smaller food vacuoles . The correlation coefficient for the food vacuole with *Pf*DHFR-TS was determined to have a mean and SEM of 0.084 and 0.032 in this experiment. There was no statistically significant correlation between DHFR-TS and the digestive vacuole, as evaluated by the one sample t test generating a P value of 0.08. Example images appear in Figure 2.4 and the resultant data is summarized in Figure 2.8.

Comparison to Endoplasmic Reticulum

The endoplasmic reticulum (ER) was also examined for correlation with the *Pf*DHFR-TS signal. The ER organelle is structured with many folds and invaginations. The ER is involved in protein production and processing, with the nuclearly associated rough ER is dotted with ribosomes all along the surface. ER Tracker Blue-White DPX dye was used to mark the ER. The observed signal correlation for ER and *Pf*DHFR-TS is

variable but has a mean and SEM of -0.073 and 0.067. There was no statistically significant correlation between DHFR-TS and the endoplasmic reticulum, as evaluated by the one sample t test finding a P value of 0.33. Example images appear in Figure 2.5 and the resultant data is summarized in Figure 2.8.

Comparison to Mitochondria via Mitotracker

The mitochondria of the malaria parasite, while not involved in energy production, still seems to be an essential, maintained organelle. As the parasite develops the volume of the mitochondria increase and the organelle branches and buds off into daughter parasites. The branched structure of the mitochondria is evident in microscopy images. The correlation coefficient of the *Pf*DHFR-TS and the mitochondria (via Mitotracker Orange) is the least variable of the organelles examined and has a mean and SEM of 0.211 and 0.038. The correlation between *Pf*DHFR-TS and the mitochondria is the best fit of the individual organelles examined and the only fit with a statistical significance, with a P value of 0.005 from the one sample t test. Example images appear in Figure 2.5 and the resultant data is summarized in Figure 2.8.

With increased focus, additional slides were prepared and dozens more images were generated to pool the results and examine if the signals coalesced or remained variable. Forty images were captured, run through image analysis, and the correlation values for DHFR-TS compared to both the mitochondria and the nucleus pooled. The result of the increase observations was the mean correlation coefficient for DHFR-TS with the nucleus was still insignificant at -0.019 with a SEM of 0.036 while the mean

correlation for DHFR-TS with the mitochondria was 0.236 with a SEM of 0.021. The P value was < 0.0001 for the correlation of DHFR-TS with the Mitotracker signal and was significant based on the one sample t test. The data is summarized in Figure 2.9 A.

We chose to evaluate the life cycle stage and effect on the correlation coefficient of parasites. 3d7 parasites were sorbitol synchronized to ring stages either 24 or 48 hours ahead of when the microscope slides were prepared. When parasites are small and in the ring stages, additional overlap is to be expected based on proximity and the limited spatial resolving power of light microscopy. The fluorescence signals of ring-stage parasites treated with DAPI were compared to DHFR-TS antibody signal and the correlation coefficient was 0.255 with a SEM of 0.099. The DHFR-TS signal was compared to the mitochondria with Mitotracker Orange dye and yielded a correlation coefficient of 0.458 with a SEM of 0.038 with ten parasite images evaluated. With the later stage parasites, the correlation observed for DHFR-TS with the nucleus, via DAPI, was 0.004 with a SEM of 0.044 but the correlation of DHFR-TS with the mitochondria was decently high and significant at 0.247 with a SEM of 0.028 in a total of 27 late stage parasites. A chart summarizing life cycle's influence on the correlation coefficient appears in Figure 2.9 B.

Comparison to Mitochondria via DHODH Antibody

A known mitochondrial protein that we could actively probe with alternate color fluorophores proved to be dihydroorotate dehydrogenase (DHODH). Antibodies from mouse serum were utilized to compare DHODH to DHFR and Mitotracker Deep Red dye

as an example for the correlation values observed between a known mitochondrial protein, DHFR-TS, Mitotracker dye, or another organelle like the nucleus. The parasites were sorbitol synchronized and evaluated in either late trophozoite/schizont or early/ring stages. Several representative parasite images are found in Figure 2.10 and a summary from many observations was compiled into Figure 2.11. For late stage parasites, the mean correlation coefficient and SEM was -0.075 ± 0.043 for DHODH antibody compared to DAPI marking the nucleus, 0.357 ± 0.061 for DHODH antibody compared to DHFR-TS antibody, 0.478 ± 0.054 for DHODH antibody compared to Mitotracker Deep Red, and 0.393 ± 0.059 for DHFR antibody compared to Mitotracker Deep Red marking the mitochondria. For ring stage parasites, the mean correlation coefficient and SEM was -0.092 ± 0.097 for DHODH antibody compared to DAPI marking the nucleus, 0.346 ± 0.076 for DHODH antibody compared to DHFR-TS antibody, 0.273 ± 0.038 for DHODH antibody compared to Mitotracker Deep Red, and 0.250 ± 0.055 for DHFR-TS antibody compared to Mitotracker Deep Red marking the mitochondria.

Comparison to Apicoplast

The apicoplast of the malaria parasite was examined using a published ACP_{leader}-GFP transfection construct [138]. The construct contains a fusion-protein with an apicoplast leader/targeting sequence and a C-terminal GFP. The signal was able to be observed with both native GFP fluorescence and with GFP-targeting Alexa Fluor 488 labelled antibodies. For consistency and to avoid photo-bleaching, GFP primary antibodies with fluorescent Alexa Fluor 488 secondary antibodies were employed for

the correlation coefficient calculations. The correlation observed was variable, from 0.353 to -0.384 with a mean of -0.056. The SEM was high at 0.124. There was no statistically significant correlation between the apicoplast and DHFR-TS, as evaluated by the one sample t test finding a P value of 0.68. Example images appear in Figure 2.6 and the resultant data is summarized in Figure 2.8.

Comparisons were made between ACP-GFP and other organelles (the nucleus and the mitochondria) to serve as controls. The apicoplast is normally adjacent to the mitochondria during the life cycle and the ability to distinguish the apicoplast from mitochondria, as marked by Mitotracker dye, was an important test for the colocalization algorithm's ability to differentiate parasite organelles. The mean Pearson correlation coefficient for the apicoplast with Mitotracker Orange was 0.055 with a SEM of 0.071. Statistically, there is no colocalization as judged by the one sample t test with a P value of 0.46. Example images appear in Figure 2.7 and the resultant data is summarized in Figure 2.8. To further serve as a control for the specificity of the ACP-GFP construct, the colocalization of the nucleus with ACP_{leader}-GFP signal of the apicoplast was also calculated from population of parasites represented in Figure 2.6 and Figure 2.7 and the resultant data is summarized in Figure 2.8. The mean correlation value was -0.033 with a SEM of 0.056. Again, there was no colocalization as judged by the one sample t test with a P value of 0.57.

HProtein-GFP Profiled by Microscopy and Correlation to Mitochondria

An alternate, protein-based marker for the mitochondria was obtained from the Prigge lab. Spalding created Dd2 parasites with an integrated copy of HProtein fused to a C-terminal GFP and published the localization findings [103]. Parasite images, including those in Figure 2.12, were obtained in order to confirm the published localization and to add confidence to future parasite permeabilization studies that would use the HProtein-GFP as a marker for a mitochondrial proteins.

Digitonin Fractionation Supports Localized *Pf*DHFR-TS

An alternate, non-microscopy based method was needed to confirm localization. Selective digitonin fractionation of parasite cell membranes was performed utilizing the HProtein-GFP containing Dd2 parasite lines created by Spadling. The HProtein-GFP parasites were previously reported as having the tagged protein localizing with the mitochondria in live cells [87, 103, 147]. HProtein-GFP was readily detected in Western blots using monoclonal anti-GFP antibody. Anti-*Pf*DHFR-TS and anti-*Pf*aldolase antibodies reacted with the native DHFR-TS and the cytosolic aldolase protein, respectively. The level of HProtein expression seemed to be, tentatively, similar to the DHFR-TS signal if not a bit higher. The blots shown in Figure 2.13 are representative experiments of those performed six times at that concentration gradient. A similar pattern was observed in another eight experiments performed with the gradient of digitonin favoring lower concentrations.

The blots obtained from digitonin permeabilization of HProtein-GFP demonstrated the HProtein-GFP releasing, primarily, between 1.4 – 0.7 mM digitonin.

This indicated that the mitochondrial membranes were sufficiently degraded to release the tagged HProtein into the supernatant of the sample. Those same samples also showed the native *Pf*DHFR-TS was released into the supernatant at concentrations greater than 0.7 mM digitonin. With *Pf*DHFR-TS, the transition was between 1.4 – 0.7 mM. In some experiments heavier-massed secondary reactivity to the *Pf*DHFR-TS antibodies were present in the pelleted fractions. These heavier signals were minimized through fast processing of the lysate and careful ice chilling whenever possible. The *Pf*aldolase bands were observed to taper more gradually between 0.7 to 0.35 and 0.18 mM, depending on the experiment. The *Pf*aldolase's half-maximal signal intensity was safely in the lower tenths of a millimolar amount of digitonin.

Discussion

Determining the localization of malarial DHFR-TS has been long overdue. With no predicted transmembrane domains or localization sequences, the DHFR-TS enzyme has been presumed to be cytosolic for years. The essentiality of DHFR-TS activity in the malaria parasite, the lethality of even partial inhibition, and the low levels of enzyme *in vivo* have all been large barriers to standard biological approaches of studying the native DHFR-TS [40, 148-150]. The generation of antibodies against the malarial DHFR-TS enzyme has been undertaken before with limited success [151]. Newer techniques in antigen prediction and peptide-based affinity isolation led to a new generation of DHFR-TS antibodies with improved performance.

The antibodies generated for *Plasmodium falciparum* DHFR-TS (and *Plasmodium vivax* DHFR-TS) proved very specific and high performing (Figures 2.1 and 2.2). With insufficient washing/blocking or parasite sample degradation, which can happen quickly, the *falciparum* antibody was observed to yield some high-molecular weight background signal whose origins have not been identified. The antibody performed well in specificity tests and proved useful for probing fixed, permeabilized cells for localization studies.

Organelle Comparison Indicates Mitochondrial Localization

With antibodies to DHFR-TS performing well, we compared the localized signals with major parasite organelles including the mitochondria, apicoplast, digestive vacuole, endoplasmic reticulum, and the nucleus. The images from the confocal microscope were thresholded to focus on the high-intensity signals and a computer algorithm employed to assess colocalization and reduce bias in analyzing the weak DHFR-TS signal. The highest Pearson correlation coefficient obtained for DHFR-TS antibody with an organelle was 0.24 with Mitotracker dye as averaged over a large population of mixed stage parasites (Figures 2.8 and 2.9 A). The fixation and permeabilization method employed favors late-stage parasites surviving to deposition on the slide. The bias towards late stages may be a factor influencing how asynchronous parasite cultures over many experiments gave a Mitotracker to DHFR-TS correlation of 0.24 but, when separated out by stage of the life cycle, the correlation was as high as 0.46 in ring stages but only 0.25 in later stage parasites (Figure 2.9 B). Comparison of DHFR-TS signal to the

mitochondria-adjacent apicoplast was investigated to add certainty to our mitochondrial characterization. We employed an established ACP_{leader}-GFP transfected D10 strain for studies with an apicoplast marker [138]. To help establish the functional range of mitochondrial protein Pearson correlation values, as measured by this confocal microscopy-based method and technique, DHODH antibody was added as a comparator to Mitotracker dye and DHFR-TS antibody in 3d7 parasites. The observed correlations for DHODH and DHFR had a mean value between 0.35 to 0.36, independent of the life cycle stage. When compared to Mitotracker dye, both proteins displayed correlations above 0.39 when in the late stage parasites, but the correlation values were lower, at 0.25, for ring stage parasites (Figure 2.11). When the standard error of the mean is taken into account, these values are nearly identical for each stage of the life cycle, further supporting of our successful measurement of *Plasmodium falciparum* DHFR-TS as a mitochondrial protein.

Digitonin Fractionation Indicates Mitochondrial Localization

An orthogonal, non-microscopy-based method to investigate localization was used to evaluate localization of DHFR-TS enzyme in the malaria parasite. Digitonin permeabilization has been used with malaria parasites and other cells based on the cholesterol content of organelle membranes differing from that of plasma membranes. A profile of the cytosolic vs organellar contents was obtained through measuring the proteins released into supernatants with differing concentrations of digitonin. The Western blot detection method employed does not permit perfect delineation of which

organelle is ruptured, but does reinforce observations of cytosolic vs organellar localization. Our comparisons using HProtein-GFP containing Dd2 parasites show that the mitochondria is ruptured at digitonin concentrations between 1.4 and 0.7 mM, while cytosolic contents release at significantly lower concentrations of digitonin, with a more gradual transition that could be due to stochastic factors or parasite life cycle stage diversity (Figure 2.13). From these experiments we observed digitonin permeabilization releasing the cytosolic proteins at concentrations approximately five times lower than where the mitochondrial protein was being released into the supernatant and DHFR-TS was releasing in the same range of digitonin concentrations as the mitochondrial HProtein-GFP.

Summary

We developed antibodies that mark the malaria DHFR-TS enzyme and applied them to demonstrate that the DHFR-TS enzyme has a sub-cellular localization in the malaria parasite. With the help of algorithmic colocalization calculations, organelle specific dyes, and both tagged and native proteins, we determined the mitochondria to be the target organelle of DHFR-TS. Further supporting the localization of DHFR-TS, we employed cell fractionation via digitonin and demonstrated localization akin to that of a previously published mitochondrial protein from the glycine cleavage system, HProtein [103].

Chapter 2 Figures

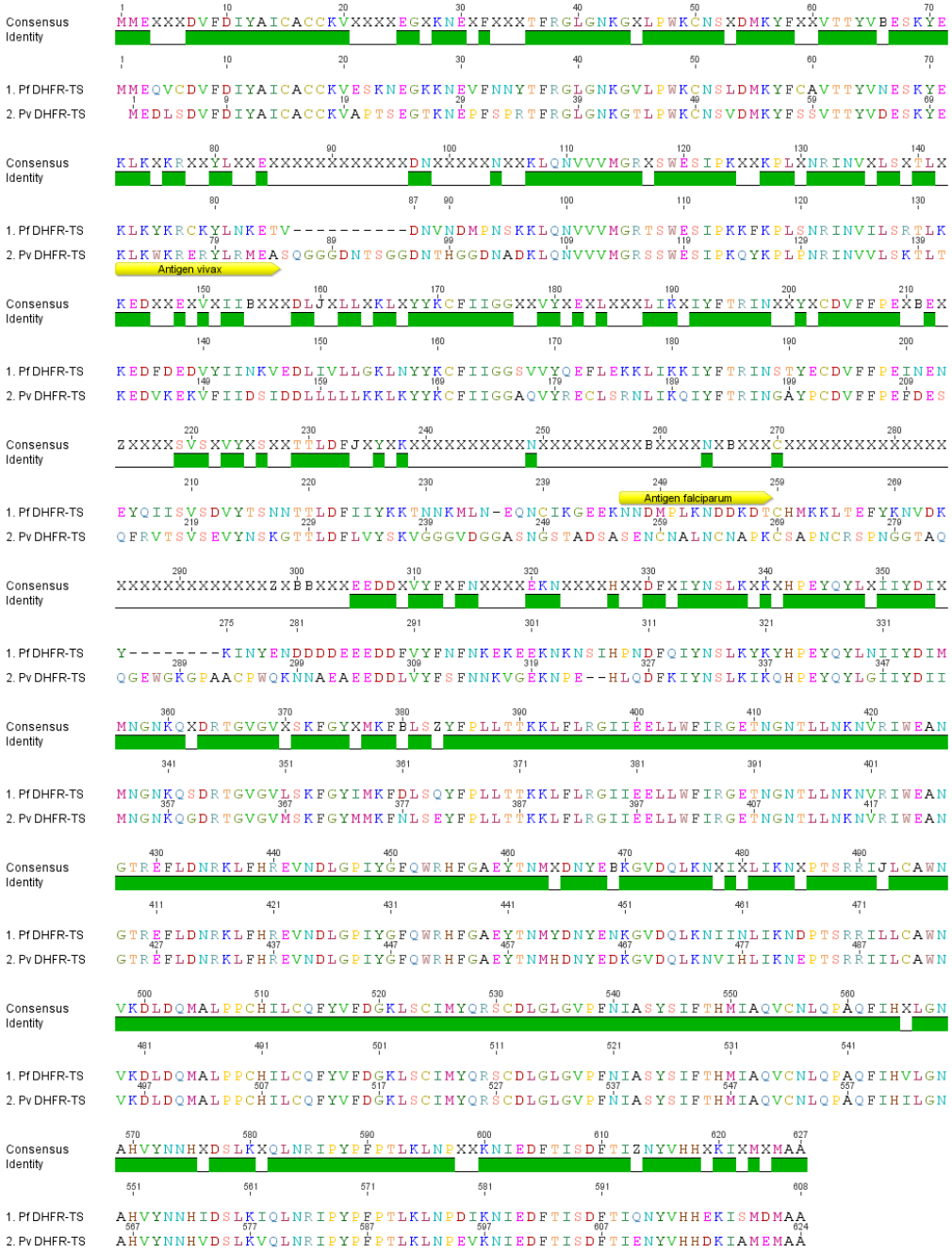

Figure 2.1 - Comparison of DHFR-TS Protein Sequences of *Plasmodium falciparum* and *Plasmodium vivax*

The DHFR domain is within the N-terminal ~220 amino acids, the TS domain comprises the C-terminal ~300 amino acids. Consensus sequences and conserved identity is indicated via the green highlights. The peptides used for antibody production and affinity purification are indicated by the yellow bars. The *P. falciparum* antigen was within the joining region between the two enzymes and the *vivax* antigen was in the DHFR region.

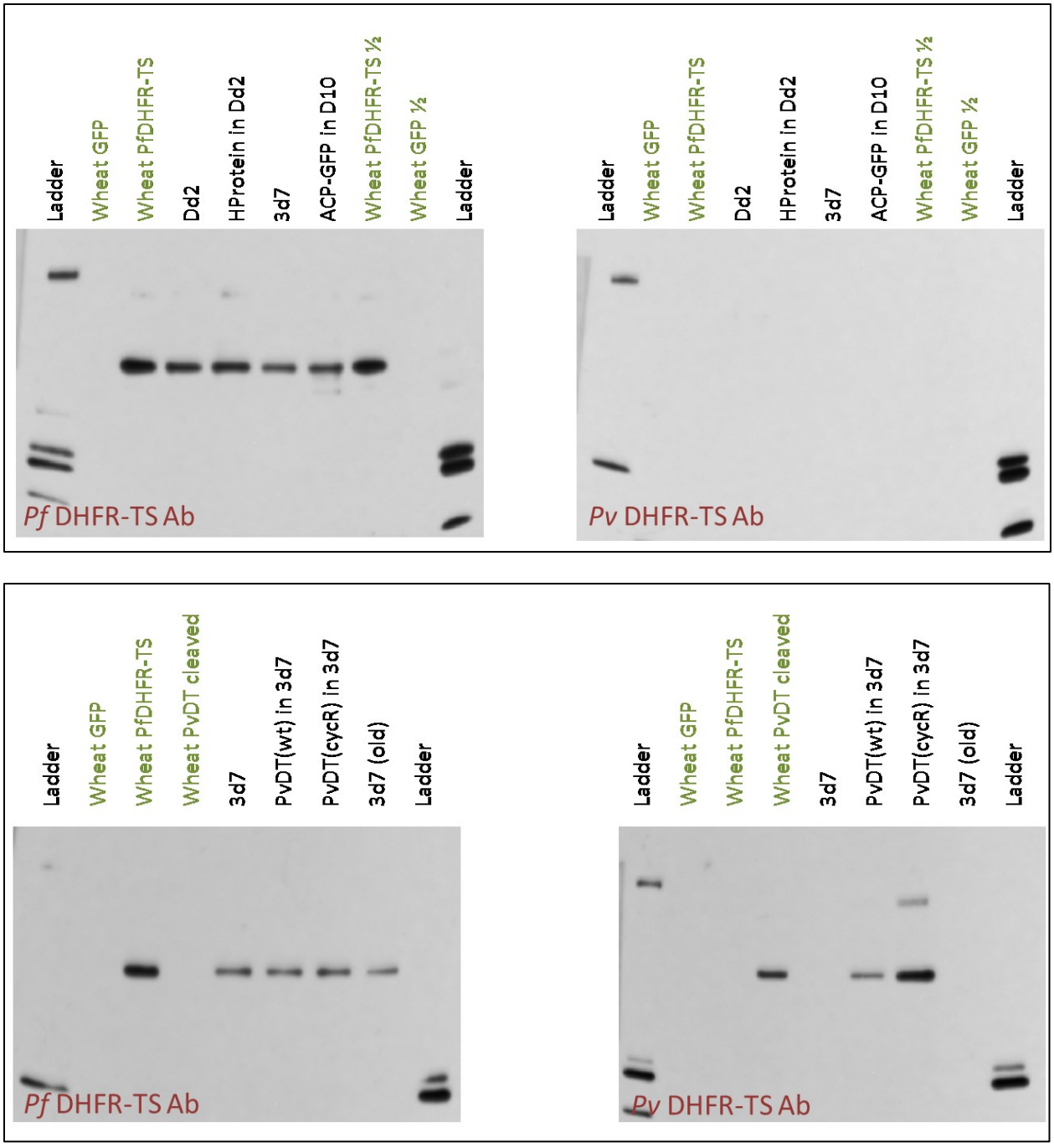

Figure 2.2 – Specificity of the Plasmodium DHFR-TS Antibodies

In figures A) and B) Western blots were performed with the antibodies to *Pf* and *Pv* DHFR-TS. Comparisons are drawn to recombinant protein produced in wheat germ, which serve as controls (lanes labelled in green). Additional parasite lines utilized for localization comparisons were also probed and antibody reactivity confirmed (labels in black). Figure B) contains transfected parasite lines more thoroughly examined in Chapter 3 as cycloguanil rescue constructs.

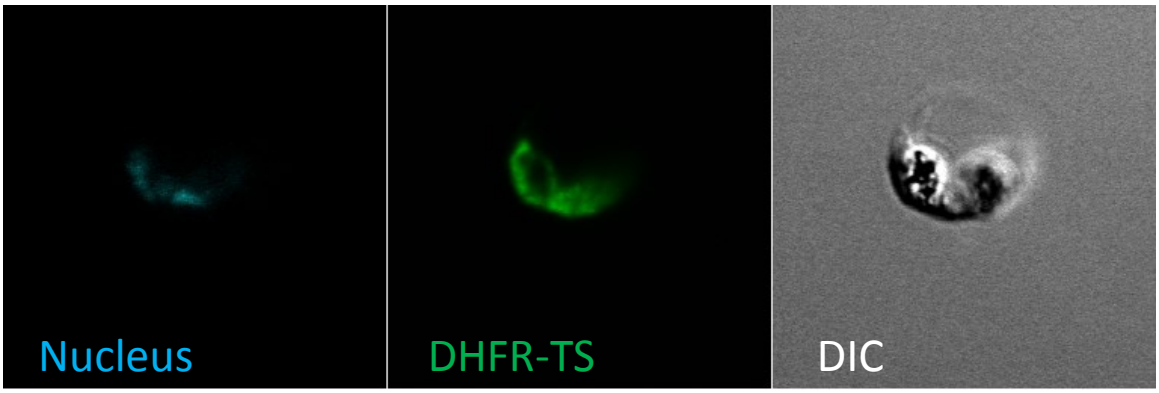

Figure 2.3 – Early Observations of DHFR Localization

Localized green signal not evenly distributed in the parasite were observed during early experiments using 3d7 parasites and antibodies to *Plasmodium falciparum* DHFR-TS enzyme. The single layer of the parasite shown above illustrates the typical appearance of DHFR-TS antibody signal, with some background in the parasite but distinct tubule-like appearance to DHFR-TS and spots of high signal intensity. The nucleus, as marked by Hoechst 33342 in teal, is shown to help establish that these are two early trophozoite stage parasites.

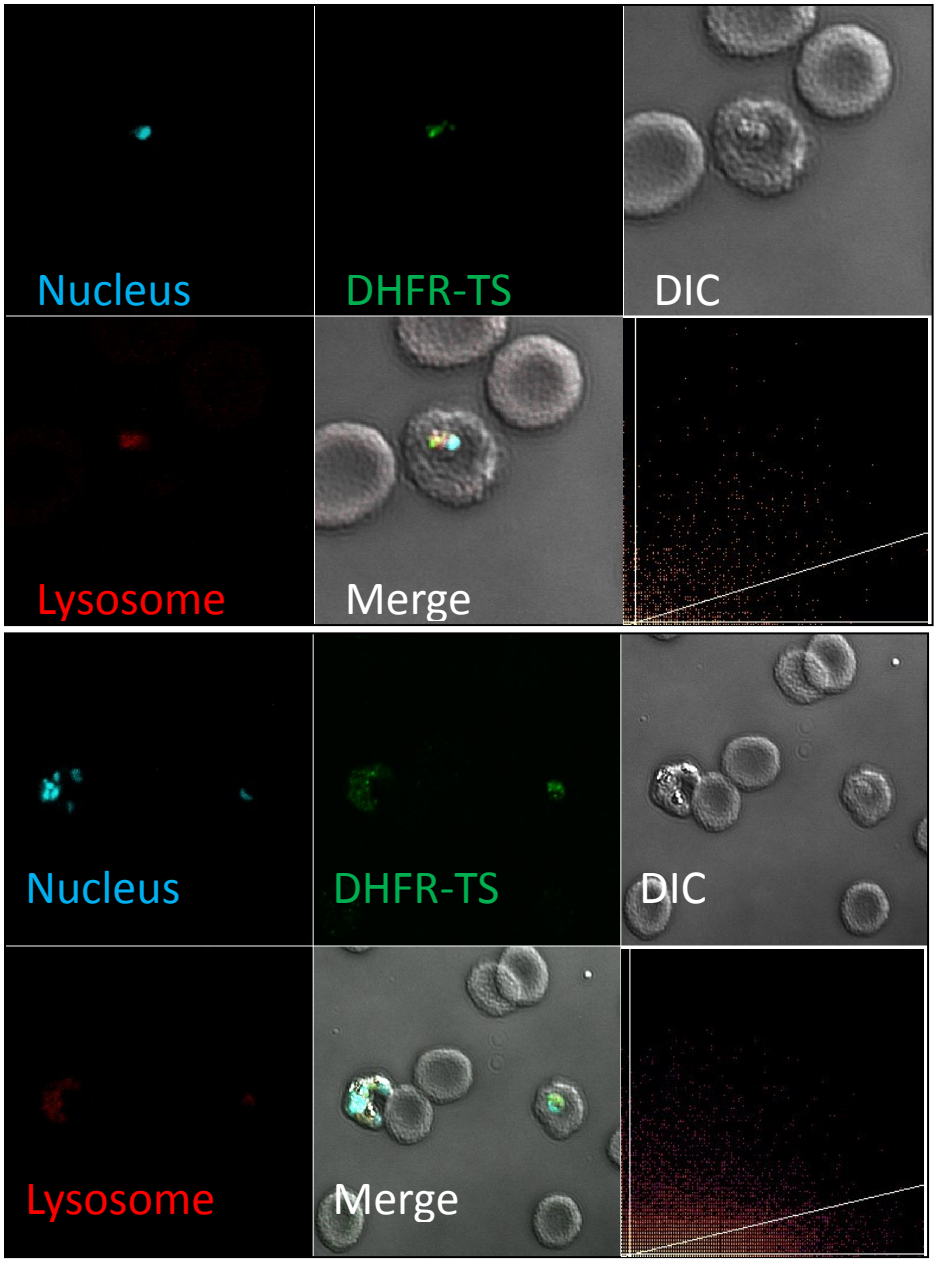

Figure 2.4 – Comparison of DHFR-TS to Nucleus and Digestive Vacuole

Confocal microscopy images were obtained of 3d7 parasites treated for a half hour with Lysotracker dye, fixed, permeabilized, and probed with DAPI and antibodies to *Pf*DHFR-TS followed by a secondary Alexa Fluor 488 antibody. DAPI (teal) indicates the nucleus, Lysotracker Red indicates the digestive vacuole, primarily, and the *Pf*DHFR-TS antibody is shown in green. The DIC image is similar to that of a simple light microscope, but allows for better capture at a set focal plane. The histogram in the lower right corner is a scatter plot of the colocalized pixels with respect to the green and red channels. In these experiments, the signal for DHFR-TS did not overlap with either the nucleus or the digestive vacuole with any statistically significant result.

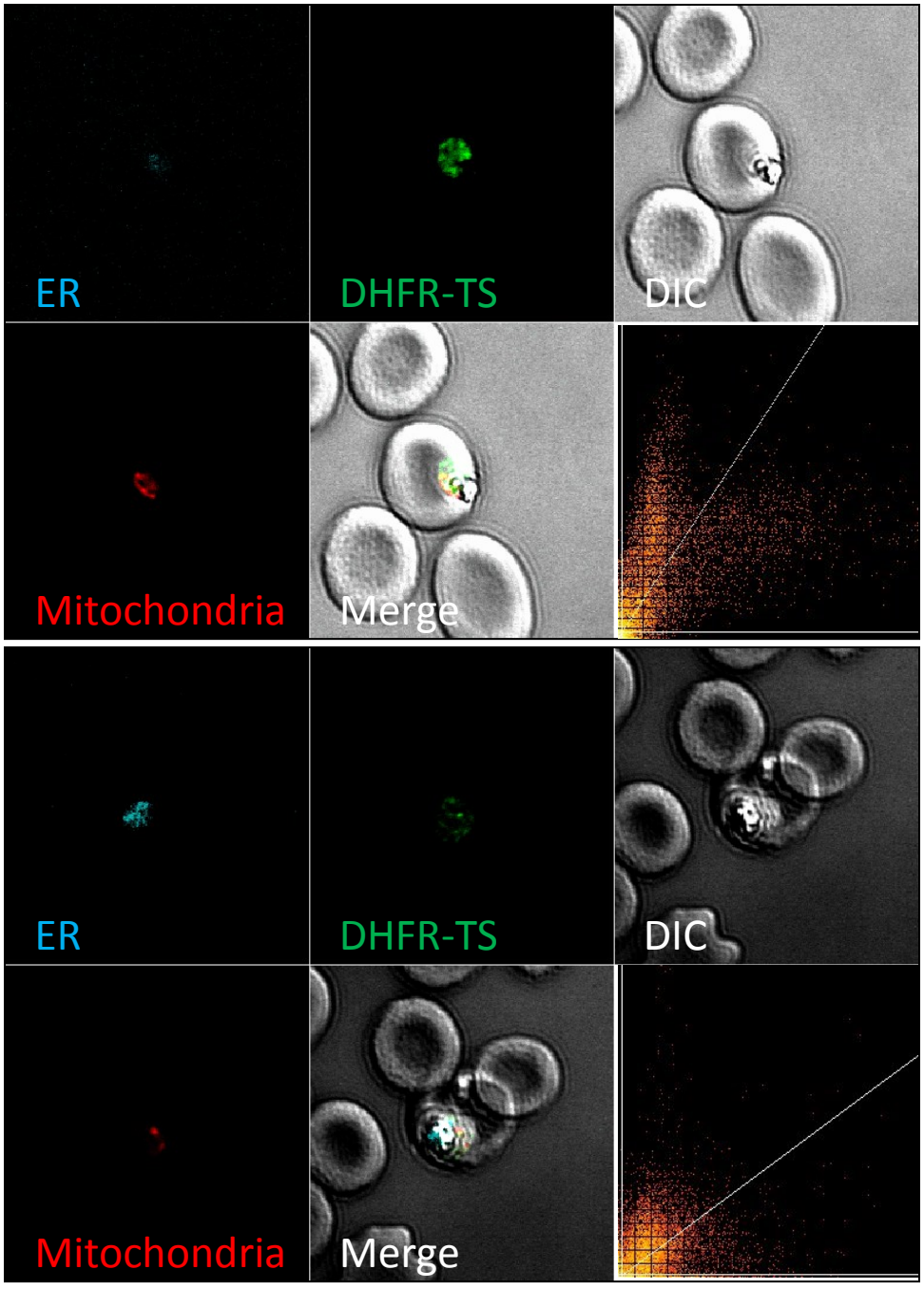

Figure 2.5 – Comparison of DHFR-TS to Mitochondria and Endoplasmic Reticulum

The above images depict 3d7 parasites treated for a half hour with Mitotracker Orange and ER Tracker Blue-White dye, fixed, permeabilized, and probed with antibodies to *Pf*DHFR-TS followed by a secondary Alexa Fluor 488 antibody. ER Tracker (teal) indicates the ER (closely associated with the nucleus), Mitotracker Orange indicates the mitochondrion, and the *Pf*DHFR-TS antibody is in green. The lower, right hand scatter plot is of the colocalized pixel signal intensity from the green and red channels. This set of experiments established DHFR-TS signal was not colocalized with the ER but was colocalized with the mitochondrion in a statistically significant way.

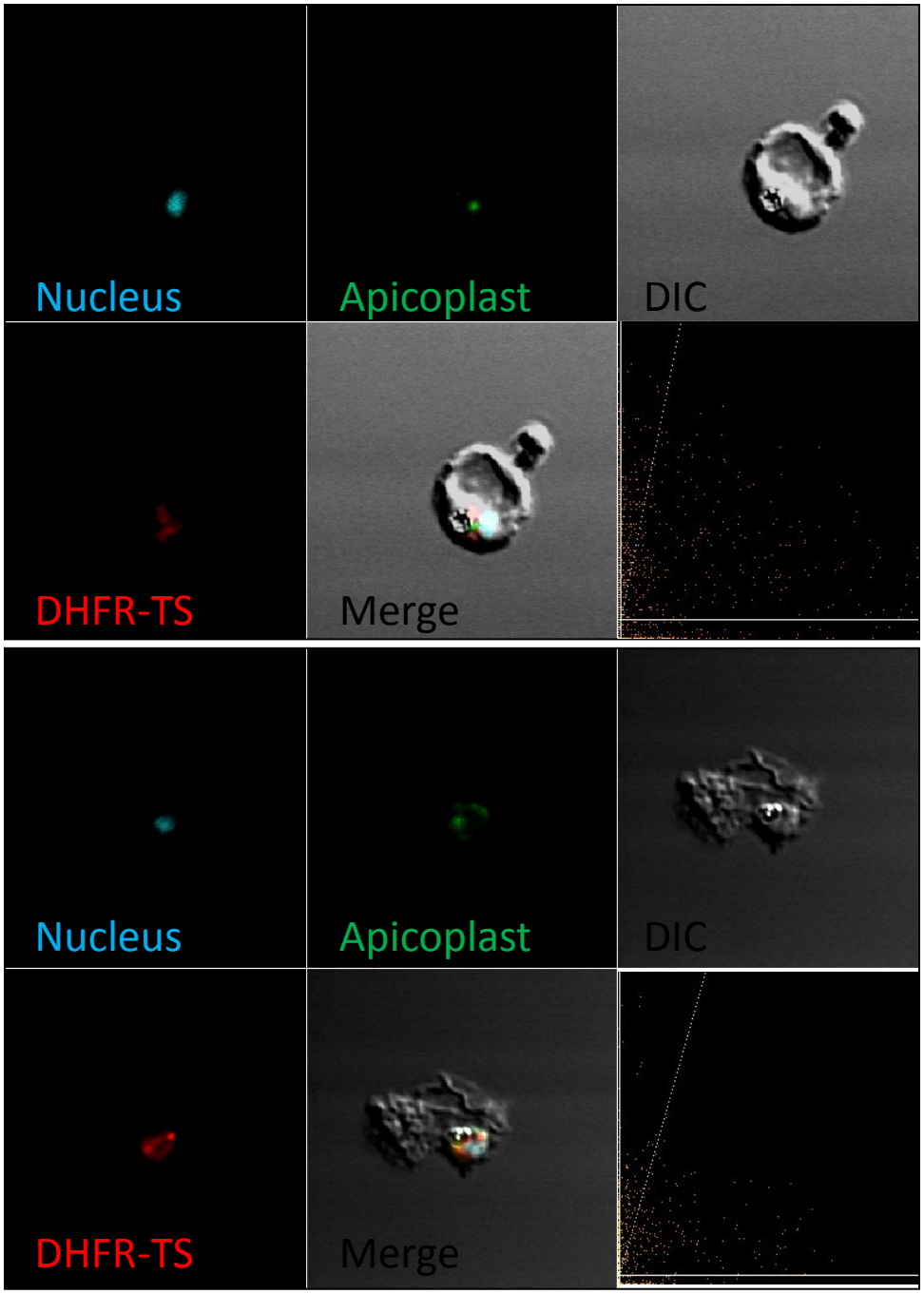

Figure 2.6 – Comparison of DHFR-TS to Nucleus and Apicoplast

Confocal microscopy images were obtained for D10 parasites containing an ACP-GFP protein which were fixed, permeabilized, and probed with antibodies to *Pf*DHFR-TS and GFP followed by secondary Alexa Fluor 488 and 532 antibodies. DAPI (teal) indicates the nucleus, the green GFP antibody signal indicates the apicoplast, and the *Pf*DHFR-TS antibody is shown in red. The histogram in the lower right corner is a scatter plot of the colocalized pixels with respect to the green and red channels. The apicoplast and DHFR-TS signals were near, but not colocalized with any statistical significance.

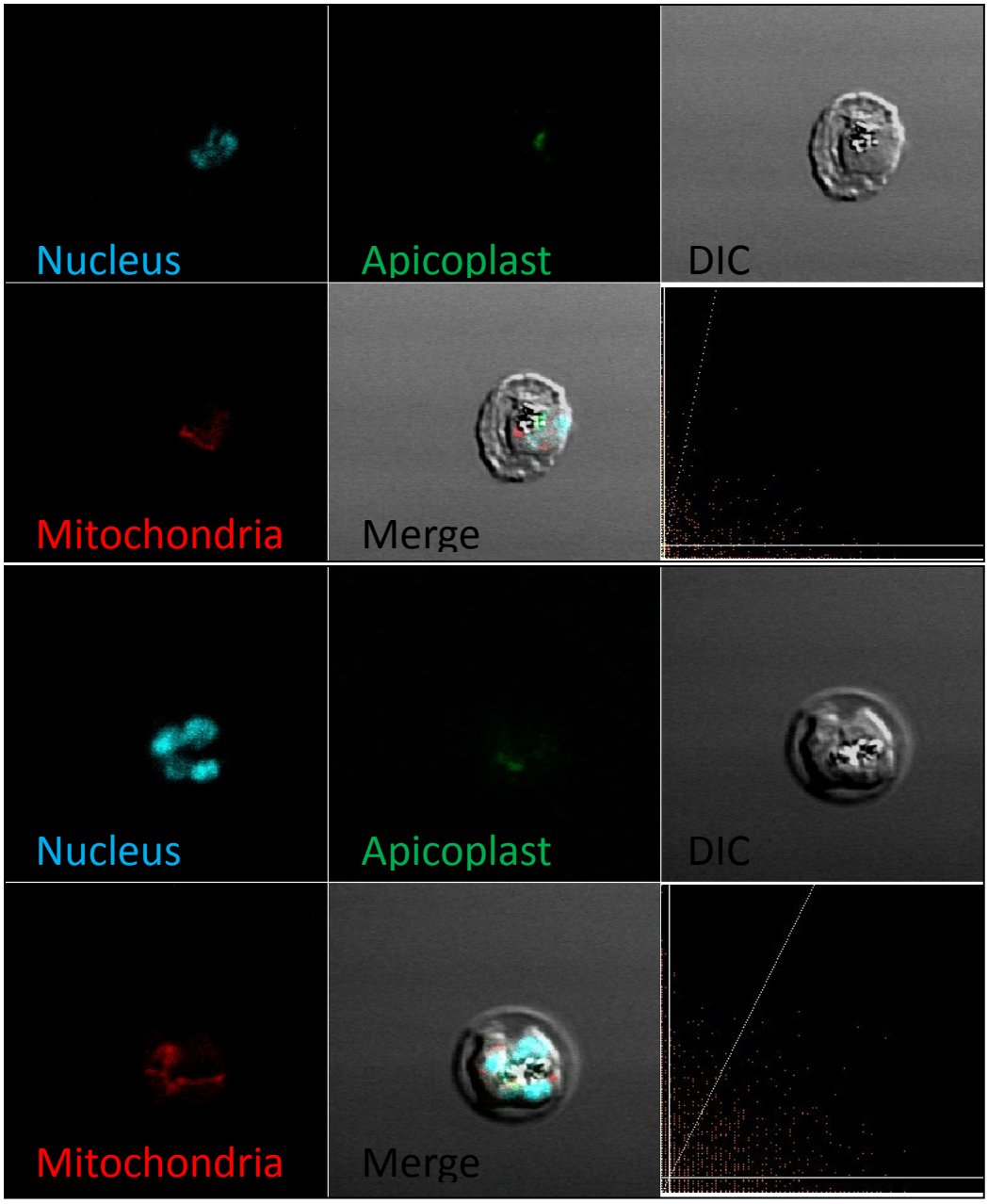

Figure 2.7 – The Apicoplast is Clearly Distinguished from the Mitochondria

Immunofluorescence microscopy was performed to establish the method's ability to distinguish apicoplastic signals from the mitochondrion. Confocal microscopy images were obtained for D10 parasites, containing an ACP_{leader}-GFP protein, which were treated with Mitotracker Orange, fixed, permeabilized, and probed with an antibody to GFP followed by secondary Alexa Fluor 488. DAPI (teal) indicates the nucleus, the green GFP antibody signal indicates the apicoplast, and the Mitotracker dye is shown in red. The histogram in the lower right corner is a scatter plot of the colocalized pixels with respect to the green and red channels.

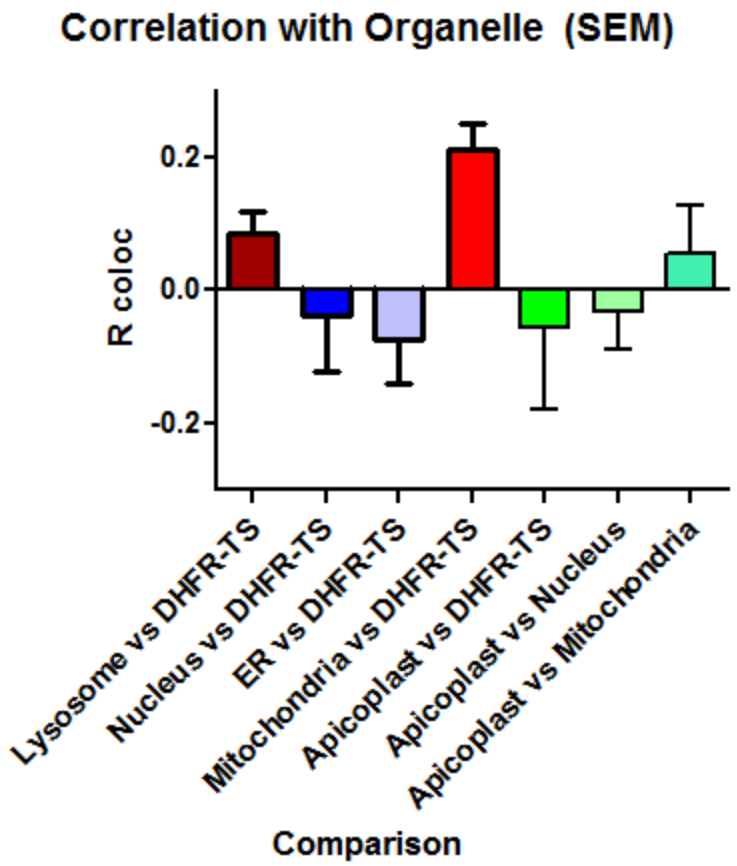

Figure 2.8 – Summary of Organelles Investigated for DHFR-TS Localization and Fit to Mitochondria

A localization survey was performed using dyes to different organelles. Colocalization of the organelle to the *Pf*DHFR-TS antibody signal was calculated using stringent thresholds and Pearson correlation coefficient methodology. The mean and standard error of the mean was calculated from at least ten images for each condition and plotted to guide further inquiry. The only correlation that registered as significant was that of DHFR-TS with the Mitochondria, with a one-sample t test P value of 0.005 in the broad survey.

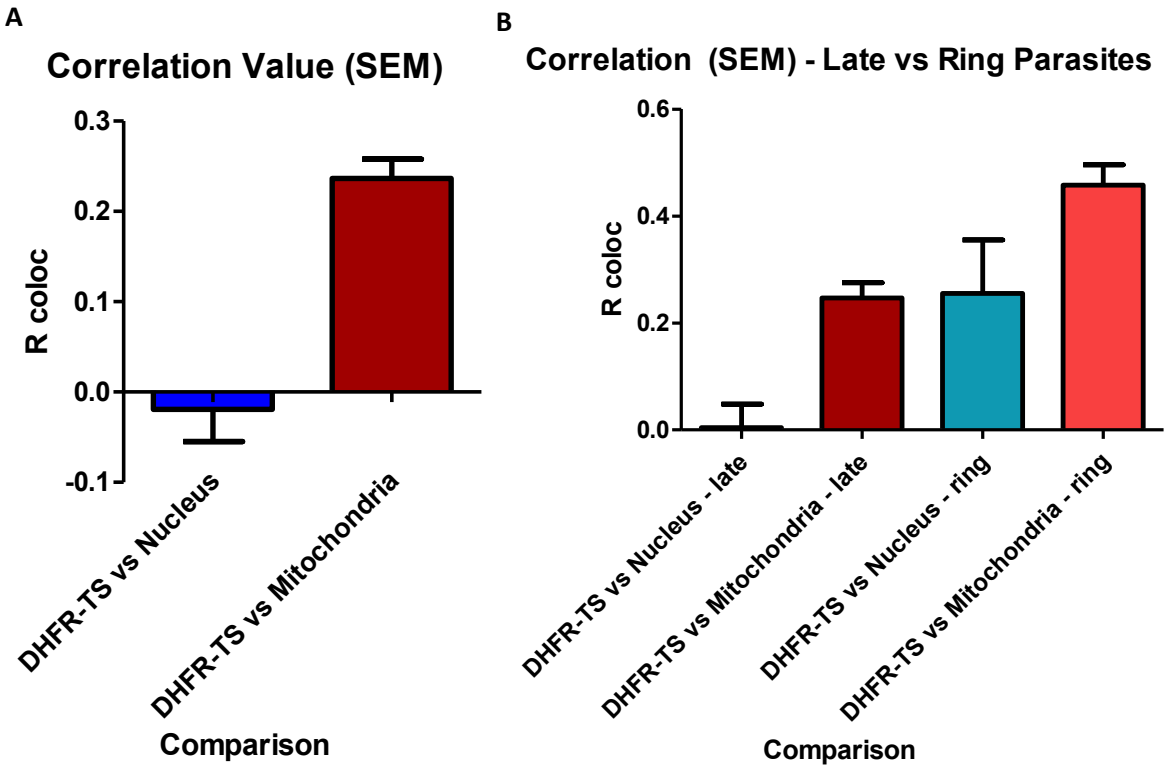

Figure 2.9 – Increased Focus of Localization, Life Cycle Stage Influences Quantification of Localization of DHFR-TS Signal

a) After a total of forty images analyzed, the *Pf*DHFR-TS antibody , when compared to Mitotracker Orange signal, coalesced at a positive value while poorly overlapping signals like *Pf*DHFR-TS compared to the nucleus coalesced closer to zero/no correlation. With the increased observations, the one-sample t test again found DHFR-TS and mitochondrial signals significant, with a P value of < 0.0001.

b) Late and early (ring) stage parasites were examined to observe any systematic bias for correlations observed based on life cycle stage. Thirteen ring-stage parasites and twenty seven late stage parasites had their full image collected, the correlation coefficients calculated, and the data binned to determine if parasite size/life cycle stage contributed to the observed correlation. The *Pf*DHFR-TS vs Mitochondria comparisons had reduced SEM ranges of approximately half the corresponding *Pf*DHFR-TS vs Nucleus comparison, indicating an ongoing lack of correlation with the nucleus and a more consistent correlation with the mitochondria.

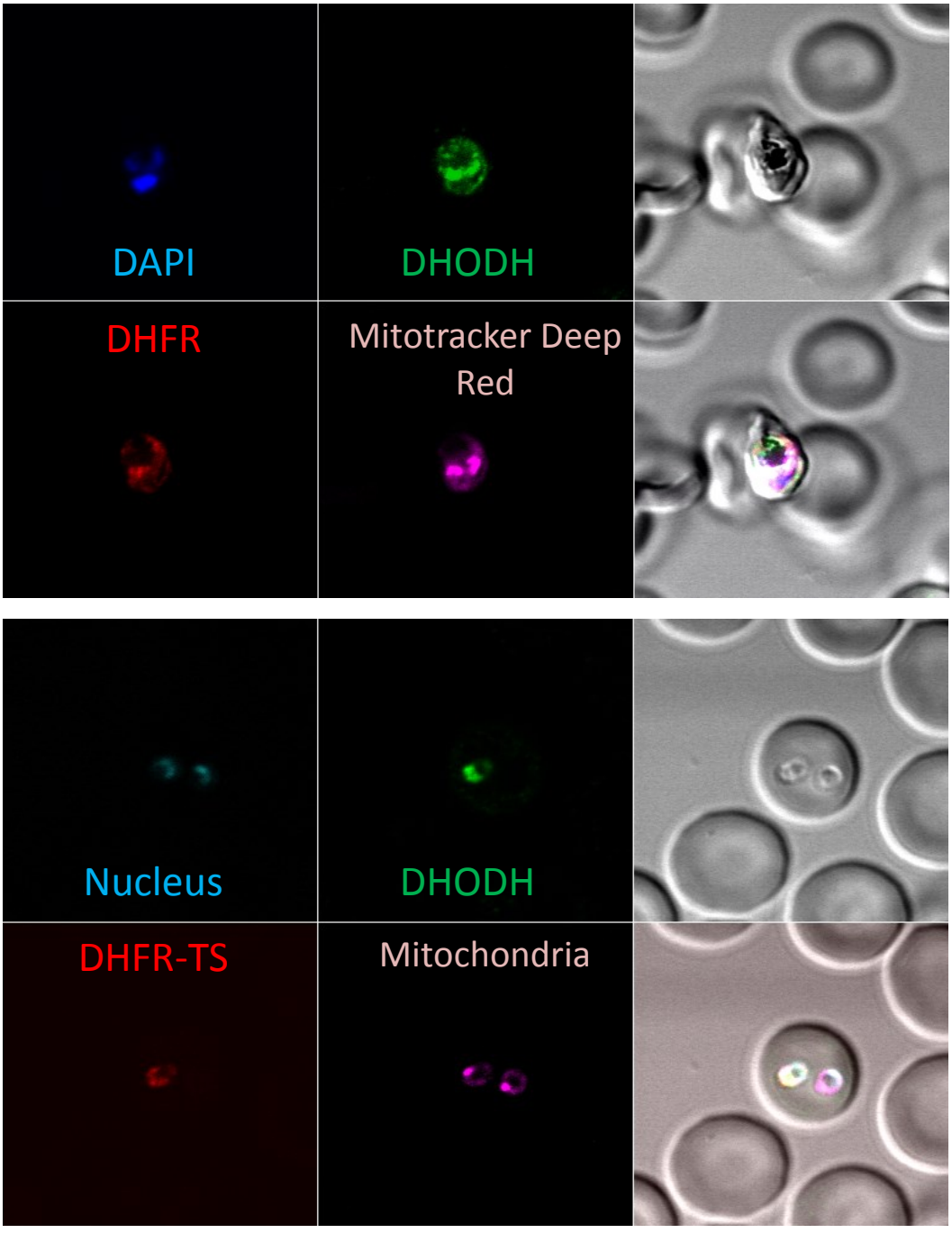

Figure 2.10 – Images of *Pf*DHODH antibody compared to *Pf*DHFR and Mitotracker Dye

Confocal microscopy images were obtained for 3d7 parasites that were treated with Mitotracker Deep Red for 30 minutes, fixed, permeabilized, and probed with antibodies to *Pf*DHFR-TS and DHODH followed by secondary Alexa Fluor 488 and 532 antibodies. DAPI treatment was added immediately before mounting. DAPI (teal) indicates the nucleus, Mitotracker Deep Red indicates the mitochondria, the green signal indicates the mitochondrial DHODH signal, and the *Pf*DHFR-TS antibody is shown in red.

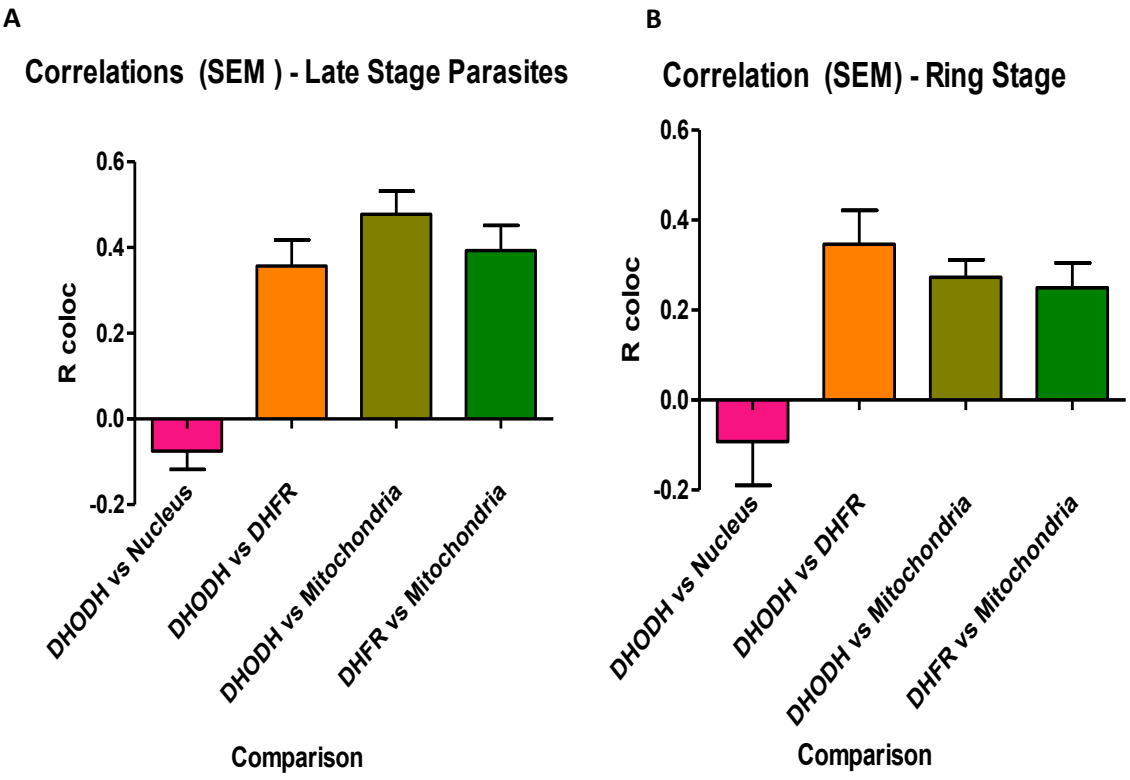

Figure 2.11 – Summary of Comparison of Mitochondrial DHODH to DHFR-TS Signal

3d7 parasites synchronized 24 or 48 hours prior were subjected to staining with DAPI (for the nucleus), *Pf*DHODH antibody (a known mitochondrial protein), *Pf*DHFR-TS antibody, and the mitochondrial dye Mitotracker Deep Red. The graphs above represent the data from a representative experiment and the analysis of A) eleven late-stage parasites and B) nine ring-stage parasites.

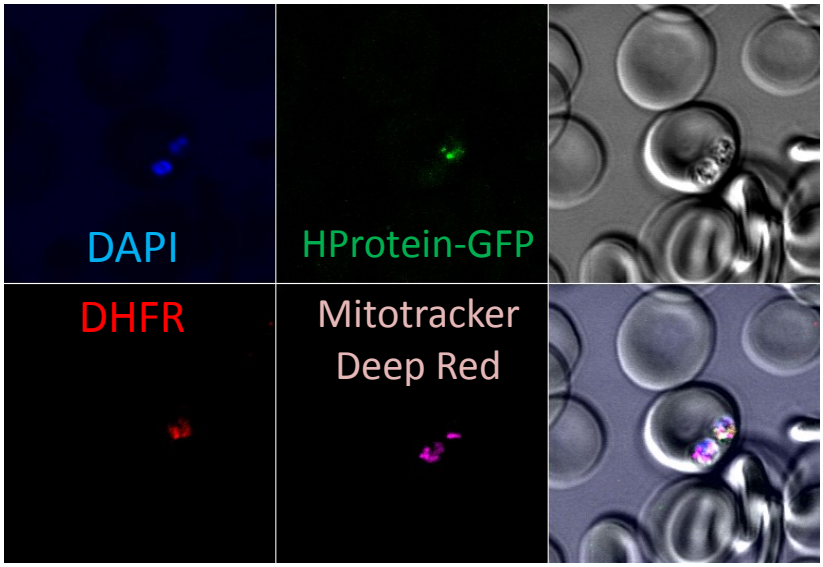

Figure 2.12 – HProtein-GFP Dd2 Parasite Line Also Marks Mitochondria

Images were captured of Dd2 parasites containing a chromosomally-integrated copy of the HProtein-GFP fusion. HProtein-GFP was thus able to serve as a mitochondrial marker. The mitochondrial marker Mitotracker Deep Red excelled at marking the parasite mitochondria, particularly in relation to the HProtein-GFP as marked by GFP antibody. DAPI was used to mark the nucleus and *Pf*DHFR-TS antibody was also reactive in the Dd2 parasite line similar to the 3d7 line which comprised the bulk of the microscopic images captured earlier.

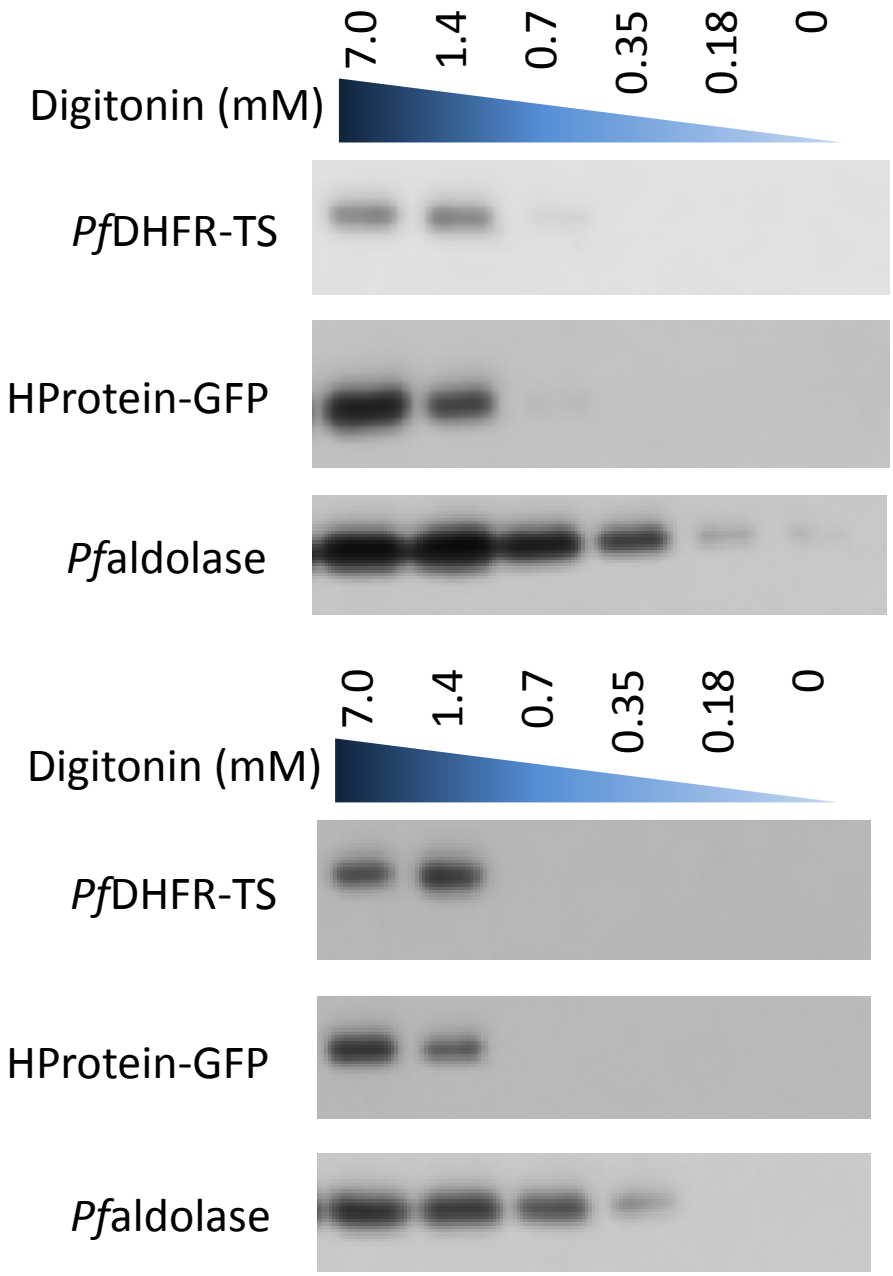

Figure 2.13 – Digitonin Permeabilization Indicates Organellar Localization of DHFR-TS

Digitonin permeabilization and Western blots of the supernatants were utilized to illustrate localization and discriminate cytosolic proteins from those contained in organelles less susceptible to digitonin. The commercial *Pf*aldolase antibody served as a marker for a strongly expressed, cytosolic protein. GFP antibody was used to mark the mitochondrial HProtein-GFP fusion. *Pf*DHFR-TS antibody was used to mark the malarial DHFR-TS enzyme, now determined to be mitochondrial. A total of fifteen experiments profiling the release were performed and the above images are representative.

Chapter 3 - A Role of Cycloguanil in the Synergy Between Atovaquone and Proguanil?

Introduction

Upon observing that *Plasmodium falciparum* dihydrofolate reductase-thymidylate synthase (DHFR-TS) was localized in the parasite, many questions related to its use as a drug target remained. In particular, two drugs considered sub-optimal as single agents have been combined to create Malarone®. Malarone® is presently a front-line drug for the prophylaxis and treatment of malaria, comprising the bulk of antimalarial drugs sold in the US in 2009 [125]. Just how the proguanil and atovaquone components of Malarone® work so effectively together is something that has been speculated upon but no mechanism has been demonstrated.

When the drug combination was proposed, the efficacy in patients was thought to arise from proguanil being converted to cycloguanil. Cycloguanil would then inhibit the folate cycle enzyme DHFR. Atovaquone contributed to the synergy by inhibiting pyrimidine biosynthesis, indirectly, through DHODH. Atovaquone would inhibit complex III of the electron transport chain and block coenzyme Q recycling. Coenzyme Q is a necessary substrate for malarial DHODH's catalytic function. Curiously, *in vitro* culture systems, which are devoid of liver-based cytochrome P450s responsible for converting proguanil to cycloguanil, also display a synergy between proguanil and atovaquone. Rather than implicate some alternate target for proguanil, we formulated a different

idea: that DHFR's inhibition by cycloguanil and atovaquone's blockade of the electron transport chain were behind the mechanism of synergy.

In order to assess the role of DHFR inhibition by cycloguanil, we drew from the many parasite isolates both from the field and the decades of researching DHFR. We would use drug sensitivity amongst these strains with known resistance-conferring point mutations to determine if DHFR drug susceptibility influences susceptibility to Malarone® and other related inhibitors. Additional parasite strains that would afford unique resistance methods to Malarone®-components or related drugs were obtained to dissect which components are involved in the synergistic method of action of Malarone®. We transfected a cycloguanil resistant form of *Plasmodium vivax* DHFR-TS into *falciparum* parasites to directly assess cycloguanil-based inhibition of DHFR with minimal uncontrolled changes to the parasite.

To further assess if cycloguanil was a contributor to Malarone®'s mechanism of action, a direct assay was developed to extract the organic components from flasks of growing parasites. The assay was tuned to capture, via analytical UPLC-MS/MS instrumentation, even trace cycloguanil conversion.

Experimental Procedures

Materials

Synthesis of Cycloguanil, 2-Chlorocycloguanil

Cycloguanil and a cycloguanil-analogue with an additional chlorine atom in the *ortho* position of the aniline were synthesized for use in subsequent experiments. The synthesis of both compounds on a 10 millimole scale was accomplished by refluxing 4-chloro-aniline or 2,4-dichloro-aniline with dicyandiamide, acetone, and hydrochloric acid (reaction scheme in Figure 3.1) [152, 153]. The resulting cycloguanil and 2-chloro-cycloguanil were found free of impurities by NMR, MS (ESI), and HPLC. The internal standard 2-chloro-cycloguanil and proguanil stocks were run through the HPLC-MS/MS protocol at 1 and 10 µM (10 µM being five times higher than the proguanil measured in any sample) to verify that no cycloguanil impurities were present.

Creation of Cycloguanil Resistant Parasites via Rescue Plasmid

In order to assess the role of cycloguanil in the mechanism of action of Malarone®, we engineered parasites that expressed a cycloguanil-resistant form of DHFR-TS from *Plasmodium vivax*. Three transfection plasmid variants were created in order to have adequate controls for genetic complementation experiments. Two variants expressed *Plasmodium vivax* DHFR-TS of either the wild type or cycloguanil resistant form. An intermediate plasmid construct, without the *vivax* DHFR-TS gene inserted, was used as a control (referred to as the "blank" plasmid). O'Neil described a *Plasmodium vivax* DHFR-TS transfection construct that conferred 1,700 fold cycloguanil

resistance to transfected *falciparum* parasites [154]. However, the construct he utilized involved a N-terminal bsd gene in frame with the DHFR-TS, a type of modification our lab has found not well tolerated by the DHFR enzyme in *Plasmodium falciparum* and has the potential to disrupt the commonly N-terminal localization signals for mitochondrial localization. We desired to create a plasmid as close to native sequence and expression levels as possible without the added time and selection issues related to chromosomal integration. The pRZ-TK-BSD2 transfection plasmid was our starting point because it contained a Blasticidin resistance expression cassette opposing another expression cassette [155]. Blasticidin selection is based on the ribosome, in contrast to antifolate-based selection used by most malaria transfection. The plasmid was modified to incorporate the *falciparum* DHFR-TS 5' UTR/promoter, the *vivax* form of DHFR-TS (wild type as well as the cycloguanil resistant form), and a rep20 element to aid in episome segregation. Figure 3.2 includes the overview of the plasmid construction.

The plasmid pRZ-TK-BSD2 was modified to remove both the thymidine kinase (TK) gene as well as the 5' calmodulin (CAM) promoter sequence. In its place was inserted an adapter sequence containing the *BlpI* restriction site, a 50 bp spacer, the *SpeI* and *NotI* restriction sites, and then the *XhoI* restriction site. To add back the physiologically relevant promoter, 830 bp of the *Pf*DHFR-TS 5' UTR was amplified and modified from 3d7 parasite genomic DNA using primers that also add *BlpI* and *SpeI* restriction sites (PfDHFR_5UTR_F_Lng GGC CGG GCT AAG CAC TTT CCT TGT AAA TGT CAT TCT TTA TAT TAA GAA GAA C and PfDHFR_5UTR_r2_Lng GGC TGG CTC GAG CGG

CCG CAC TAG TAA AAA GGA GAA AAT ATA AAT ATA TAA ATA AAT AAA). The 5'UTR was inserted into a pGEM-T Easy vector for sequencing before being excised via double restriction digest and inserted into the digested, adapter-containing pRZ-BSD +Adapter plasmid, replacing the 50 bp spacer.

The cycloguanil-resistant *Plasmodium vivax* DHFR-TS gene was based on the AMRU-1 strain referenced by O'Neil as GenBank Accession DQ244115 [45, 154, 156]. The resistant DHFR sequence was overlaid on the full length *Plasmodium vivax* DHFR-TS gene from Sal-1 strain (GenBank Accession XM_001615032 and PlasmoDB ID PVX_089950) and the indicated point mutations added to the Sal-1 sequence (Figure 3.3). The wild type Sal-1 DHFR-TS gene and cycloguanil resistant (cycR) AMRU-1 DHFR-TS gene with four point mutations were obtained in native codons from GenScript with a *SpeI* restriction site at the 5' end and *XhoI* at the 3' end (Figure 3.4). The genes were excised from Genscript's plasmid using the *SpeI* and *XhoI* restriction enzymes and inserted into a similarly digested pRZ-BSD +Adapter +PfUTR backbone to make a functional transfection plasmid.

A 550 bp section of rep20 sequence was amplified from pHHyDHOD–GFP plasmid obtained from the Vaidya lab, which itself was derived from the reduced rep20 element-containing pHHMC*/3R0.5 plasmid published by O'Donnel[52, 157]. The amplification was performed using the primers Rep20_3RS_F and Rep20_3RS_r containing the *HindIII* and *SalI* restriction sequences as well as auxiliary *EcoRI* and *BlpI* sequences. The *HindIII* and *SalI* sites were used to insert the rep20 sequence at the 3'

end the expression cassette following the *Plasmodium vivax* DHFR-TS gene while the backup *EcoRI* and *BlpI* sites would allow for insertion at the end of the Blasticidin resistance gene expression cassette or between the opposing expression cassettes if needed. The sequence of primer Rep20_3RS_F is GGA CCG AAT TCG CTA AGC AAG CTT CTA TAT TTG TTA AAT TAA GAC CAA ACT TAG TAC C and the sequence of primer Rep20_3RS_r is GGA CCG AAT TCG CTT AGC GTC GAC TAC TTT CAC TAA TAT AGG TCC TAT CAT AAC TAA C with the *HindIII* and *SalI* sites underlined, respectively. Following PCR, the rep20 element was agarose gel purified and then ligated into a pGEM-T Easy vector for plasmid production purposes.

The pRZ-BSD *Plasmodium vivax* DHFR-TS transfection plasmids were further enhanced by incorporation of the rep20 element following the *Pv*DHFR-TS expression cassette. Digestion of the target pRZ plasmid and pGEM-T Easy with the rep20 element with both the *HindIII* and *SalI* restriction enzymes was sufficient to linearize both template and insert. The rep20 element was gel purified, ligated into the digested pRZ template, and the resulting plasmid (Figure 3.2 C) was produced, sequenced, and then further transfected into 3d7 parasites per established "preloaded erythrocyte" protocols.

Methods

Parasite Transfection Using Preloaded Erythrocytes

Parasite transfection was accomplished using a method where erythrocytes were electroporated to load them with plasmid DNA and the malaria parasites were allowed

to invade the pre-loaded red blood cells and spontaneously uptake the plasmid. The protocol is based on the low current, high capacitance method published by Fidock and adapted to preload erythrocytes prior to invasion by Deitsch [111, 158]. The pre-loaded erythrocyte method has been found 5 to 180 times more effective than direct electroporation [159].

High salt electroporation media called “cytomix” was made from DEPC treated water with 120 mM KCl, 0.15 mM $CaCl_2$, 2 mM EGTA, 5 mM $MgCl_2$, 25 mM HEPES, and 10 mM pH 7.6 K_2HPO_4/KH_2PO_4 as described by Wu [160]. The cytomix was filtered through a bottle-top 20 micron Millipore filter to sterilize. Cytomix formula was stable at room temperature for many months but prolonged storage at 4 °C resulted in salt precipitates.

Relatively fresh erythrocytes were processed, as usual for cell culture, then combined 1:1 v/v with cytomix, spun down at 4,000 rpm in a swinging bucket centrifuge, and the supernatant removed. This high salt parasite pellet was used for transformations. For each transformation, 100 µg of plasmid (under 100 µL volume) was combined with 200 µL of the salt-washed erythrocyte pellet, and an additional ~100 µL of cytomix was added bring the total volume to 0.4 mL in a 0.2 cm gap Bio-Rad electroporation cuvette (#165-2086). The erythrocytes were electroporated at 310 V, 950 µF and then removed from the cuvette into a parasite culture flask with additional media washes. The cultures were grown with daily media changes and as-needed red blood cell additions until the selection agent had killed most untransformed parasites.

The selection agent was added 48 hours after the initial transformation. Cultures were subjected to media changes every other day and smears were used to assess parasite emergence starting one week after the transfection was performed. Three to four weeks was the minimum time for parasites to emerge from this procedure, with slower growing transformants emerging a week or more later.

Assay for Anti-Plasmodial Activity (EC_{50})

Parasite growth and the effects of various inhibitors were assayed based on parasite metabolic activity using a modified Desjardins radioisotope method [161]. The assay measures the incorporation of ^{3}H-hypoxanthine to quantify parasite survival and growth. The 96-well plates were setup with triplicate wells containing 180 uL of parasitized erythrocytes (1% parasitemia and 0.5% hematocrit) to which 20 uL of 10% DMSO drug intermediate was added. The drug solutions were made up in 100% DMSO stocks and arrayed in plates, then transferred into RPMI-1640 to create the intermediate 10% DMSO plate. Procedurally, atovaquone solubility issues observed during larger experiments with low DMSO intermediates were best avoided by quick handling of intermediate drug plates during assay setup. Each assay plate contained a DMSO only/No Drug control. The assays were incubated at 37°C for 48 hours in an atmosphere of 90% N_2, 5% CO_2, and 5% O_2. Radioactive ^{3}H hypoxanthine solution (0.25-0.5 µCi per 50 µL of complete media) was added to the wells and the parasite plates incubated another 24 h. At the end of the assay plates were placed in a -80 °C freezer overnight to halt growth and help with cell lysis. The plates were thawed and DNA

harvested onto glass fiber filters (Inotech Biosystems IH201A) with an Inotech Biosystems Cell Harvester. The mats were washed with three rinses of ~40 mL of Milli-Q water per plate. The filters were then secured in plate-format cartridges (Packard Omnifilter) and permitted several hours to dry. After fully drying, 30 µL of Microscint-O scintillation fluid (Perkin Elmer) was added to each well using a 12 channel pipette and the plate sealed with a TopSeal-A adhesive film (Perkin Elmer). Radioactive nucleotide incorporation was quantified using a TopCount scintillation counter with counts collected for 2 minutes per well. The data was then reduced to growth rates relative to DMSO control at each data point and pooled into Graphpad Prism 5.01 . The data was plotted, curves fit , and the data reduced to EC_{50} tables where appropriate. The curves were generally best fit via nonlinear curve fitting with automatic data point rejection. Each assay was repeated at least three times before a representative experiment was chosen for presentation.

Solid Phase Extraction and Quantification of Proguanil Conversion via LC-MS/MS

3d7 malaria parasites were cultured in 30 mL volume T75 flasks under standard conditions for 24 hours in the presence of 100 nM proguanil alone, 100 nM atovaquone alone, 100 nM atovaquone and 100 nM proguanil, or 100 nM proguanil that was added just before the red blood cells and parasites were harvested from the media. Additionally, a separate flask with all the media and red blood cell content, but no malaria parasites was cultured with 100 nM proguanil. The red blood cell pellet

containing the parasites was harvested by centrifugation in a swinging bucket centrifuge at 2,000 x g for 5 minutes. The supernatant was removed, leaving a 0.7 mL pellet to which 100 picomoles of a 2-chlorocycloguanil internal standard was added. In early experiments the blood pellet was lysed by freezing at -80°C overnight before adding internal standard. Later experiments were performed under more harsh conditions, via adding the internal standard and then sonicating ice-chilled samples for 30 seconds using a Heat Systems Ultrasonics Inc., Model W185 Cell Disrupter with a micro tip at 30 watt output. The resulting 0.7 mL blood pellet became more translucent and was then adjusted to 70% acetonitrile to precipitate cellular proteins. The tube was centrifuged at 10,000 x g for 20 minutes at 4 °C. The supernatant was then aliquotted into 1.5 mL tubes and speed vacuumed. The dry samples were resuspended in 100 µL of acetonitrile and water 1:1, combined into a single tube, and speed vacuumed again. The sample was then resuspended in 50 µL of acetonitrile and water 1:1 before being loaded into an auto sampler vial and stored at 4 °C before analysis. The following fragmentations were monitored during the run: 2-chloro-cycloguanil 286.1-229.1, 286.1-58.0; proguanil 254.2-170.2, 254.2-153.0; cycloguanil 252.2-195.2, 252.2-153.1, 252.2-58.0 .

A standard curve was constructed from 6 to 9 samples in acetonitrile:water 1:1 containing proguanil, cycloguanil, and 2-chloro-cycloguanil at concentrations from 5,000 to 0.5 nM. Extraction efficiencies were compared by adding three different concentrations of mixed standards to the 0.7 mL red blood cell and parasite pellet

during work up and comparing the resulting samples to the standard curve. The peak areas of the most responsive ion fragments of each drug across all samples were recorded, the internal standard used to normalize each run's extraction efficiency individually, and the resulting areas were compared to the standard curve to determine the drug concentration in each sample.

Results

Single Drug Susceptibility Profiles

Malaria parasite growth and drug survival assays (EC_{50}s) were performed to assess the effects of selected antimalarial drugs. To establish baselines for the effects of the drug combination Malarone® (proguanil and atovaquone), we first profiled the susceptibility to single drugs as well as relevant combinations. Proguanil's metabolite, cycloguanil, and a biguanide drug also reported as synergistic with atovaquone, synthalin, were assayed [105]. Inhibitors of complex III of the electron transport chain, the target of atovaquone, were also profiled [162]. Growth was assessed by ^{3}H-hypoxanthine uptake assays conducted following 48 hours of drug exposure in standard, 20% serum supplemented RPMI-1640 media. Experiments were performed using the common lab strains 3d7, FCR3, D6, Dd2, and TM90 C2A as well as the non-standard lab strains/drug-resistant lines B/G9, SB1-A6, and TM90 C2B. A series of single-agent antimalarial drugs related to Malarone® were assayed and resulted in the parasite growth data shown in the representative experiment in Figure 3.5.

Proguanil

The growth inhibitory effects of proguanil were examined at drug concentrations as high as 100 µM. The individual results of the proguanil EC_{50} are reported in Figure 3.5 and Table 3.1. Of the parasite lines tested, nearly all parasite strains tested display similar EC_{50} drug inhibition profiles of around 10 µM (3d7 13 µM, B/G9 12 µM, FCR3 15 µM, Dd2 15 µM, TM90 C2A 14 µM). Moderate sensitivity was observed with SB1-A6 and TM90 C2B lines at 8.0 and 8.2 µM, respectively. The D6 parasite strain, a strain very susceptible to many drugs, stood out with a sensitivity of 0.43 µM.

Cycloguanil

The levels of drug resistance observed for cycloguanil are quite a bit more variable than other drugs discussed. The EC_{50} of the most cycloguanil-sensitive lines were in the low nanomolar range (D6 2.8 nM and SB1-A6 3.2 nM). The most common lab strain, 3d7, was moderately less susceptible to cycloguanil (3d7 15 nM) and is generally regarded as the baseline standard for a "sensitive to antifolates" phenotype. More pronounced resistance was observed with strains carrying known point mutations in the DHFR gene (Table 3.5) which resulted in low micromolar sensitivity (FCR3 1.8 µM and Dd2 2.9 µM). The highest level of cycloguanil resistance was observed in the parasite strains B/G9 and the TM90 C2A and C2B variants (B/G9 19 µM, TM90 C2A 35 µM, and TM90 C2B 18 µM).

Atovaquone

Atovaquone is a particularly potent antimalarial drug with activity in the single nM range for most strains of malaria. Atovaquone potency was assessed via ^{3}H-hypoxanthine uptake and yielded EC_{50}s of - 3d7 4.6 nM, B/G9 8.9 nM, FCR3 1.9 nM, Dd2 6.2 nM, and TM90 C2A 14 nM. Moderate sensitivity was observed in the D6 line at 0.15 nM. High levels of resistance were observed in the SB1-A6 and TM90 C2B lines (98 and 69 µM, respectively). The SB1-A6 and TM90 C2B strains are expected to have pronounced resistance to atovaquone due to their previous exposure and acquired resistance to an experimental acridone-based electron transport chain inhibitor or atovaquone, respectively.

Myxothiazol

Additional parasite growth assays were performed using inhibitors of two active sites of complex III in the electron transport chain, myxothiazol and antimycin A. The results of these alternate complex III inhibitors are reported in Figure 3.6 and Table 3.1. Parasites exposed to myxothiazol are well grouped in their sensitivity. The majority of the parasite lines are sensitive around the several hundred nanomolar level (3D7 360 nM, B/G9 460 nM, Dd2 370 nM, and TM90 C2A 750 nM). The most myxothiazol-sensitive lines tested were the FCR3 and D6 strains at 100 nM and 68 nM, respectively. Significant resistance to myxothiazol was observed in the TM90 C2B and SB1-A6 parasite lines (TM90 C2B 9 µM and SB1-A6 53 µM). The fact that atovaquone binds to the same

Q_0 active site as myxothiazol is predictive of the resistance displayed by the TM90 C2B and SB1-A6 strains.

Antimycin A

Parasites exposed to antimycin A were difficult to quantify given the limited solubility of antimycin A in our culture media. Antimycin A binds the alternate Q_i site of complex III of the electron transport chain. The majority of the parasite lines display moderately sensitive to antimycin A (3d7 9.6 µM, B/G 6.6 µM, and Dd2 5.5 µM). D6 and FCR3 parasites, at 840 and 1,000 nM, were more sensitive than the majority of parasite lines. TM90 C2A, TM90 C2B and SB1-A6 appeared highly resistant to antimycin A with the TM90 C2A strain EC_{50} at 96 µM but the TM90 C2B and SB1-A6 strains resistance extending above the 100 µM maximum concentration assayed.

Synthalin

Synthalin is a commercially available, alternate biguanide drug reported to inhibit parasite growth and act synergistically with atovaquone [105]. Synthalin's structure, a 10 carbon hydrocarbon chain with guanidine on each end, cannot be activated to a cycloguanil-like structure. Any biguanide-specific targets that were evident for proguanil might carry over into synthalin, particularly any components of synergy. As a single agent antimalarial, the majority of the synthalin EC_{50}s were in the upper tens of micromolar range (3d7 121 nM, B/G9 37 nM, D6 35 nM, Dd2 34 nM, SB1-

A6 67 nM, TM90 C2A 55 nM, TM90 C2B 47 nM). Only the FCR3 parasite line seemed to appreciably differ in sensitivity to synthalin, at only 4.1 nM.

Drug Synergy Profiles

Low concentrations of atovaquone have been implicated in creating a susceptibility to proguanil that is synergistic in nature. The relatively consistent response of parasite strains to proguanil alone, varied response to atovaquone, and even more varied response to cycloguanil, proguanil's active form, inspired the profiling of parasite growth in response to both components of Malarone®, atovaquone and proguanil across a broad range of parasite strains. A number of variations on the design were performed, with the best display of synergistic response from experiments where a low nanomolar amount of atovaquone was kept fixed as the concentration of proguanil was varied. Due to the growth inhibition by atovaquone being varied, the inflection point of the proguanil curve is being reported rather than the true, non-drug treated 50% growth inhibition point. To help quantify synergy, something we will call a "Synergy Shift Ratio" was calculated by dividing the concentration of half maximum inhibition of the biguanide by the half maximum inhibition of that parasite strain's biguanide with atovaquone. High Synergy Shift Ratios represent higher levels of a synergistic drug action. A representative experiment's inhibition curves are displayed in Figure 3.7 and the interpreted EC_{50}s and Synergy Shift Ratios are reported in Table 3.2 . Against a single drug, most parasite strains were susceptible to proguanil with an EC_{50} around 10 micromolar. The D6 parasite strain is more sensitive with an EC_{50} of 430

nanomolar. When a small amount of atovaquone was added, many parasite lines exhibited a significant shift in the half-maximal growth inhibition concentration of proguanil. At 0.4 nM atovaquone added to the proguanil, the most significant shift was in FCR3's EC_{50} value being reduced 7 fold compared to proguanil alone. With 1 nM atovaquone added to the flasks of proguanil treated parasites, proguanil's observed EC_{50} was, again, significantly shifted in the FCR3 strain (56 fold compared to proguanil alone) as well as in the 3d7 and Dd2 strains (at 81 fold and 6 fold shifts). When atovaquone was increased to 5 nM, the EC_{50} had shifted in most parasite lines, indicating a phenomenon where some parasite lines may require relatively high amounts of atovaquone to achieve synergy. The parasite strains that displayed a synergy shift at lower atovaquone concentrations (3d7, FCR3, and Dd2) were also shifted in the 5 nM atovaquone with proguanil treatment group at 100, 153, and 107 fold shifts, respectively. Additionally, the B/G9, SB1-A6, and TM90 C2A parasite strains had synergistic shifts of 34, 12, and 79 fold, respectively. Curiously, the D6 parasites, which are the most susceptible to atovaquone, did not seem to display a synergy shift nor did the TM90 C2B parasite line.

Another experiment was designed to examine if biguanides were consistent in their synergistic potency against parasites already experiencing atovaquone-based disruption of the electron transport chain. We examined the theory proffered by Srivastava *et al* that biguanide potency was achieved through a leaky complex III that was only exposed after atovaquone's disruption of the major driving force of the

electropotential gradient [124]. Malaria parasite lines were drug treated at grouped concentrations calculated to be approximate to the EC_{70} concentrations of atovaquone (0.2 nM for D6, 1.5 nM for 3d7, B/G9, and FCR3, 5 nM for Dd2 and TM90 C2A, 100 nM for SB1-A6 and TM90 C2B) with a variable proguanil. The SB1-A6 and TM90 C2B strains are highly atovaquone resistant, so the 100 nM was a practical limit and not the EC_{70}. The Synergy Shift Ratio for proguanil and high levels of atovaquone was calculated by dividing the concentration of half maximum inhibition of the biguanide by the half maximum inhibition of that parasite strain's biguanide with EC_{70} atovaquone. Again, high Synergy Shift Ratios represent higher levels of a synergistic drug action. The ^{3}H-hypoxanthine uptake/cell growth curves for a representative experiment are displayed in Figure 3.8 and interpreted in Table 3.3. The Synergy Shift Ratio of proguanil with atovaquone was high in the 3d7, FCR3, TM90 C2A, and Dd2 parasite lines, resulting in a proguanil potency shifts of 148, 158, 163, and 100 fold, and modest in B/G9 and SB1-A6 parasite lines, resulting in synergy shifts for proguanil potency of 43 and 41 fold. The synergy of synthalin and atovaquone at its EC_{70} value was similarly evaluated as high in the TM90 C2A parasite line, at 126 fold, and modest in FCR3, 3d7, and B/G9 parasite lines, with potency shifts of 42, 16, and 16 fold. The parasites displaying proguanil and atovaquone synergy had some members in common with the synergy between the synthalin biguanide and atovaquone, but some inconsistent members and a differing order of sensitivities cast doubt on the source of synergy being the same target(s). We then directly evaluated if proguanil's conversion to cycloguanil was involved in the *in vitro* observations of synergy.

Direct UPLC-MS/MS Evidence for Cycloguanil Formation

Individual T75 flasks of parasites were grown at the same 100 nM proguanil and 100 nM atovaquone concentrations described by Painter while studying Malarone® synergy [52]. Flasks were grown with proguanil but not parasites, proguanil or atovaquone alone in the presence of parasites, and conditions with both proguanil and atovaquone with parasites for a 24 hour period. The extraction efficiency of the method with BondElut C18 columns was variable; between 10 – 30% was a typical recovery achieved while creating the standard curve. Upon normalizing the internal standard to the standard curve, it was possible to reasonably quantify the levels of drugs recovered from the red blood cell pellet, although run to run variation was high. The level of proguanil extracted from the 1 mL red blood cell pellet was 22 ± 3 µM, 18 ± 4 µM, 15 ± 4 µM, and 0 from the conditions of no parasites, proguanil alone with parasites, proguanil and atovaquone with parasites, and atovaquone alone with parasites, respectively. The level of cycloguanil measured in that same pellet was determined to be 9 ± 3 nM, 14 ± 2 nM, 16 ± 2 nM, and 0 from the conditions of no parasites, proguanil alone with parasites, proguanil and atovaquone with parasites, and atovaquone alone with parasites, respectively, when averaged across experiments. The data is summarized in Figure 3.10. The presence of cycloguanil is remarkable and not something that depends on parasite metabolism.

Drug Rescue with Cycloguanil Resistant *Plasmodium vivax* DHFR-TS

Rescue plasmids were constructed to transfect malaria parasites with a cycloguanil resistant form of DHFR-TS from *Plasmodium vivax* in order to evaluate a theory that proguanil was activated to cycloguanil in the flasks of parasites. The transfected parasites were evaluated for their susceptibility to the proguanil and atovaquone components of Malarone®, cycloguanil, and various concentrations of proguanil mixed with atovaquone. Continual selection with Blasticidin was required to maintain the episomal plasmids. The growth inhibition curves from a representative experiment using the transfected parasites appears in Figure 3.11 and the data is summarized in Table 3.4. The difference between the drug susceptibility of parasites containing plasmids was minor, from 9.5 µM for 3d7 parasites without drugs to 6.4 – 3.4 µM for parasites assayed for proguanil. Atovaquone susceptibility was not appreciably altered in the transfected parasites, all displaying EC_{50}s near 1 nM. A moderate level of cycloguanil resistance was conferred to parasites transfected with the cycloguanil resistant form of *Pv*DHFR-TS. Parasites had a cycloguanil susceptibility of 5.5 to 5.9 nM without the addition of *Pv*DHFR-TS enzyme (for 3d7 and the pRZ (blank) transfectant, respectively). The wild type form of the *Pv*DHFR-TS enzyme conferred slight levels of resistance (16.5 nM, 3 fold) in some experiments, but the resistance was not significant enough to be faithfully reproduced in all experiments. Cycloguanil resistant *Pv*DHFR-TS-containing parasites were between 10 and 37 fold more resistant to cycloguanil compared to the EC_{50} obtained for the wild type *Pv*DHFR-TS transfectants or between 27 and 60 fold more resistant when the cycloguanil resistant *Pv*DHFR-TS parasites are

compared to the transfection control pRZ (blank). The cycloguanil resistant form of *Pv*DHFR-TS did produce an unusual curve shape in ^{3}H-hypoxanthine uptake assays and the shallow slope contributed to uncertainty in the EC_{50}. When the transfected parasites were treated with proguanil and a 1 nM amount of atovaquone, the EC_{50}s were fairly consistent at between 38 and 95 nM for the parasite lines. No significant shift in the level of synergy between 1 nM atovaquone and proguanil was observed relative to proguanil alone.

Digitonin Permeabilization of *Pv*DHFR-TS-Containing Parasites

Digitonin-based selective membrane permeabilization was performed on the 3d7 parasites transfected with *Plasmodium vivax* DHFR-TS expression plasmids. As shown in the experiment depicted in Figure 3.12, the un-mutated, wild-type *Pv*DHFR-TS protein levels became extracellular at digitonin concentrations between 0.7 mM – 0.35 mM, similar to the pattern observed for aldolase (a cytosolic protein) releasing between 0.7 mM to 0.35 mM. The native *Pf*DHFR-TS was released into the supernatant between 1.4 mM and 0.7 mM. The cycloguanil-resistance point mutations incorporated in *Pv*DHFR-TS did not alter the digitonin permeabilization profile observed. The cycloguanil-resistant *Pv*DHFR-TS was probed with the same antibody as wild-type *Pv*DHFR-TS and was also released into the supernatant between 0.7 mM - 0.18 mM. In that same experiment, the cytoplasmic marker *Pf*aldolase was also observed to release between 0.7 mM - 0.18 mM. In contrast, the *Pf*DHFR-TS was released into the supernatant between 1.4 and 0.7 mM digitonin concentrations. These results indicate

that our *Pv*DHFR-TS proteins were cytoplasmic and not localizing like the native *Pf*DHFR-TS.

Discussion

Proguanil Sensitivity

Proguanil is a relatively weak antimalarial in parasite cultures. While effective in the human body due to pro-drug activation to cycloguanil, the proguanil administered to parasite cultures requires very high concentrations to kill parasites. The levels of proguanil necessary to kill parasites in cultures are not achieved in human plasma following standard oral doses [107, 163]. The parasites' susceptibility to proguanil was a relatively uniform response, with EC_{50}s between 8 and 15 µM in all strains but D6 parasites. The D6 strain was the most susceptible to proguanil (at 430 nM) and is 20 times more sensitive than the SB1-A6 experimental strain that was derived from D6 (which measured at 8,000 nM). SB1-A6 was created from D6 parasites via repeated rounds of selection with an experimental antimalarial that targets the electron transport chain [162]. The Riscoe lab that created the SB1-A6 line has been investigating the genetic basis for that strain's resistance and may, in the future, have additional insight about the causes for the reduced proguanil sensitivity in that parasite line.

Cycloguanil Sensitivity

Cycloguanil acts on the same DHFR active site as pyrimethamine, an antimalarial drug used for decades until resistance became well established in the field [164-166].

Widespread use of antifolate-based antimalarial drugs, including pyrimethamine and proguanil/cycloguanil, has resulted in many parasite isolates with different DHFR point mutations contributing to varied levels of cycloguanil resistance. A summary of the DHFR point mutations amongst parasite strains used in this study is found in Table 3.5. Both the D6 and SB1-A6 parasite lines are very sensitive to cycloguanil, with 2.8 and 3.2 nM EC_{50}s. 3d7 parasites are slightly more resistant to cycloguanil with a 4.6 nM EC_{50}. The Dd2 strain is a DHFR triple mutant and FCR3 has a unique double mutant genotype that contributes to moderate cycloguanil resistance, at 2.9 and 1.8 μM, respectively. B/G9 parasites are a transgenic parasite strain with an incorporated human DHFR gene, which confers an extreme cycloguanil resistance of 19 μM. The TM90 C2A and TM90 C2B strains have a DHFR quadruple mutant genotype and are highly resistant to cycloguanil at 35 and 18 μM $EC_{50,}$ respectively. The observed sensitivity to cycloguanil agrees with the trends expected from the point mutations known for each parasite line, as well as the incorporation of a transgenic human DHFR to the B/G9 strain. Human DHFR is not appreciably inhibited by cycloguanil. The order of sensitivities to proguanil and cycloguanil are divergent, with little similarity beyond D6 being the most sensitive strain to both drugs.

Atovaquone Sensitivity

Atovaquone potency is typically in the low nanomolar to sub-nanomolar range in EC_{50} assays. Many early experiments with large panels of parasites were not of suitable quality due to issues with atovaquone's solubility in RPMI media as DMSO decreased.

Adjustments were made, requiring careful dilutions of drug plates with RPMI-1640 intermediate concentration plates and timely handling to avoid precipitation effects. The solubility observation could also be related to a report of lipid level influence on atovaquone EC_{50} measurements, as drug stocks and intermediates were made in RPMI-1640 and added to serum-supplemented media (with associated lipids) containing the live parasites [167]. The majority of the cell lines assayed were predictably sensitive to atovaquone in the 5 - 14 nM range with both extra-sensitive (D6 and FCR3, at 0.15 and 1.9 nM) and resistant exceptions (SB1-A6 and TM90 C2B, at 98 and 69 μM). The SB1-A6 line was derived from the D6 isolate after exposure to increasing levels of an electron transport chain inhibitor, 3-(6,6,6-trifluorohexyloxy)-6-amino-acridone, with stepwise increases from 100 nM to 5,000 nM over 4 weeks [162]. The mechanism(s) by which SB1-A6 parasites display such strong electron transport chain inhibitor resistance while simultaneously possessing mitochondria that, when made into free lysates, possess enzymes that are inhibited by those same electron transport chain inhibitors, are not yet elucidated. The TM90 C2B isolate is related to the TM90 C2A isolate as it is derived from the patient who provided the TM90 C2A isolate whose infection recrudesced after atovaquone monotherapy, yielding TM90 C2B [54]. The TM90 C2B strain is reported to have differences in the expression of several components of the electron transport chain's complex III and complex IV as well as glycolysis [168]. The TM90 C2B line is also known to have a point mutation in the cytochrome b gene at amino acid 268 (Tyrosine to Serine). Mutations at codon 268 have been found to decrease the efficiency of the

enzyme and interfere with the quinone oxidation (Q_O) site targeted by atovaquone [168-170].

Alternate Electron Transport Chain Inhibitors (Myxothiazol and Antimycin A)

The SB1-A6 and TM90 C2B parasite lines were selected with atovaquone or atovaquone-like compounds until they developed drug resistance. Additional electron transport chain inhibitors targeting complex III were also screened to evaluate if atovaquone susceptibility was unique compared to other complex III inhibitors. Antimycin A is a bacteria-derived antibiotic that acts on the Q_i site of complex III. Myxothiazol is a ubiquinone analog that acts on the Q_O site of complex III, the same site that atovaquone binds in. The reason for screening both inhibitors is that both sites are necessary for complex III, an essential component of the electron transport chain of the mitochondrion, to function. Due to the many parasite strains being studied, some with known resistance to atovaquone and like compounds, we needed to evaluate which parasites may be displaying reduced atovaquone susceptibility instead of a reduced reliance on the electron transport chain. Probing the same complex would also provide an avenue for evaluating if any off-target effects of atovaquone were partly responsible for its anti-parasitic activity.

Parasites exposed to antimycin A in the ^{3}H-hypoxanthine uptake assay elicited a wide range of responses. The majority of EC_{50}s for antimycin A were in the single micromolar range (Table 3.1 - FCR3 1 µM, Dd2 5.5 µM, B/G9 6.6 µM, and 3d7 9.6 µM). The D6 parasite line was the most susceptible at 840 nM and the TM90 C2A, SB1-A6,

and TM90 C2B parasite lines were the most resistant (at 96 μM and above). The relatively weak potency of antimycin A made it difficult to evaluate if parasites susceptible to atovaquone were displaying a similarly ranked susceptibility to antimycin A. To a first approximation, parasite strains of high and low sensitivity to atovaquone displayed a similarly ordered sensitivity to antimycin A. The intermediate sensitivities were not of the same order. It was noticed that antimycin A had difficulties with precipitation in 10% DMSO intermediate plates sufficient to leave some traces on the plastic culture plates. Comparison to another report of antimycin A potency differs significantly and casts doubt on our protocols being appropriate for this compound[162]. The low potency and high expense of antimycin A created a significant barrier to its use in drug synergy experiments and discouraged further experimentation.

Parasites exposed to myxothiazol displayed a similarly broad range of EC_{50}s in parasite growth assays, generally achieving EC_{50} values 50 to 100 fold higher than the value of atovaquone (Table 3.1). Notable exceptions to the trend were the most sensitive parasites, D6 at 68 nM and its 450 fold increase, and the least sensitive parasites, SB1-A6 and TM90 C2B at 53 and 9 μM, which were 2 fold and 8 fold less potent than atovaquone on the same parasite strains. The ordering of sensitivity to atovaquone mirrors that found in myxothiazol, as one might expect with the same Q_0 active site inhibited by both compounds. It is known that the TM90 C2B parasite line has a Y268S mutation in cytochrome b that decreases atovaquone's potency but SB1-A6

parasites were not found to have any mutation in cytochrome b and the mechanism of its resistance remains unknown [162].

Alternate Biguanide (Synthalin Sulfate)

While not actively used as an antimalarial agent, the biguanide drug synthalin sulfate has been reported to be synergistic with atovaquone and electron transport chain inhibition [105]. The drug synthalin was developed as a functional analog of Metformin. Metformin resulted following a progression from lilac extracts to guanidine in the early 1900s to Metformin [171]. Synthalin was utilized to treat diabetes but was withdrawn in the 1940s due to liver toxicity and other drugs have since displaced it [172-174]. Synthalin also lead to the pentamidine class of drugs to treat trypanosomiasis [175]. Structurally, synthalin is comprised of two guanidines linked through a 10 carbon hydrocarbon chain. Synthalin is incapable of being metabolized to cycloguanil.

The potency of synthalin against many parasite lines was determined, using the EC_{50} growth assay, for use as a baseline for further synergy tests. The majority of the parasite lines had drug susceptibilities around 40 nM (Table 3.1). SB1-A6 parasites had an EC_{50} slightly elevated at 67 nM and 3d7 parasites were the most resistant at 121 nM. The most sensitive strain was FCR3 at 4 nM. Despite reports of synthalin's synergy with atovaquone being like that of proguanil, there is no discernable pattern for susceptibility to synthalin alone that matches up with that of the biguanide proguanil (Table 3.3).

Drug Synergy Trends

The panel of lab adapted parasite isolates was treated with variable concentrations of proguanil combined with small, 0.4 – 5 nM amounts of atovaquone. Proguanil and atovaquone have been implicated as a synergistic drug combination with unproven theories about the mechanism [59]. Our experiments (Figure 3.7 and Table 3.2A) were able to capture the synergistic shift of proguanil with fixed concentrations of atovaquone. Comparing the potency of proguanil with atovaquone to cycloguanil, parasite strains susceptible to cycloguanil order similarly, but not identically, to proguanil with atovaquone. For example, at 1 nM atovaquone and varied proguanil the EC_{50} from least to greatest orders as 3d7, D6, FCR3, SB1-A6, Dd2, B/G9, TM90 C2A, and TM90 C2B while cycloguanil susceptibility orders as D6, SB1-A6, 3d7, FCR3, Dd2, TM90 C2B, B/G9, and TM90 C2A. At a single atovaquone concentration, the proguanil and atovaquone potency is similar to that of cycloguanil. With differing amounts of atovaquone added to proguanil, our experiments (Figure 3.7 and Table 3.2B) illustrated that some parasite lines (FCR3, 3d7, and possibly Dd2) display susceptibility to drug synergy between proguanil and atovaquone potentiated at low concentrations of atovaquone, but others (B/G, TM90 C2A, and possibly the SB1-A6 line) only display synergistic shifts at higher concentrations of atovaquone. In this set of experiments, in strains where strong synergy was noted between proguanil and atovaquone, the level of proguanil needed to reach half-maximal growth was reduced by around 100 fold compared to proguanil alone. Oddly, two parasite lines exhibiting extreme atovaquone

sensitivity and extreme insensitivity, D6 and TM90 C2B, display no significant synergy between atovaquone and proguanil, instead measuring less than a fourfold difference from the potency of proguanil alone.

Drug synergy between proguanil and atovaquone has also been characterized as a general synergy between biguanides and atovaquone [59]. To help delineate if any cycloguanil-specific mechanisms were in play, we attempted to measure the synergy between a biguanide that can't make cycloguanil, synthalin, with atovaquone and compare to the Malarone® drug combination. In the biguanide-synergy comparison, we incorporated higher concentrations of atovaquone calculated to be inhibitory against each parasite line to more directly illustrate any drug synergy (Figure 3.8 and Table 3.3). The Synergy Shift Ratio for synthalin with atovaquone ranged from 1 to 126 fold, with the ordering from high to low of TM90 C2A 126 fold, FCR3 42 fold, 3d7 and B/G9 16 fold, Dd2 6 fold, and D6, SB1-A6, and TM90 C2B having shifts of less than fourfold (within the range of experimental variation). When put in an order of magnitude, drug susceptibility compares well with the pattern observed for proguanil with atovaquone (TM90 C2A 163 fold, FCR3 158 fold, 3d7 148 fold, Dd2 100 fold, B/G9 43 fold, SB1-A6 41 fold, and D6 and TM90 C2B being fourfold or less). As the single drug EC_{50}s for synthalin and proguanil widely differed in strain susceptibility, the pattern for both proguanil and synthalin when combined with atovaquone is surprising. The magnitudes of the Synergy Shift Ratios fluctuate but the ordering is reasonably well preserved (except for B/G9 and Dd2 exchanging positions and SB1-A6 displaying no synergy between the synthalin and

atovaquone combination). The D6 and TM90 C2B parasites not displaying synergy between both biguanides and atovaquone was remarkable and suggests these parasite lines may have some unidentified similarity that contributes to lack of synergy between proguanil and atovaquone.

A theory of a secondary proguanil-based sensitivity playing a role in the synergy is perhaps bolstered by the results with TM90 C2B parasites. TM90 C2B has a known atovaquone-specific point mutation in the cytochrome b gene (Y268S) and did not display proguanil and atovaquone synergy [54, 168]. Also interesting, the SB1-A6 parasites displaying moderate synergy between proguanil and atovaquone but the progenitor D6 line not displaying biguanide and atovaquone synergy hints at a complex set of changes that have occurred in the D6 parasites that even the lab that created SB1-A6 has not yet identified.

We profiled the drug susceptibilities of different parasite isolates as an efficient way to examine parasites with differing DHFR mutations, but relying on isolates may also introduce complications. Different lab-cultured parasite isolates have very different histories, including the length of continuous culture in media, known antimalarial drug treatments and acquired resistance, and differing changes resulting from long term asexual culture (a bias towards fewer gametocytes, inability to produce both sexes of gametocytes, loss of cytoadherence, and reduced folate uptake abilities for example)[176-182]. In order to more thoroughly remove genetic variation and establish a role for cycloguanil in Malarone® drug treatment, assays were performed to assess if

cycloguanil was generated under *in vitro* culture conditions. We also developed a transfection-based rescue construct that would impart parasites with a cycloguanil resistant form of DHFR-TS enzyme.

Mass Spec Determination of CG and PG Levels from *In Vitro* Cultures

The proguanil and cycloguanil drugs are organic molecules that could be extracted from cell cultures via solid phase extraction techniques. The internal standard of 2-chloro-cycloguanil was added just prior to lysis of the blood and parasite pellet, allowing for a way to correct for variations in recovery efficiencies. Detection was initially performed on a Waters Micromass Quattro Micro QTQ in the Chemistry Department but the cycloguanil signal could barely be detected above the noise. A Waters Micromass Quattro Premier XE UPLC QTQ system in the Medicinal Chemistry department, which combines a higher pressure HPLC with a more sensitive mass spec, proved more reliable at detecting the faint signal of cycloguanil.

Solid phase extraction from a 30 mL culture flask recovered between 13-30 % of the drugs present in the flask. When corrected to the standard curve via extraction efficiencies from added internal standard, the levels of drugs could be quantified. The amount of proguanil, typically from 15 - 22 µM in the injected 50 µL sample is significant and suggests some sequestration in the red blood cell pellet. The UPLC system was employed for greater resolution in lower volumes, essentially allowing for more of the sample to be injected into the Triple Quadrupole Mass Spectrometer. The UPLC system was able to detect peaks for cycloguanil that were significant relative to the noise and

ultimately measured between 9-17 nM. We were able to quantify how proguanil added to the culture flask contents was converted to small amounts of cycloguanil. The observed ~0.07% conversion would expose flasks of parasites given 100 nM proguanil to only 0.07 nM cycloguanil; an amount the EC_{50} indicates is too low to expect cycloguanil to be the sole source of lethality.

A hypothesis to explain the synergy between proguanil and atovaquone had been formulated that involved atovaquone potentiating the activation of proguanil to cycloguanil. That hypothesis was not supported by roughly equal, but extremely low, levels of cycloguanil being found in all the flasks treated with proguanil. Another theory emerged that atovaquone, via disruption of the electron transport chain, perturbed the ability of the parasite to localize the target of cycloguanil, DHFR. Two possible potencies could involve a localized concentration of DHFR enzyme in the mitochondria that is essential for survival or the mitochondria could be a privileged compartment that affords some measure of protection from drugs. In both cases, the disruption of localization may be what registers as synergistic increases in potency.

Resistance Plasmids

In order to further dissect any relationship between cycloguanil and the Malarone® drug resistance, we constructed a transfection plasmid that would express a cycloguanil-resistant form of the *Plasmodium vivax* dihydrofolate reductase-thymidylate synthase gene based on mutations in the AMRU-1 isolate. The enzyme's template and our natural comparator was the non-cycloguanil resistant form of *Pv*DHFR-TS from the

Sal-1 strain (wild type). *Plasmodium falciparum* parasites of the 3d7 strain were transfected with the plasmids to supplement their physiology. Significant considerations were given so the episomal transfection system would not be extremely dissimilar to the native DHFR-TS's expression strength. The transfected *Pv*DHFR-TS enzyme was kept in the native *vivax* codon sequence and the gene's expression driven by 830 bp of the *falciparum* DHFR-TS 5' UTR. When profiled for cycloguanil susceptibility (Figure 3.11), the slope of the growth inhibition curve for the cycloguanil resistant pRZ-*Pv*DT (cycR) parasite line was shallow in comparison to the wild type enzyme. Hill slope differences are frequently is considered a marker for more complex interactions than a single target. The shallow slope also led to significant variability in interpreting values for the level of cycloguanil resistance conferred by the AMRU-1 mutations, but the values were between 10 to 40 fold resistant compared to the wild type *Pv*DHFR-TS transfectant and 27 to 60 fold resistant compared to parasites that underwent a mock transfection and selection (pRZ blank). The moderate cycloguanil resistance did not correlate with any noticeable change in susceptibility to the proguanil and atovaquone components of the drug Malarone®. The initial theory of cycloguanil being at the heart of proguanil and atovaquone's synergistic activity was in conflict with the resultant lack of rescue from proguanil with atovaquone. There are many ways to interpret the finding. One theory for why these constructs might not have been successful is that, despite our efforts to use the native coding sequence and promoter, the transgenic enzyme introduced was not sufficiently conserved from *Plasmodium vivax* to *Plasmodium falciparum* to be functionally equivalent. The moderate shift in

cycloguanil susceptibility supports this notion, as the point mutations introduced have been reported to confer three orders of magnitude resistance to cycloguanil when using a different transfection system for the AMRU-1 enzyme [45, 154]. Another theory to explain why the transfected *Pv*DHFR-TS was not able to confer more resistance is that the native enzyme might need to be present and active in a particular location in the parasite. Following the observation of localization of *Pf*DHFR-TS to the mitochondria, the localization of the *Pv*DHFR-TS enzyme produced in these transgenic parasites was also examined using digitonin permeabilization.

Digitonin-based Fractionation of *Pv*DHFR-TS Transfectants

Experiments were performed utilizing selective digitonin permeabilization of the 3d7 *Plasmodium falciparum* parasites that had been transfected to express *Plasmodium vivax* DHFR-TS. The blots obtained from these experiments (Figure 3.12) hinted at a relatively strong production of *Pv*DHFR-TS protein in the cell. Although Western blots are not a quantitative technique, the relatively short exposure times compared to native *Plasmodium falciparum* DHFR-TS suggest a greater abundance of the *vivax* protein. Digitonin fractionation on both *vivax* DHFR-TS containing parasite lines showed the cytosolic protein, aldolase, was released from the parasite at similar digitonin concentrations as the *Plasmodium vivax* DHFR-TS protein. The native *Plasmodium falciparum* DHFR-TS only appeared in the supernatant of the higher digitonin concentration samples, indicating organellar localization not shared with the *vivax* protein. The cycloguanil-resistance point mutations incorporated in *Pv*DHFR-TS did not

alter the digitonin permeabilization profile observed. Both constructs were actively producing the *Pv*DHFR-TS protein in the parasites but the digitonin permeabilization profile, and likely the localization, of the *Pv*DHFR-TS protein produced differed from that of the *Pf* native DHFR-TS.

Summary

In summary, our investigations into the synergy of proguanil and atovaquone started from a theory that cycloguanil was at the root of this combination. This theory was assisted when we analyzed the contents of flasks treated with drugs and found that the cell culture conditions were actively producing small quantities of cycloguanil from the proguanil. Parasite strains were profiled and their susceptibility to electron transport chain inhibitors was of a similarly ordered lethality. Cycloguanil sensitivities were similar to the combination of proguanil and atovaquone, but not in all parasite strains. Proguanil, cycloguanil, and the biguanide synthalin all have very different potencies against parasites but the proguanil and high atovaquone combination and synthalin and high atovaquone susceptibility profiles were similar. We sought to remove strain-related variation through direct genetic transfection to create a parasite resistant to cycloguanil. The transfected parasites were resistant to cycloguanil but not to the combination of proguanil with atovaquone. As the native DHFR-TS enzyme was localizing differently from the introduced cycloguanil resistant DHFR-TS, the enzyme we introduced may have been limited in what functions it could rescue with a different organellar exposure.

Chapter 3 Figures

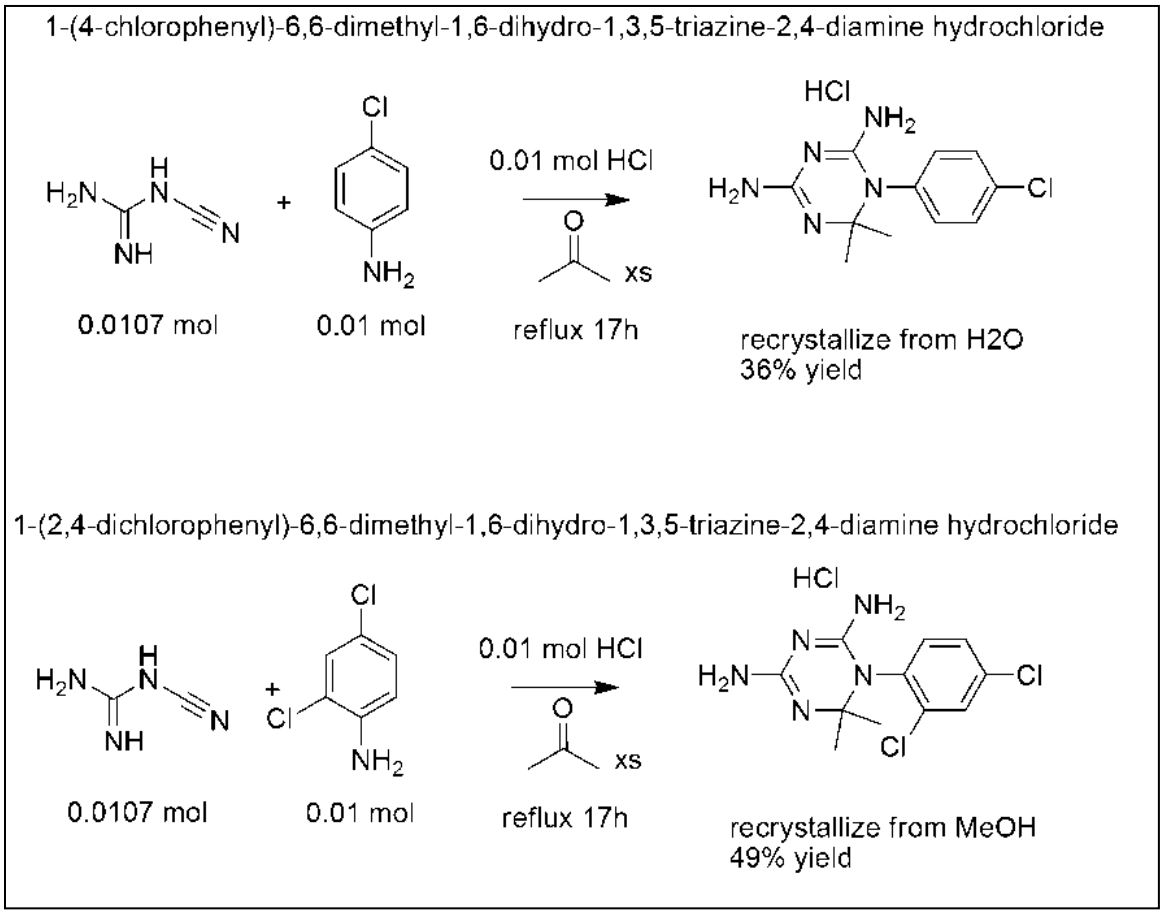

Figure 3.1 - Scheme for Synthesis of Cycloguanil, 2-Chloro-cycloguanil

The synthesis of cycloguanil and 2-chloro-cycloguanil was carried out by refluxing 10.7 millimoles of dicyandiamide, 10 millimoles of the corresponding aniline, 10 millimoles of hydrochloric acid, and 5 mL of acetone overnight. The precipitate was recrystallized from either water or methanol (as indicated). HPLC and ESI-MS verified the product and purity of the product. The 2-chloro-cycloguanil was to be used as an internal standard for HPLC-MS/MS experiments and was run through the appropriate detection system at concentrations 10x higher than expected to ensure no trace cycloguanil was present/detectable with that method.

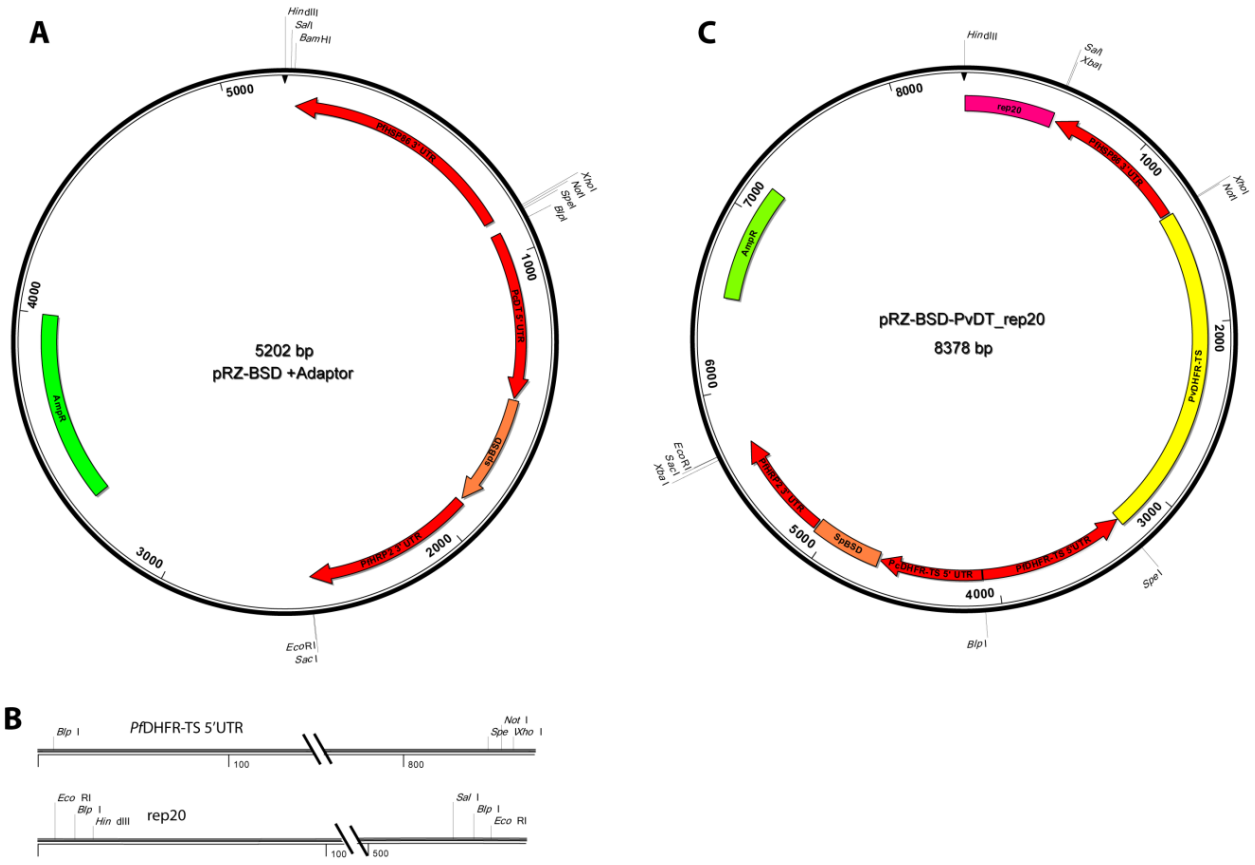

Figure 3.2 – Construction of *Plasmodium vivax* DHFR-TS Rescue Plasmid

Above is the plasmid construction scheme for the *Plasmodium vivax* DHFR-TS transfections**.** A) Depicts the pRZ-BSD +Adaptor plasmid obtained from removing extraneous pRZ-TK-BSD2 elements and inserting the synthetic primer sequence of restriction sites. B) Depicts the Plasmodium falciparum DHFR-TS 5' UTR used as a promoter and rep20 element. Both were modified with the indicated restriction sites using PCR from either 3d7 genomic DNA or the pHHyDHODH-GFP plasmid. All domains were sequenced in cloning vectors before being added to the transfection vector. C) Depicts the completed construct after the native *Pf*DHFR-TS 5' UTR promoter, rep20 segregation promoter, and *Pv*DHFR-TS gene elements were added. Plasmid maps generated with Lasergene.

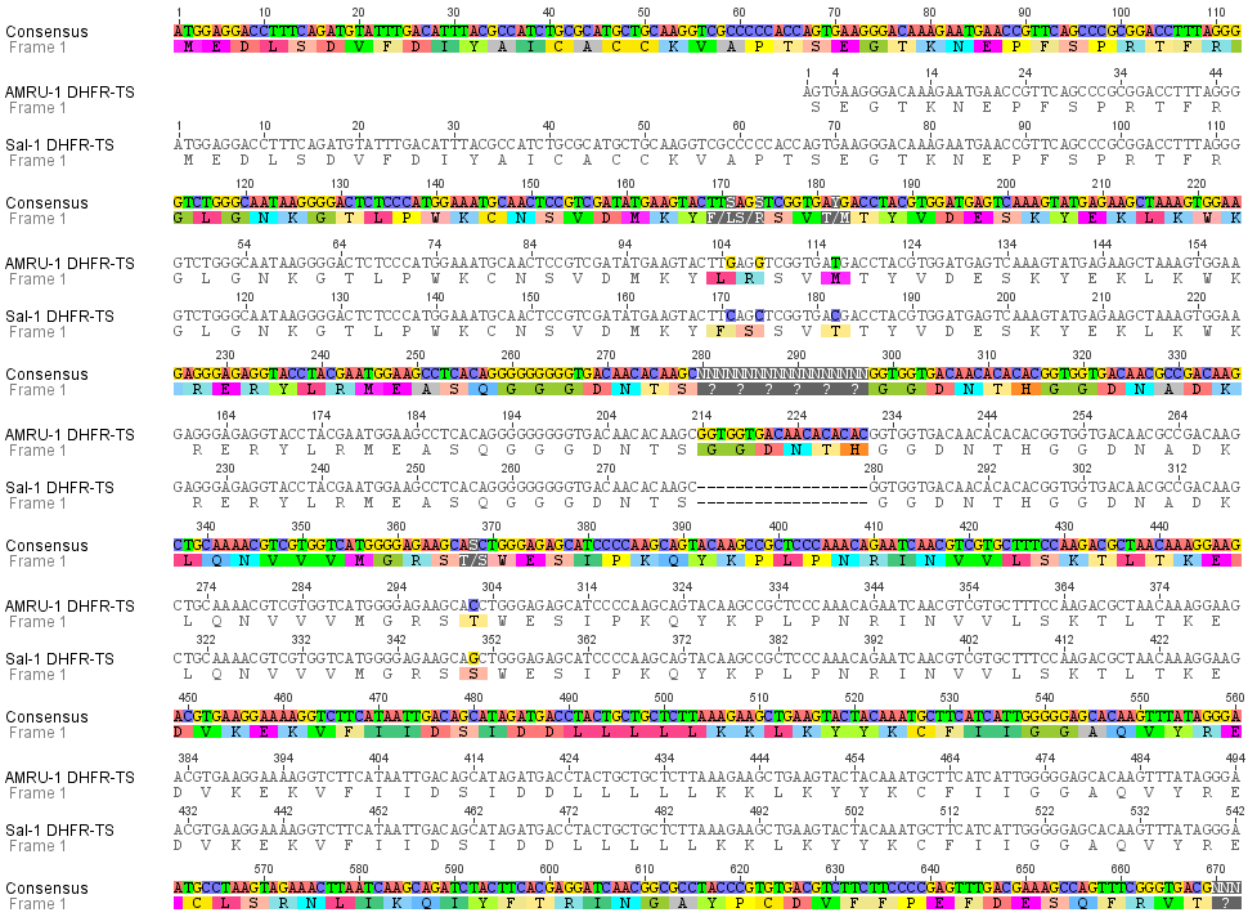

Figure 3.3 – Comparison of *Plasmodium vivax* DHFR Nucleotide Sequences

Depicted is the sequence alignment of overlapping portions of the *Plasmodium vivax* DHFR-TS AMRU-1 (cycloguanil resistant) and Sal-1 (cycloguanil sensitive/wild-type) gene sequences. The nucleotide sequence sources for *Plasmodium vivax* DHFR-TS of wild-type Sal-1 is GenBank Accession XM_001615032 and AMRU-1 cycloguanil resistant type is GenBank Accession DQ244115. The AMRU-1 sequence has four point mutations that have been identified as contributing to antifolate resistance but the repeat element at 93 – 99 was not indicated as contributing to the phenotype and was not preserved during plasmid construction. Nucleotide alignment generated with Lasergene.

Figure 3.4 – Comparison of Plasmodium vivax DHFR-TS Protein Sequences

Protein sequence comparison of *Plasmodium vivax* DHFR-TS -wild-type (wt) and cycloguanil resistant (cycR) in native codons. The figure depicts the lalign results for the full protein sequence of *Plasmodium vivax* wild-type (Sal-1) and cycloguanil resistant (AMRU-1) variants expressed by the episome transfection constructs. The four point mutations identified as responsible for resistance, which were preserved in the synthetic gene constructs, are indicated by the gold boxes. The Lalign protein alignment was generated with Geneious.

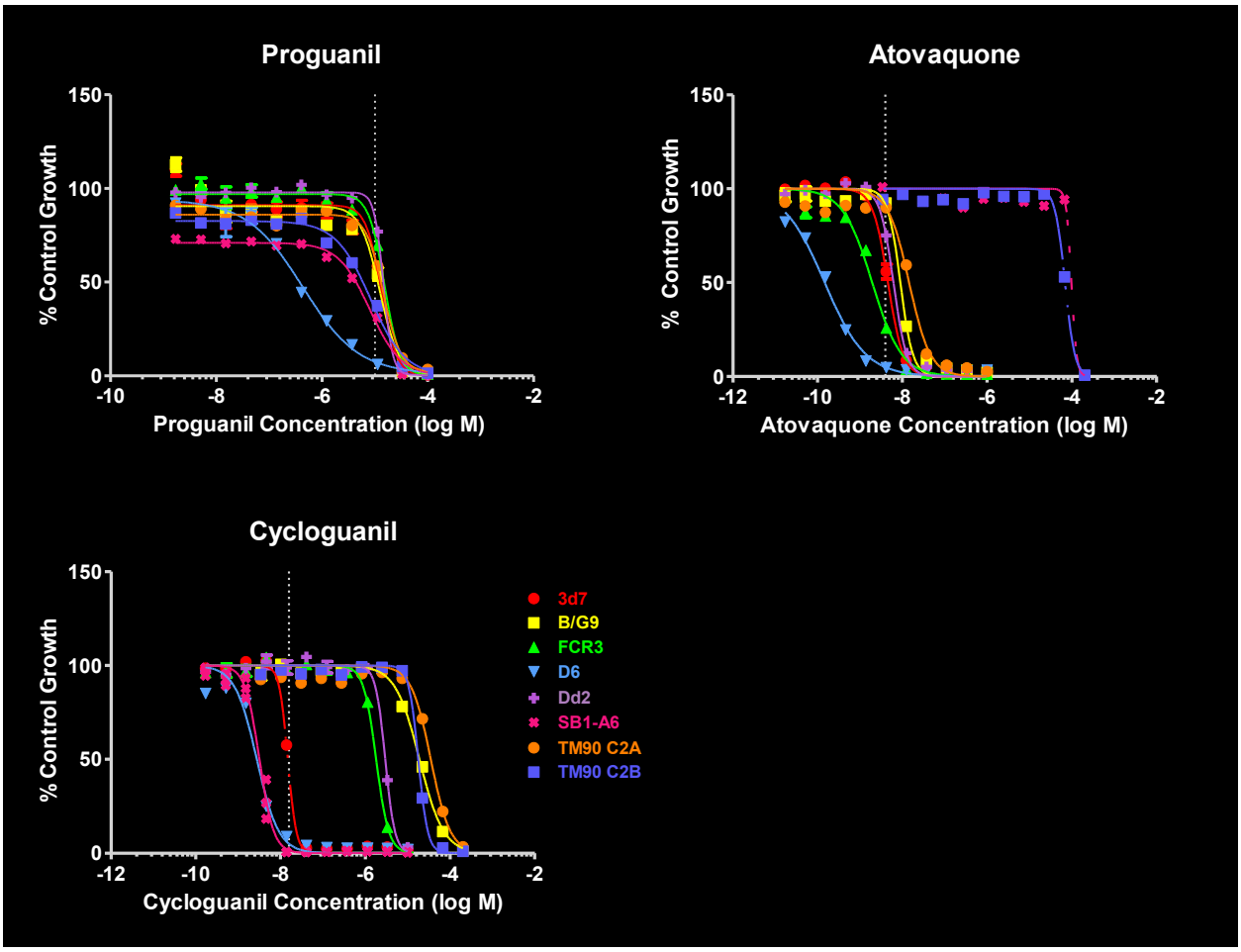

Figure 3.5 – Single Antimalarial Parasite Growth Assays

Parasite growth over a 48 hour drug treatment period was assessed using $^{3}H^{-}$hypoxanthine uptake assays. The EC_{50} of the reference strain, 3d7, is indicated by a vertical dashed line. Individual values are summarized in Table 3.1.

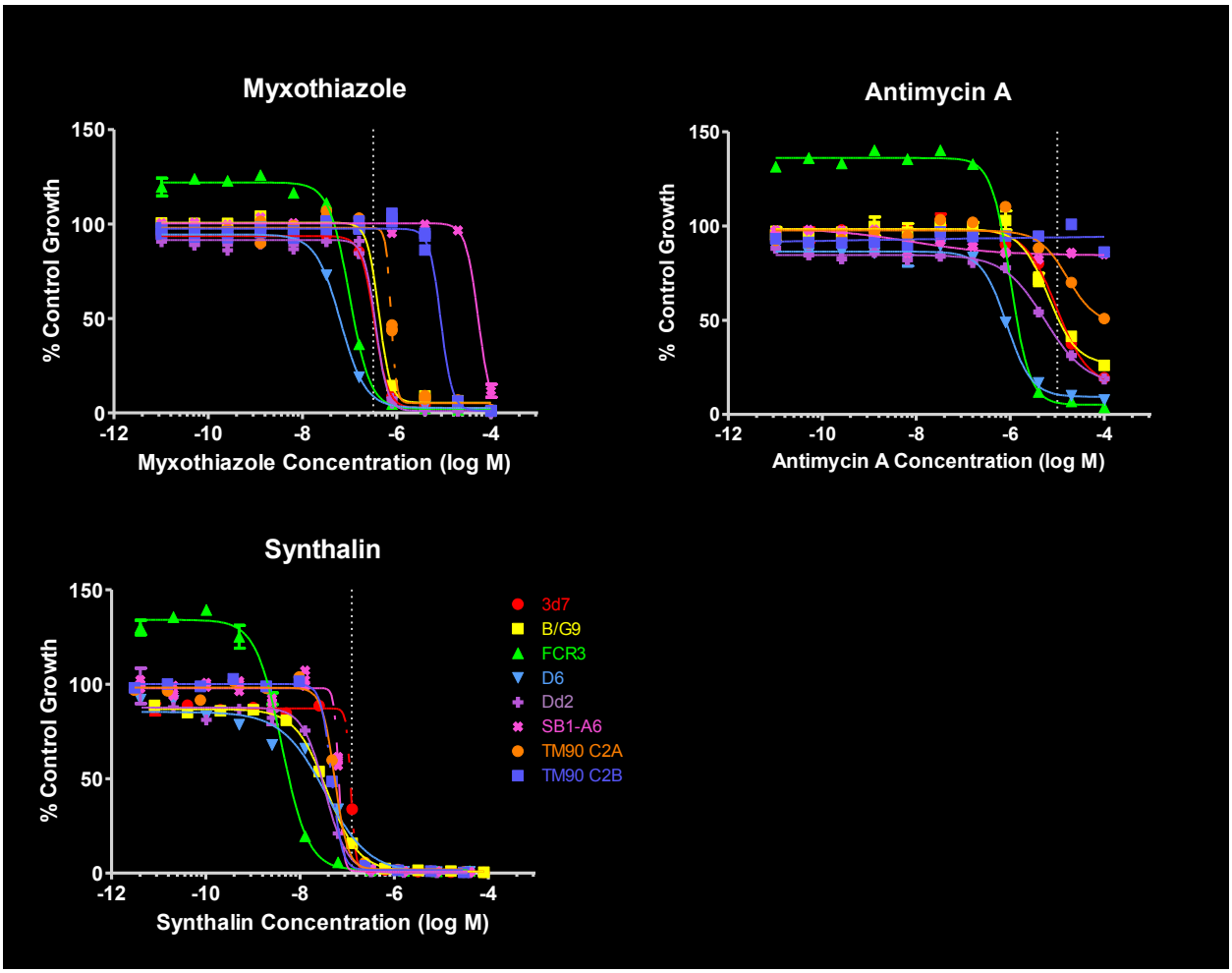

Figure 3.6 – Electron Transport Chain/Alternate Biguanide Single Antimalarial Parasite Growth Assays

Parasite growth over a 48 hour drug treatment period was assessed using ^{3}H hypoxanthine uptake assays. The EC_{50} of the reference strain, 3d7, is indicated by a vertical dashed line. Individual values are summarized in Table 3.1.

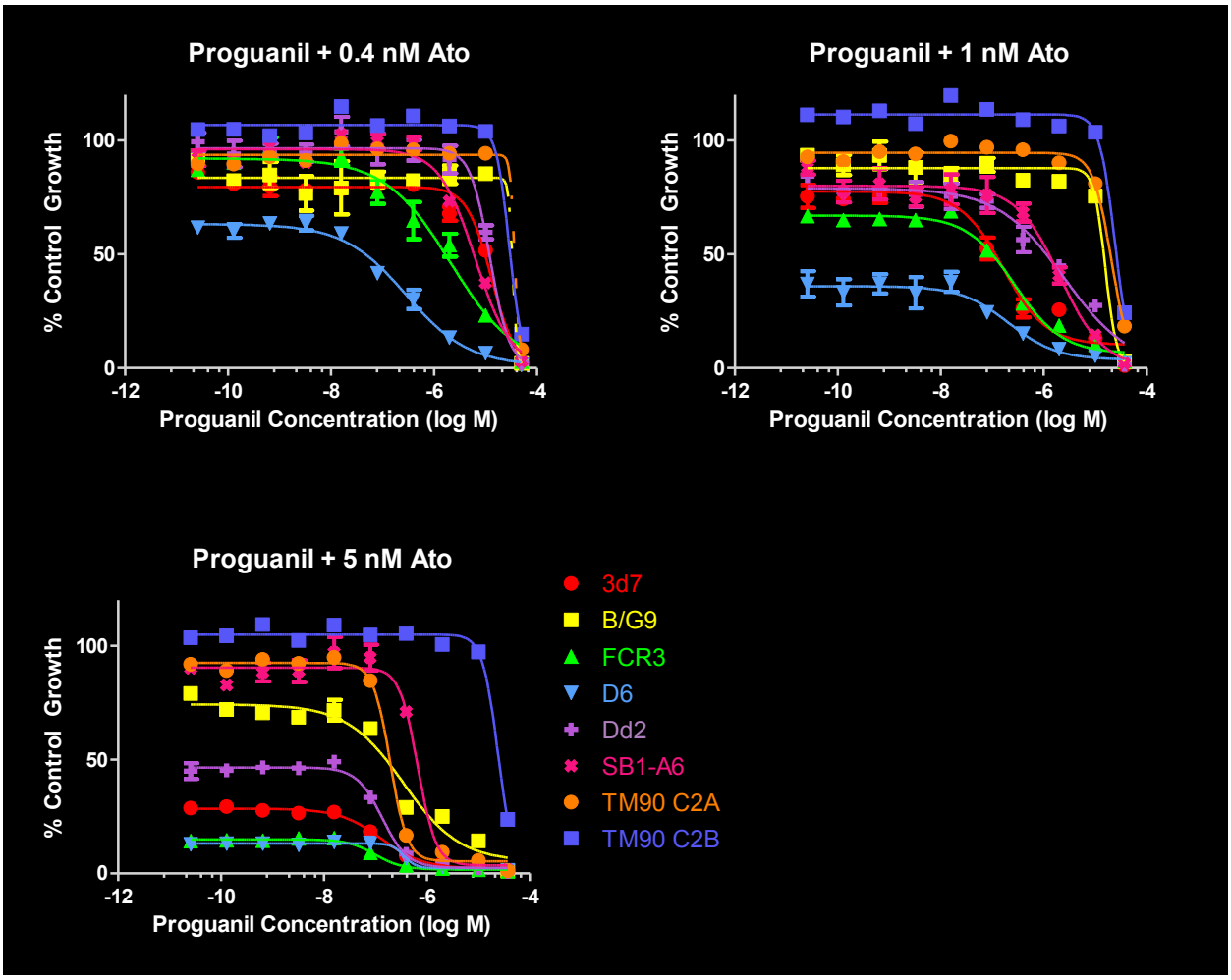

Figure 3.7 – Malarone® Drug Synergy Growth Assays

Parasite growth over a 48 hour drug treatment period was assessed using ^{3}H hypoxanthine uptake assays. Parasites were treated with a set 0.4, 1, or 5 nanomole concentration of atovaquone while proguanil concentrations were varied. Individual values are summarized in Table 3.2.

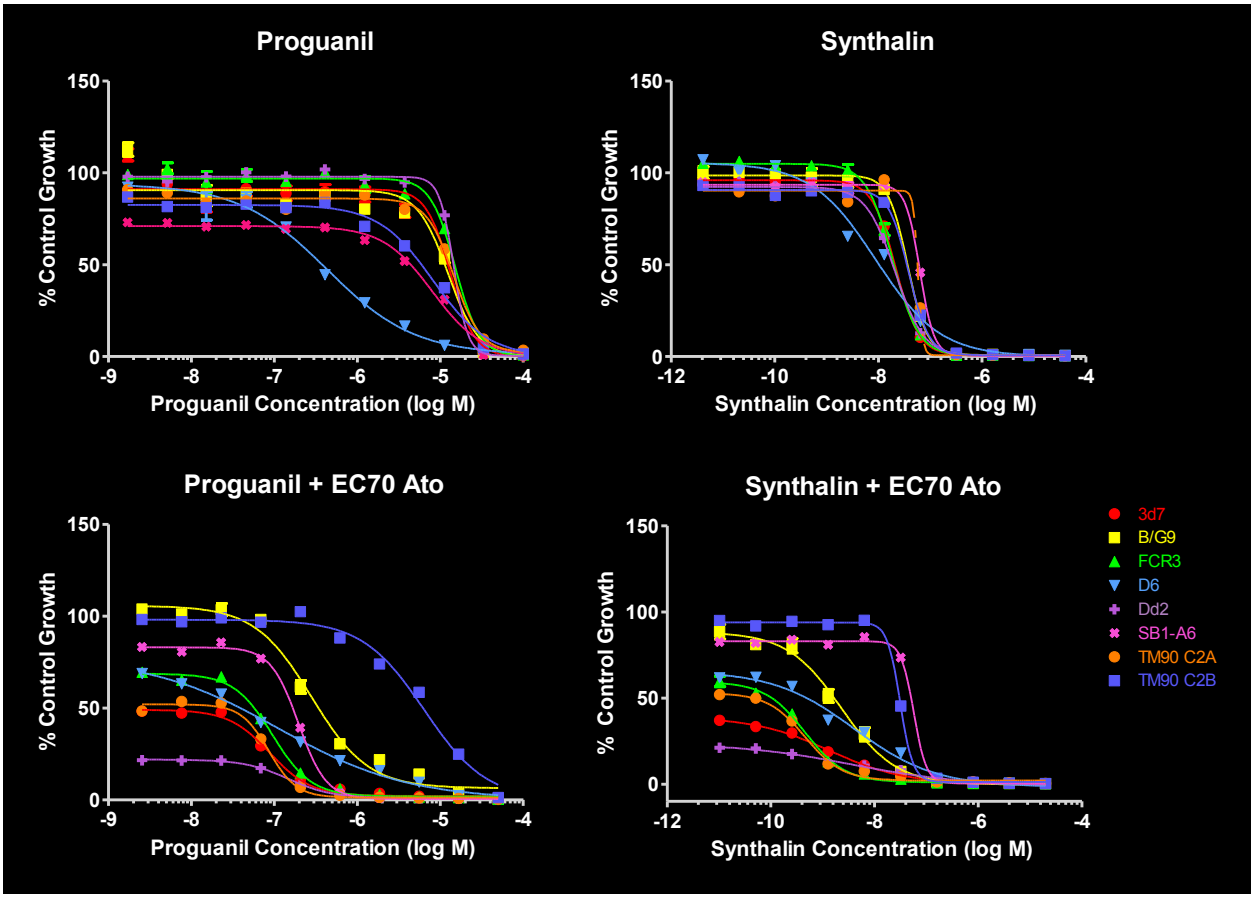

Figure 3.8 – Growth Assays Evaluating Synergy of Biguanides with Effective Concentrations of Atovaquone

Parasite growth over a 48 hour drug treatment period was assessed using ^{3}H hypoxanthine uptake assays. Parasites were treated with a set concentration of atovaquone calculated to achieve 70% growth inhibition alone, although actual results differed, while proguanil concentrations were varied. The individual EC_{50} values and synergy ratio are summarized in Table 3.3.

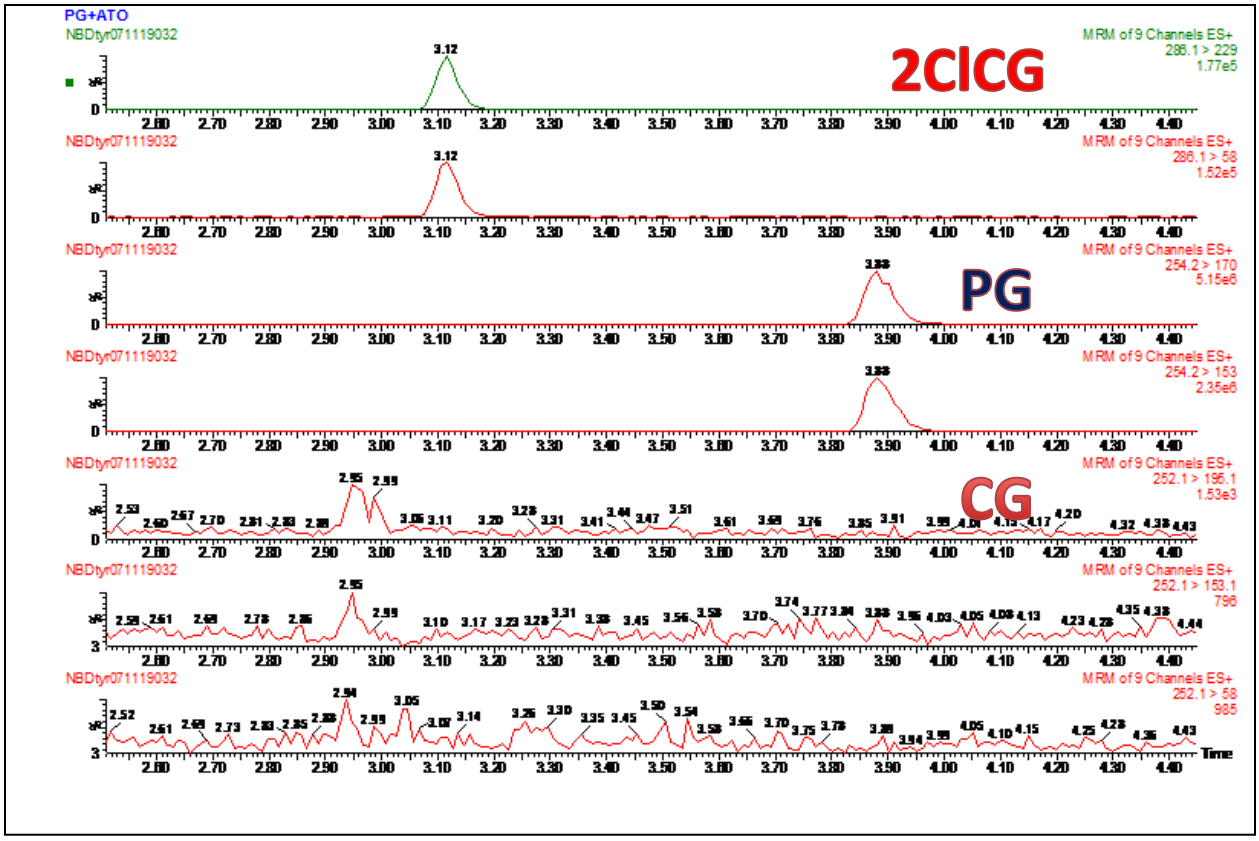

Figure 3.9 – An Example Extracted Ion Trace from UPLC-MS/MS of Flask Extracts

The elution profile and ion trace depicted is from a representative run from the *in vitro* cultures of 3d7 parasites treated with 100 nM of proguanil with 100 nM of atovaquone for 24 hours prior to solid phase extraction. Internal standard of 2-chlorocycloguanil was added to the red blood pellet immediately prior to extraction and analysis. The minor peaks for cycloguanil did not appear above the noise level of the HPLC instrument present in the Chemistry department at the time and a UPLC instrument at Medicinal Chemistry was utilized. The consistent cycloguanil signal in all three indicative ion fragmentations helps establish certainty around the important finding of low levels of proguanil activation to cycloguanil. In this run, extraction efficiency was between 13-25% for the individual compounds, as based on the extraction efficiency of the standard curve.

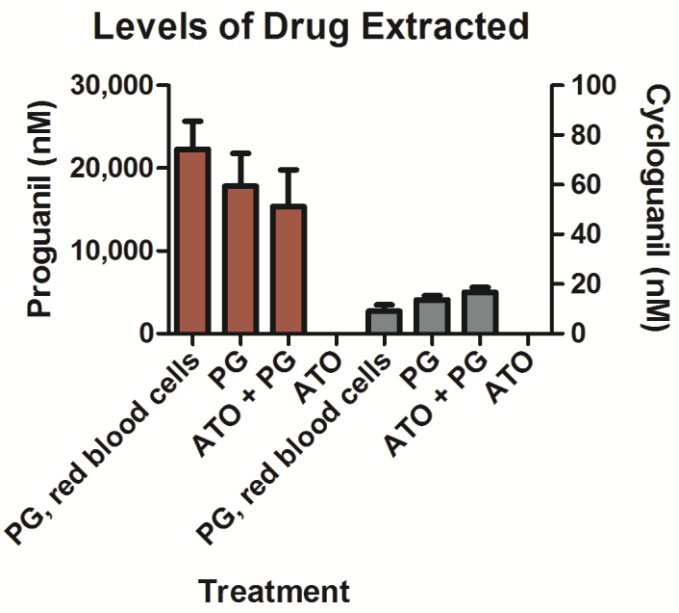

Figure 3.10 – Summary of Cycloguanil Recovered from *In Vitro* Treated Flasks

The solid phase extraction and UPLC-MS/MS assay of cell culture flask contents permitted quantification of drug quantities present in the isolated sample. The mean ± SEM level of proguanil extracted from the 1 mL red blood cell pellet was 22 ± 3 µM, 18 ± 4 µM, 15 ± 4 µM, and 0 from the conditions of no parasites, proguanil alone with parasites, proguanil and atovaquone with parasites, and atovaquone alone with parasites, respectively. The level of cycloguanil measured in that same pellet was determined to be 9 ± 3 nM, 14 ± 2 nM, 16 ± 2 nM, and 0 when averaged across at least four experiments with the same conditions. At less than 0.1% conversion, the amount of cycloguanil recovered would not be enough for the whole flask of parasites or even red blood cells to be dosed much beyond the EC_{50} concentration of 15 nM. The level of cycloguanil present could, however, contribute to other mechanisms of lethality triggered by drug treatment.

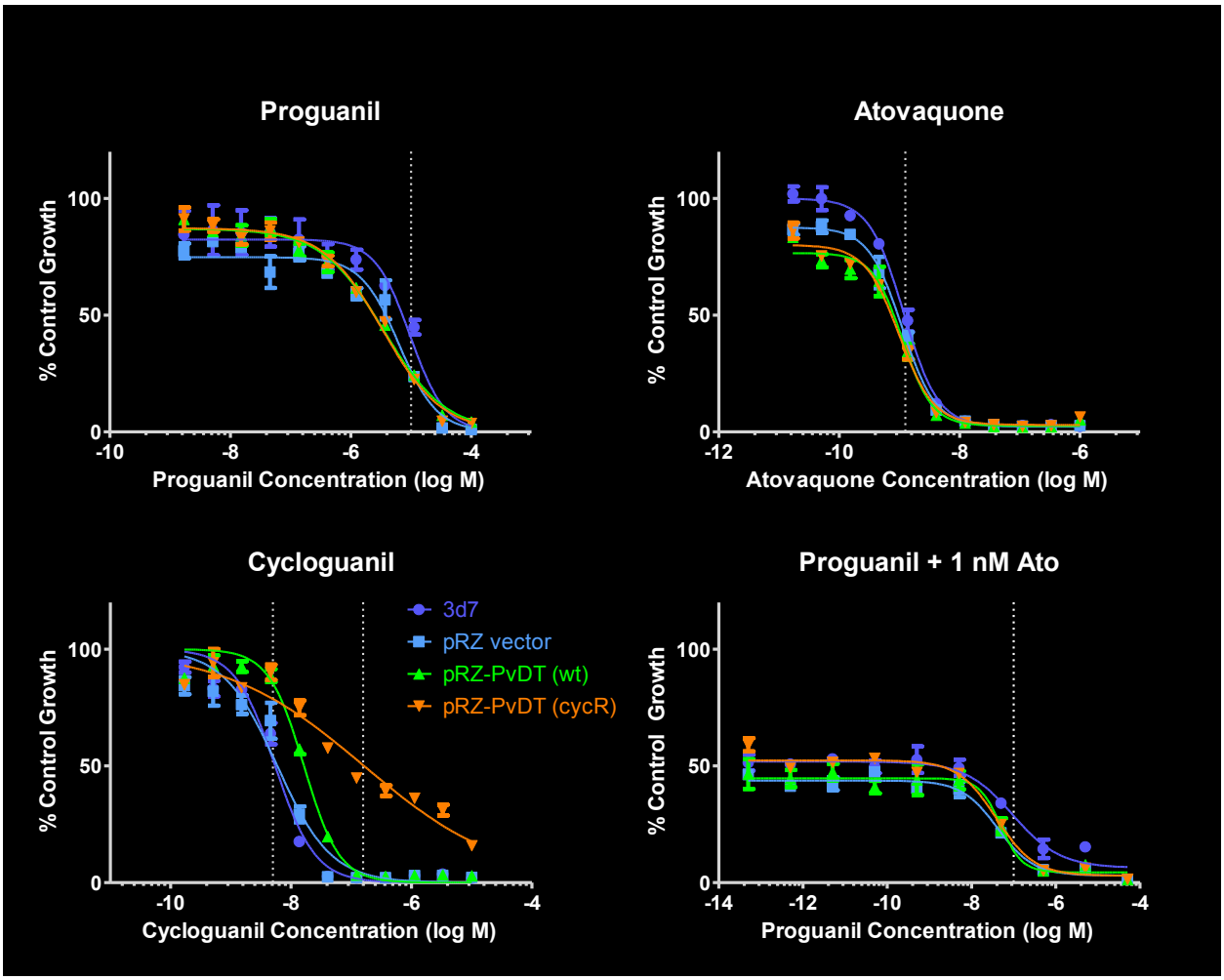

Figure 3.11 – Transfected Cycloguanil Rescue Constructs and Drug Susceptibility

Parasites were transfected with *Plasmodium vivax* DHFR-TS of either a wild type (wt) or a cycloguanil resistant (cycR) form reported to confer 1,700 fold resistance in a stronger expression system. The pRZ plasmid used here was modified to be driven by the native promoter sequence of *Plasmodium falciparum* DHFR-TS by inserting 800 bp of the 5' untranslated region. The episomal plasmid and extra *Pv*DHFR-TS gene produced did little to shift proguanil and atovaquone susceptibility. The wild type *Pv*DHFR-TS gene conferred slight resistance to cycloguanil (three fold or less) but the mutated, cycloguanil resistant *Pv*DHFR-TS conferred greater resistance to cycloguanil, between 27 – 60 fold as compared to blank plasmid or 9.7 – 37 fold as compared to wild type *Pv*DHFR-TS transfectants. The growth profile of transfected parasites with a 1 nM amount of atovaquone and variable amounts of proguanil was not appreciably different across the parasite lines assayed.

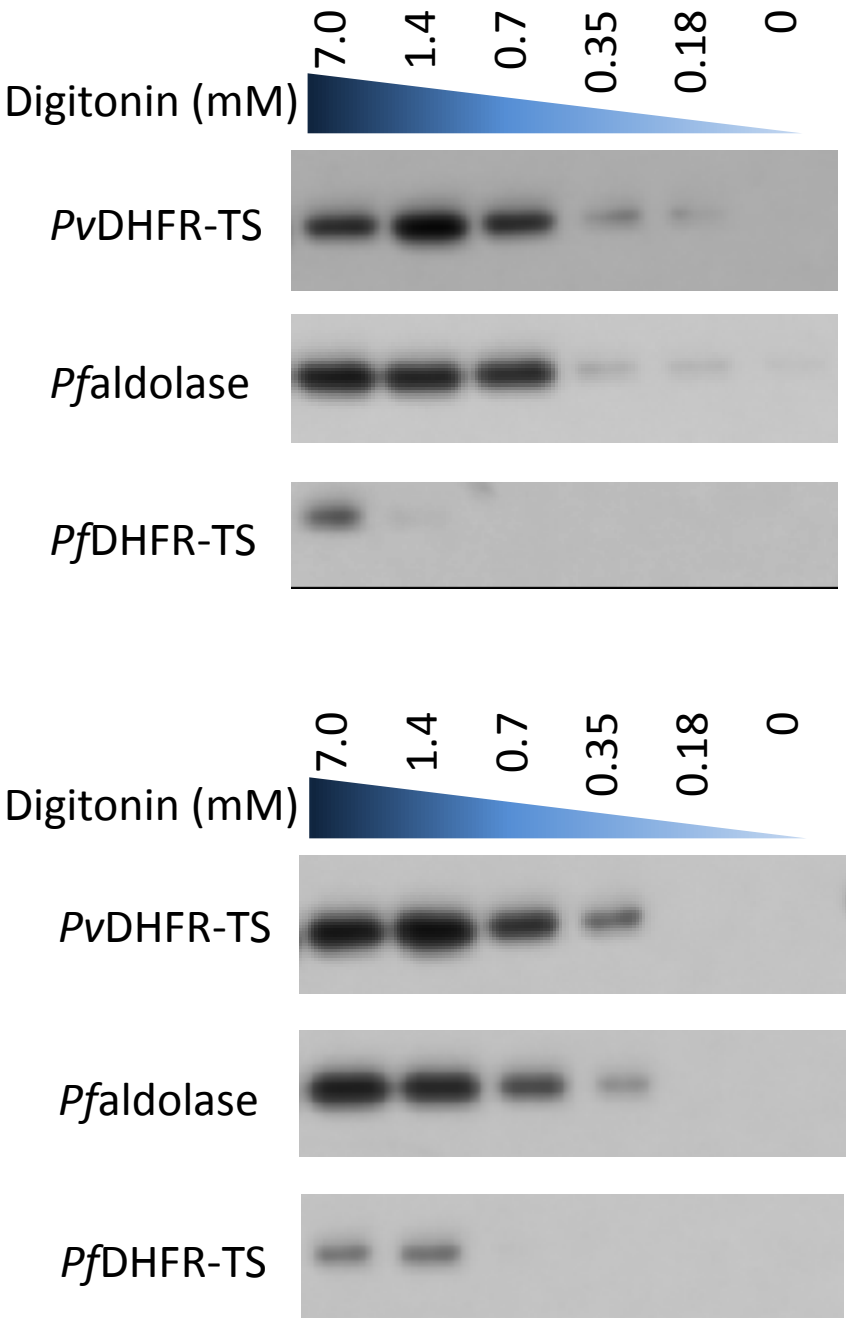

Figure 3.12 – Digitonin Permeabilization Profile of Transfected *vivax* DHFR-TS Constructs

Transfected parasites were treated with digitonin at differing concentrations to generate supernatants that were probed via Western Blot. The profile of the released *vivax* form of DHFR-TS more closely matches the release of the cytosolic protein, aldolase, than the native *falciparum* DHFR-TS. The wild type and the cycloguanil resistant *vivax* DHFR-TS containing parasites appear in the top and bottom panels, respectively.

Chapter 3 Tables

	3d7	B/G9	FCR3	D6	Dd2	SB1-A6	TM90 C2A	TM90 C2B
Proguanil	13,000	12,000	15,000	430	15,000	8,000	14,000	8,200
Cycloguanil	15	19,000	1,800	2.8	2,900	3.2	35,000	18,000
Atovaquone	4.6	8.9	1.9	0.15	6.2	98,000	14	69,000
Myxothiazol	360	460	100	68	370	53,000	750	9,000
Antimycin A	9,600	6,600	1,000	840	5,500	>100,000	96,000	>100,000
Synthalin	121	37	4.1	35	34	67	55	47

Table 3.1 - Compiled EC_{50}s (nM) for Single Drugs

Parasites from many different isolates were assayed for cell growth after 48 hours of drug exposure. All values reported in nanomoles per liter. Certain drugs with very steep curves triggered high enough error values to be considered estimates by Prism and are annotated with the value in red.

A

	3d7	B/G9	FCR3	D6	Dd2	SB1-A6	TM90 C2A	TM90 C2B
Proguanil	13	12	15	0.43	15	8.0	15	8.2
Proguanil + 0.4 nM Ato	13	34	2.1	0.29	12	6.4	37	29
Proguanil + 1 nM Ato	0.16	16	0.27	0.21	2.5	2.1	21	24
Proguanil + 5 nM Ato	0.13	0.35	0.098	0.36	0.14	0.67	0.19	24

B

	3d7	B/G9	FCR3	D6	Dd2	SB1-A6	TM90 C2A	TM90 C2B
PG/(PG+0.4Ato)	-	-	**7**	-	-	-	-	-
PG/(PG+1Ato)	**81**	-	**56**	-	**6**	-	-	-
PG/(PG+5Ato)	**100**	**34**	**153**	-	**107**	**12**	**79**	-

Table 3.2 – Compiled EC_{50}s (µM) for Proguanil and Atovaquone Mixtures and Synergy Shift Ratios (bold)

In table (A) parasites from many different isolates were assayed for cell growth after 48 hours of exposure to a mixture of variable amounts of proguanil with a fixed concentration of atovaquone. All values reported in micromoles per liter. Table (B) provides a summary of the Synergy Shift Ratio observed for each parasite strain, as calculated by the half-maximal growth inhibition of proguanil alone divided by the half-maximal growth inhibition of proguanil with atovaquone at a fixed concentration. All Synergy Shift Ratios where the determined EC_{50} concentrations differed by fourfold or less were omitted in order to highlight only the larger, synergistic variations.

	3d7	B/G9	FCR3	D6	Dd2	SB1-A6	TM90 C2A	TM90 C2B
Proguanil	13,000	12,000	15,000	430	15,000	8,000	14,000	8,200
Proguanil + EC_{70} Ato	88	280	95	110	150	195	86	6,400
PG/(PG+Ato)	**148**	**43**	**158**	**4**	**100**	**41**	**163**	**1**
Synthalin	22	37	19	8.9	21	63	58	39
Synthalin + EC_{70} Ato	1.4	2.3	0.45	4.1	3.8	57	0.46	31
Syn/(Syn+Ato)	**16**	**16**	**42**	**2**	**6**	**1**	**126**	**1**

Table 3.3 - Compiled EC_{50}s (nM) for Biguanides with EC_{70} Atovaquone and Synergy Shift Ratios (bold)

All values reported in nanomoles per liter and were the result of 48 hours of drug exposure. Synergy Shift Ratios were calculated by dividing the effective concentration to inhibit half the parasite growth for each biguanide by the value obtained for the combination of the biguanide with atovaquone at 100 nM for SB1-A6 and TM90 C2B, 5 nM for Dd2 and TM90 C2A, 1.5 nM for 3d7, B/G9, and FCR3, and 0.2 nM for D6 parasites. The magnitude and ordering of susceptibility to the synergistic combination appears divergent.

	3d7	pRZ (blank)	pRZ-PvDHFR-TS (wt)	pRZ-PvDHFR-TS (cycR)
Proguanil	9,700	6,400	3,500	3,400
Atovaquone	1.2	1.1	1.1	1.0
Cycloguanil	5.5	5.9	16.5	160
Proguanil + 1 nM ATO	95	41	49	38
PG/(PG+1ATO)	**100**	**150**	**70**	**90**

Table 3.4 - Compiled EC_{50}s (nM) for Malarone-related Antimalarials with Transfected Parasites and Synergy Shift Ratios (bold)

All values reported in nanomoles per liter and were the result of 48 hours of drug exposure followed by ^{3}H hypoxanthine uptake assays. EC_{50}s, particularly in the case of the proguanil with 1 nM atovaquone condition, were interpreted from half-maximal observed growth for individual strains. In an alternate experiment with greater cycloguanil resistance, the shape of the pRZ-PvDHFR-TS (cycR) curve for cycloguanil inhibition was elongated such that 9.4, 7.3, 12, and 440 nM were the observed concentrations for cycloguanil EC_{50} but lack of resistance to other drugs was consistent.

Strain	DHFR Codon						Notes
falciparum	**16**	**51**	**59**		**108**	**164**	
3d7	A	N	C		S	I	
D6	A	N	C		S	I	
SB1-A6	A	N	C		S	I	D6 derived
FCR3	V	N	C		T	I	
Dd2	A	I	R		N	I	
TM90 C2A	A	I	R		N	L	
TM90 C2B	A	I	R		N	L	cytochrome b Y268S
B/G9	A	I	R		N	I	+ human DHFR
vivax	**33**	**57**	**58**	**61**	**117**	**133**	
Sal-1	S	F	S	T	S	N	
AMRU-1	S	L	R	M	T	N	

Table 3.5 – Common Antifolate-Related DHFR Point Mutations in *Plasmodium* Parasites

The DHFR point mutations among various lab strains studied are indicated above. Mutations from strains considered "wild type" are highlighted in red and the table is arranged such that descending down the column imparts increasing levels of pyrimethamine (and cycloguanil) resistance. The B/G9 strain, despite being a triple mutant of Dd2 lineage, has extreme pyrimethamine resistance due to the human DHFR enzyme incorporated into its genome. *Plasmodium falciparum* codons 59 and 108 have been implicated as analogous to *Plasmodium vivax* codons 58 and 117. Also indicated is the TM90 C2B cytochrome b point mutation conferring atovaquone resistance. SB1-A6 parasites were selected with a drug similar to atovaquone until it had acquired significant resistance to electron transport chain inhibitors via an unknown mechanism.

Chapter 4 - Significance and Future Prospects

Significance

Antimalarial drugs have been targeting the folate cycle and DHFR since the 1940s. DHFR has been an antimalarial drug target for so long that large swaths of continents have populations of malaria parasites with established resistance to drugs that inhibit DHFR. A PubMed search for "malaria DHFR" results in hundreds papers but "malaria DHFR localization" yields no indication that the enzyme's localization has ever been demonstrated experimentally. Some of the same features that made DHFR a great drug target (low levels of enzyme and the polypeptide's essentiality in performing two catalytic steps in the folate cycle) also make it incredibly difficult to perform significant biological assays with the native malaria protein. Due to several ongoing investigations related to mitochondrial proteins and connections to DHFR inhibition, we decided to apply science's new generation of to determine the localization of native malarial DHFR-TS. We sought to avoid changing the native protein with epitope tags, avoid overexpression, and perform manipulations with a toolset limited by how commonly DHFR-based selection is employed.

Antibodies were generated from a panel of antigenic DHFR-TS peptides. The antibodies advanced through via multiple booster immunizations proved to be highly specific, beyond what our lab has been able to obtain using recombinant proteins [40, 183]. Malaria parasites were fixed, probed with the DHFR-TS and Alexa Fluor tagged antibodies, and a confocal laser scanning microscope utilized to generate a three

dimensional image of the malaria parasite. The malaria parasite is so small that the diffraction limits of light microscopy actually result in parasite images that are, at optimal settings, less than 100 voxels across and only about 5 voxels thick. Early studies demonstrated DHFR-TS antibodies bound and showed an odd patterning that involved more features than would be expected for a cytosolic protein, but the signal was still faint.

Advanced image analysis methods were employed to evaluate localization of the faint DHFR-TS signal with an unbiased eye. A panel of parasite organelles was evaluated to confirm that the DHFR-TS pattern aligned with that of the mitochondria. Beyond Mitotracker dye, we also employed an established HProtein-GFP fusion protein and the canonically mitochondrial membrane associated DHODH enzyme as additional markers for the mitochondria to compare with DHFR-TS. Digitonin-based selective membrane permeabilization and recovery of organellar contents served to generate additional confidence in our finding of a mitochondrial localization for *Plasmodium falciparum* DHFR-TS enzyme.

Preliminary drug susceptibility profiling of different parasite strains was responsible for leading us to develop a theory whereby cycloguanil was playing a key role in the synergistic action that makes Malarone® a successful drug. When viewed with a limited set of parasite isolates (3d7, D6, FCR3, SB1-A6, and TM90 C2B) the pattern of susceptibility to combinations of proguanil with atovaquone follows a similar susceptibility to that observed for cycloguanil. The drug susceptibility pattern also

resembles the order that would be predicted by known DHFR point mutations in the parasite strains. When additional parasite lines were brought into the comparison and the drug interactions more thoroughly calculated, the picture became murkier. Some parasite strains were not observed to display any synergy between proguanil and atovaquone; a feature reported of TM90 C2B bearing cytochrome b point mutation Y268S. However, D6 parasites also did not display synergy.

Folate uptake mechanisms, which vary in their preservation by different parasite isolates, are known to influence *in vitro* assessment of antifolate drugs. The published information regarding parasite uptake of exogenous folates is limited, but could impact susceptibility to a DHFR inhibitor like cycloguanil [184-186]. Both Dd2 and 3d7 parasites are implicated in their ability to utilize exogenous folates, but between incomplete literature on the topic and the curious change to non-synergy from TM90 C2A to TM90 C2B via cytochrome b mutation, chasing down folate uptake effects would have been a significant deviation. A full profiling of the folate salvage abilities of all eight parasite strains might elucidate if it influences the proguanil and atovaquone synergy.

In attempts to clarify the role of cycloguanil in parasites treated with proguanil and atovaquone, two investigations were launched to directly address cycloguanil. One inquiry involved using solid phase extraction of the organic components of flasks treated with Malarone® and component drugs to assess if any proguanil was being converted into cycloguanil, despite lack of a hepatic system. This would address some of the controversy surrounding proposed mechanisms of synergy. Another project was to

engineer parasites that had been directly modified to impart cycloguanil resistance. We created a rescue plasmid to impart cycloguanil resistance using a related *vivax* DHFR-TS and examined Malarone® susceptibility. Significant efforts were made to avoid over-expression and not disrupt any potential leading localization sequences by keeping a native *Plasmodium falciparum* DHFR-TS promoter, not adding additional GFP-type protein tags, and keeping the gene in the native *Plasmodium vivax* codons.

The direct quantification of cycloguanil extracted from flasks of parasites was successful in that trace amounts of cycloguanil were measured from flasks treated with proguanil. However, with 100 nM of proguanil applied to the flask's contents, the 0.07% converted to cycloguanil would be ineffective against DHFR unless some mechanism for sequestration was occurring in the parasite. Solid phase extraction efficiencies from the bulk culture remained sub-optimal at under 30%. Optimization of the extraction and quantification method was not pursued further as results of rescue plasmid experiments and more promising findings related to DHFR localization developed. However, the tools developed could be further improved and put to use to actively pursue which components (media, time, heat) are necessary or influential in converting proguanil to cycloguanil *in vitro* and possibly developed into a pulse-chase profile of what happens with this conversion before and after exposure to another drug.

Cycloguanil rescue constructs were created and validated as conferring modest cycloguanil resistance (significantly less than was reported in a different transfection system that used an antifolate-based selection for plasmid maintenance). The

observed cycloguanil resistance with the appropriate plasmid was not observed in the same parasites treated with a synergistic combination of Malarone®. Further investigation of the localization of the added *Pv*DHFR-TS enzyme using digitonin-based membrane permeabilization revealed that our construct may not have been a fully functional replacement. The bulk of the *Pv*DHFR-TS enzyme was isolated from the cytosolic fractions and may not have been able to replicate any DHFR-TS function requiring localization to the mitochondria.

Malarial DHFR has been studied for decades and even well-funded organizations and drug companies have yet to explain the synergy of Malarone® *in vitro*. It was a difficult undertaking for our academic lab with our resources to explain how this drug combination works, but combining drug target elucidation with complex biological processes like localization would not be expected to be easy.

Future Prospects

In this thesis we uncovered interesting, biologically relevant localization surrounding the well-established antimalarial drug target DHFR. We have pushed the boundaries of what can be observed in fluorescence, laser scanning confocal microscopy with a very low abundance enzyme. The brightest, most biologically compatible fluorophores were employed for these studies and we still needed to push further to determine localization. We integrated advanced image analysis techniques in order to establish the mitochondrial localization of *Plasmodium falciparum* dihydrofolate

reductase-thymidylate synthase enzyme and validated the algorithm with additional mitochondrial dyes and the membrane-bound mitochondrial protein dihydroorotate dehydrogenase.

Explorations into malaria parasite drug action, particularly those that may involve DHFR, are challenged by the limited genetic tools available. The majority of transfection systems for malaria utilize either human DHFR or drug resistant apicomplexa DHFR enzyme, leaving Blasticidin one of the only other avenues for selection. Commonly employed protein fusion epitopes such as GFP were avoided over concerns of unnatural localization possibilities. As with many other organelles, few experimentally established controls are available for mitochondrial localization with malaria. With the data from the native enzyme indicating a mitochondrial localization, one could create a fused DHFR-GFP construct in order to generate follow-up images that may also show mitochondrial signals. The biological relevance might be reduced, but the images from such a construct might be easier for the larger community to acknowledge.

Another method to support mitochondrial localization could be to isolate parasite mitochondria with nitrogen bomb cavitation and gradient centrifugation. Rupture of parasites via gas bubbles has potential to be rather harsh and destructive, but it may be used to attempt to detect high levels of DHFR protein in the mitochondrial fractions vs cytosol. Another method would have DHFR-TS protein crosslinked via formaldehyde or another chemical means and tryptic digests and MS analysis used to

evaluate if the DHFR-TS fragments were in sufficient proximity to other mitochondrial proteins to detect an increased crosslinking to mitochondrial proteins compared to crosslinking to non-mitochondrial/cytosolic protein.

A more ambitious effort would be to create new, fluorescently labelled DHFR inhibitors that are biologically compatible and bind covalently. While methotrexate is usually taken into parasites (and additional glutamic acid moieties attached) our experience was the raw enzyme inhibition was retained but bioavailability disrupted after coupling Alexa Fluor 488 or fluorescein to the glutamic acid moiety of methotrexate. A better tolerated fluorescent label or fluorescent molecule incorporated directly into a binding moiety could result in a more bio-compatible fluorescent tag for DHFR's active site. However, folic acid is a substrate for several enzymes and even minor changes to the molecule would create a need to establish the new fluorescent label's specificity prior to use as a label of DHFR.

Efforts to investigate the synergy behind Malarone® proved to be more confounding than initially expected. While a cursory examination of synergy between proguanil and atovaquone followed the trends of cycloguanil resistance, some noted exceptions and the inconsistent patterns with another reportedly synergistic biguanide, synthalin, and atovaquone cast some doubt on a cycloguanil-based mechanism. Our panel of different parasites suggests that the process of drug selection performed on D6 parasites that created the SB1-A6 strain may have also restored proguanil sensitivity and possibly a synergistic response to proguanil and atovaquone. It is hoped that further

profiling by the lab that created the parasite lines (which has more direct access to the source strain) will eventually elucidate what changes resulted in the SB1-A6 strain obtaining its unique resistance to electron transport chain inhibition while also shifting proguanil sensitivity and restoring Malarone® synergy.

An important feature of antifolates related to parasite drug susceptibility is the ability of different parasite lines to salvage folates from media. A more thorough understanding of which parasite lines retain the ability to uptake folates from media and the rate could provide insight into which parasites were experiencing DHFR-related effects. Similarly, while we've observed the result of DHFR-TS localization to the mitochondria organelle, the determining sequences and pathway DHFR-TS traverses to enter the mitochondria has not been investigated.

Flasks of media and red blood cells, after the addition of proguanil, yielded minute amounts of cycloguanil that could be detected by UPLC and Triple Quadrupole Mass Spectrometry. We employed three indicative ion fragmentations to remove ambiguity in cycloguanil identitification. Which components of the media and factors that result in the activation of proguanil to cycloguanil was not well investigated due to more promising localization observations. One method to add more confidence to this conversion (and perhaps create a tool for pulse-chase studies) would be to create an isotopically labelled proguanil that would yield a similarly labelled cycloguanil. The most direct routes for the synthesis of proguanil with commercially available isotopes that would be significantly shifted involved U-^{13}C p-chloroaniline.

The localization of the cycloguanil resistant *Pv*DHFR-TS protein produced by the rescue plasmid was subjected to digitonin permeabilization only recently. Efforts made to preserve all possibility of localizing similar to native enzyme appear to have been insufficient. Genetic manipulation of parasites can be a long process but it would be instructive to determine the drug potencies of parasites containing a more targeted version of the rescue construct. A known mitochondrial targeting/leader sequence, like that found in DHODH, could more assuredly drive localization to the mitochondria. With enough cycloguanil resistant DHFR-TS driven into the mitochondria ahead of any electron transport chain inhibition, perhaps a greater resistance to cycloguanil would be observed as well as a possible shift in the susceptibility to proguanil and atovaquone.

Appendix 1: Auxiliary Experiments

Introduction

Over the course of this project, many experiments were performed that were indicative, but don't exactly fit into the story of this thesis. One idea was to use commercially produced, fluorescently labelled methotrexate as a marker for DHFR enzyme by binding to the active site. While fluorescently labelled methotrexates were able to bind and inhibit the recombinant enzyme, the label seemed to interfere with target accessibility in raw parasites. Another series of experiments attempted to profile the parasite's response to drug treatment and how that influences localization. The difficulty is, however, that the signal from DHFR is already fairly weak and the influence of lethal amounts of drugs would be anticipated to kill the parasite.

Experimental Procedures

Materials

DHFR Active Site Label – Methotrexate

The common use of DHFR enzyme as a resistance selection marker in many assays has resulted in commercially available fluorescently tagged methotrexate (MTX). Methotrexate is a known, tight inhibitor of the malarial DHFR-TS enzyme [187]. Invitrogen/Life Technologies was our source for methotrexate conjugated to Alexa Fluor 488 *(*M23271) and methotrexate conjugated to fluorescein (M1198MP). When used as

an enzyme active-site label, the fluorescent folate analog would be a uniquely specific way to examine localization.

Methods

DHFR-TS Activity Assay Using 96-Well Plate Reader

The DHFR activity assay was modified from a cuvette based assay to be performed in a 250 µL reaction volume in a 96 well micro plate with up to 48 samples run at a time and data collected for 10 minutes. The concentrations of substrate were not modified, at 100 µM each DHF and NADPH, but the amount of enzyme was reduced to permit longer data sampling and minimize data lost during plate preparation. The working buffer (Buffer A) was created from 20 mM K_2PO_4 pH 7.0, 0.1 mM EDTA, 10% glycerol, and 10 mM DTT (added fresh before use as its breakdown seems to absorb at 340 nM). To minimize pipetting operations, three separate solutions were combined in the assay plate immediately before running. The solution containing the inhibitor was prepared first using serial dilutions in a 400 µL/well 96 well plate and contributed 35 µL to the final reaction volume. The other solutions were a 139 µM DHF solution in Buffer A that was able to be kept at room temperature and contributed 180 µL to the total reaction. The final solution, 714 µM NADPH and DHFR enzyme in Buffer A, was kept on ice and additional DHFR titrated in as necessary. The reaction was arrayed such that no outside wells of the 96 well plate were used for inhibitor (they have the greatest temperature fluctuation and were only used for no-inhibitor positive controls) and 5 replicate wells for each concentration were read at a time, up to half the plate being

setup and run during the same one to two minutes of pipetting into the assay plate. UV-permissive PMA polymer 96 well plates were used for the assay. To establish the correct amount of DHFR for an activity measurement at 340 nM of -0.02 to -0.025 Abs/min, DHFR enzyme was added in aliquots to the DHFR+NADPH solution and un-inhibited test reactions of 35 µL Buffer A, 180 µL DHF solution, and 35 µL of NADPH + enzyme solution were performed. After several additions, the appropriate activity would generally yield a linear change in absorbance for the 8-10 minute run and, depending on sample conditions, would remain acceptable for about 40 minutes before additional DHFR enzyme would need to be added and the rate of reaction verified.

For assay plates, inhibitor (in Buffer A and whatever DMSO was necessary) was arrayed from the inhibitor stock plate into the assay plates. For the other solution components basins were used to help speed up use of an 8 well pipette. DHF solution was dispensed from a basin that was at room temperature and a basin set in ice was used as the receptacle for the chilled NADPH + enzyme solution. 180 µL of the DHF solution was added to the wells of the plate which was rapidly followed by 35 µL of the NADPH + enzyme solution. The assay plate was then loaded into the plate reader, a 10 second high intensity mix step was programed to run, and then the plate was read for absorbance at 340 nm every 30 seconds for 10 minutes to yield the linear activity measurement. Pyrimethamine was often included as a negative control for its ability to inhibit enzyme activity. For most IC_{50}s, both halves of a plate were devoted to each compound such that 12 concentrations were used to construct the IC_{50} curve.

Results

Active Site Marker (Fluorescently Labelled Methotrexate) Not Cell Permeable

We desired to leverage the DHFR active site binding ability of methotrexate by using fluorescently tagged methotrexates as a probe for DHFR in microscopy studies. However, adding the fluorescent label to the MTX molecule has the potential to reduce the binding ability of methotrexate.

The ability of the fluorescently labeled methotrexates to inhibit the *Pf*DHFR-TS enzyme was examined using split, recombinant DHFR + TS enzyme [183]. In the NADPH consumption assay the DHFR (+ TS) enzyme, NADPH, and dihydrofolic acid were combined with various concentrations of methotrexate, methotrexate conjugated to Alexa Fluor 488, or methotrexate conjugated to fluorescein. The reaction progress was monitored as a function of time on a UV-Vis absorbance plate reader measuring at 340 nm. Methotrexate and the fluorescently labeled versions all produced similar low nanomolar IC_{50} inhibition levels, at 1.5 to 3.8 nM (Figure A1.1 A). The experiment demonstrates that the covalently bound fluorescent label does not significantly disrupt the ability of the methotrexate molecule to inhibit the DHFR enzymatic reaction.

In contrast, parasites assayed for the EC_{50} in the presence of methotrexate and fluorescently labeled methotrexates for 48 hours showed that while methotrexate is

lethal to the parasite with an EC_{50} of 11 nM the fluorescent label conjugation results in an approximately 200-fold elevated EC_{50} of ~2,200 nM (Figure A1.1 B).

Malarone® Drug Exposure – A Slow Change?

Eventually, we desired to see if the localization of DHFR-TS was disrupted by Malarone® treatment. A perfect experiment was made more difficult by our inability to rescue from proguanil and atovaquone with *Pv*DHFR-TS, so we took a straight-forward approach to see what was observable. Asynchronous cultures of integrated HProtein-GFP expressing Dd2 parasites from the Prigge lab were exposed to 100 nM of both proguanil and atovaquone or 100 nM of chloroquine 12, 3, and 0 hours prior to workup. Previous experiments with live cell imaging utilizing just Mitotracker and the native GFP fluorescence had indicated significant loss of fluorescence by 24 hours. The treated samples were processed, the nucleus marked with DAPI, and images captured on the confocal microscope.

The colocalization values for drug-treated parasites that were imaged were extremely variable. Additionally, analysis was confounded by the signal for the mitochondrial HProtein-GFP fading in a significant population of parasites by 12 hours. While the parasites were able to be imaged, in this set of experiments it was difficult to see if the proguanil and atovaquone signal was changing at a rate faster than chloroquine, a fast-acting drug with a different target from that suspected for Malarone®.

Discussion

Fluorescently Labelled Methotrexates

Commercially available fluorescently labelled methotrexates were also investigated for use in labelling fixed cells at the DHFR active site and for any localization after irreversibly binding to the enzyme. The presence of the fluorophore attached to the glutamic acid moiety was not appreciably disruptive to DHFR enzymatic activity as measured on the native enzyme (Figure A1.1 A). However, the fluorophore interfered with the ability to kill whole cells and resulted in a 200 fold reduction in potency (Figure A1.1 B), presumably due to reduced uptake or triggered deactivation mechanisms. The inability to use bioaccumulation processes to help drive DHFR labelling by fluorescent methotrexates limited their use to methods that could bypass parasite membranes and permeability issues.

The fluorescently labelled methotrexates were attempted to be used as probes for confocal microscopy, being applied in methods analogous to an antibody, but the minor amount of fluorescent signal obtained could not be discriminated from that of background fluorescence of the fixed samples. It is possible the DHFR active site is simply unable to bind an inhibitor after being fixed, proteins cross-linked, and cell membranes washed away by detergents as a part of the sample preparation process.

Malarone® Drug Exposure

Examination of localization of proteins as a parasite is also being given a lethal amount of drug is not a process that is easy to tease a cause and effect relationship out of. We'd hoped that a rescue construct that would replace DHFR's function would assist our studies, but ultimately that rescue construct was ineffective against the proguanil and atovaquone combination. Despite not having a way to control for protein turnover that would allow us to distinguish the fade of old proteins from the generation of new ones and our mitochondrial marker being influenced by the same protein turnover, we performed a limited number of experiments examining the effect of proguanil and atovaquone treatment on localization of DHFR in HProtein containing parasites. The results were inconclusive, with rather large error bars and processing issues related to attempting repeatable thresholding of images as the signals faded.

With a more clever design involving the ability to control when the proteins are actively transcribed and possibly the introduction of a modified amino acid that could be detected by antibody might make this a type of examination more complete. If our rescue construct worked, it would have been interesting to see if the native DHFR-TS localization was disrupted by drug treatment. Unfortunately, the long and difficult process of genetic manipulation in malaria parasites did not permit free experimentation with such designs.

Appendix 1 Figures

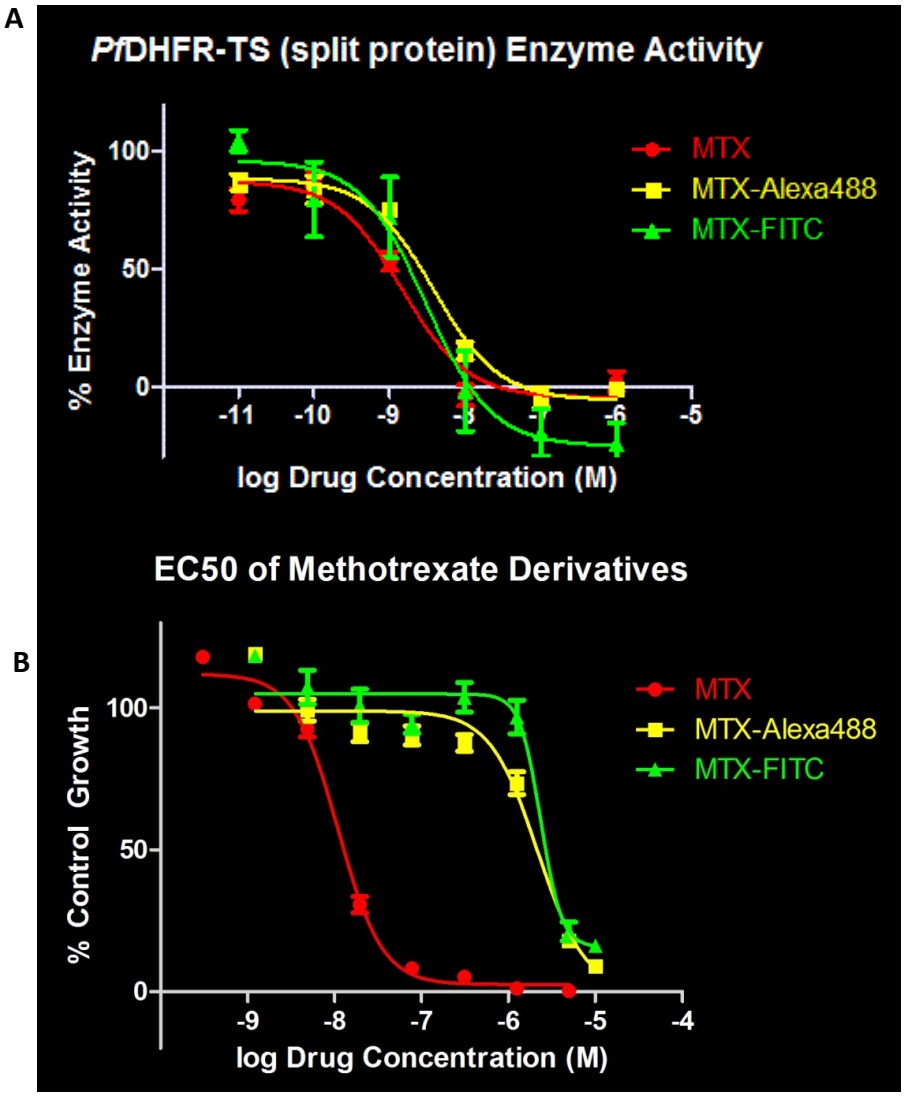

Figure A1.1 – Fluorescently Labelled Methotrexate Not Able to Penetrate Cells

Following several experiments where fluorescently-tagged methotrexates were unsuccessfully attempted to be used as markers for DHFR-TS enzyme, a more thorough failure analysis was performed. In experiment A) DHFR-TS enzyme activity was assayed in the presence of methotrexate and the fluorescently labelled analogs and the observed inhibition was between 1.3 and 3.8 nM. B) When whole parasites were treated for 48 hours with the methotrexates, the fluorescent labels result in a 200-fold loss in potency in whole cells (shifting from 11 nM to 2,200 – 2,400 nM), suggesting uptake and drug permeability may be preventing standard methotrexate potency.

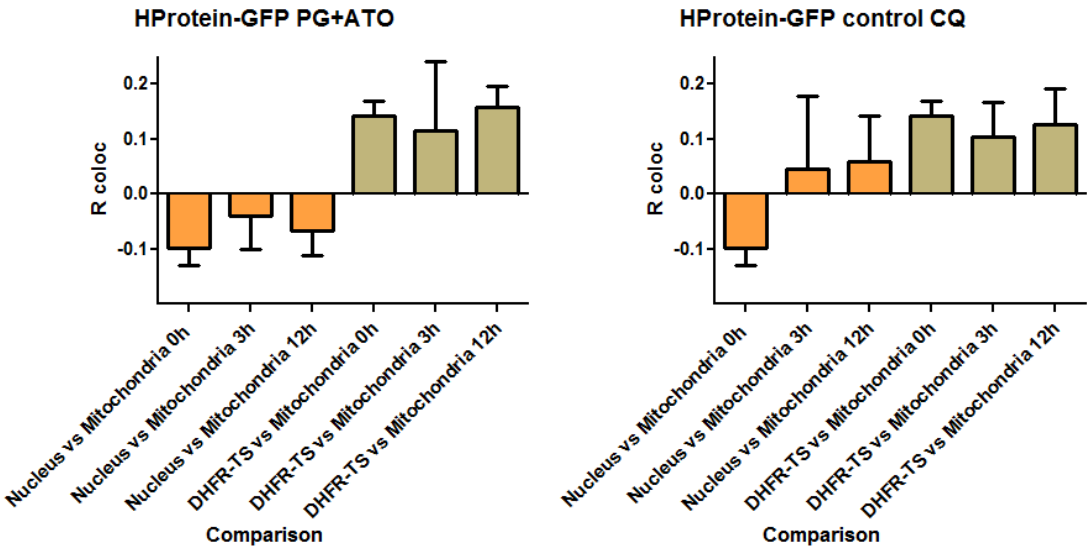

Figure A1.2 – Limited Observations of Drug-Treated Parasites Uncertain

HProtein-GFP containing Dd2 parasites were treated with 100 nM proguanil and atovaquone or 100 nM chloroquine for 3 or 12 hours prior to slide preparation. Overall, colocalization values did not appear to drastically change. Confounding the analysis, the mitochondrial HProtein-GFP signal was reduced by 12 hours, an unknown rate of protein turnover makes it difficult to judge which are new localization events vs the loss of old, and a protocol where images are thresholded individually makes for a shifting baseline and may lose data about the quantities of enzyme present.

Appendix 2: General Experimental Procedures

Materials

Digitonin Permeabilization Reagents

Digitonin was procured from Sigma Aldrich (D141) and prepared as either a 40 or 50 mg/mL stock in DMSO. Parasite wash buffer was prepared from PBS with 3% w/v sucrose and a tablet of cOmplete, EDTA-free protease inhibitor cocktail (Roche). Antibodies used were rabbit polyclonal anti-*Pf* aldolase HRP conjugated (abcam ab38905, 1 mg/mL), mouse monoclonal anti-GFP (clone B2) (Santa Cruz sc9995, 0.2 mg/mL), rabbit polyclonal anti-*Pf* DHFR-TS (GenScript custom, 0.6 mg/mL), rabbit polyclonal anti-*Pv*DHFR-TS (GenScript custom, 0.6 mg/mL), HRP conjugated goat anti-mouse (Santa Cruz sc2301, 0.4 mg/mL), and HRP conjugated goat anti-rabbit (Santa Curz sc2302, 0.4 mg/mL).

Western Blot Reagents

Lysis buffer for malaria parasite samples was composed of 50 mM Tris pH 8.0, 5 mM EDTA, and 0.5 % Triton X 100 in water. Additionally, Bio-Rad Laemmli 2x Sample Buffer was used for loading the samples. For wet transfers performed overnight, a 500 mL volume of 10x Bio-Rad wet transfer solution was made from 15 g Tris Base, 72 g of glycine, and 2.5 g of SDS and made up as a 1x solution with 10% methanol for immersive transfers. TBST solutions were made with 0.1% Tween from 1L of a 10x stock comprised of 88 g NaCl, 24 g TrisCl, 5.6 g Tris base, and 10 mL of Tween 20 all adjusted to pH 7.6 after preparation of the stock as well as after preparation of each 1x working solution.

General Methods

Continuous Growth of Blood-Stage Parasites

Plasmodium falciparum blood-stage parasites and transfectants were cultured with human erythrocytes at 2% hematocrit in RPMI-1640 media (Life Technologies #22400-89 +Glu +25 mM HEPES) supplemented with 20% human serum using a protocol previously described [188]. Cultures were maintained in sterile conditions in a biosafety level 2 hood. All instruments and equipment were purchased sterile, sterilized by 70% ethanol spray, or filtered using bottle-top 20 micron filters. All culture waste was either mixed with bleach to 10% v/v to sterilize or collected in autoclave bags and autoclaved according to University of Washington regulations prior to disposal.

Continuous parasite culture required fresh blood, media, and, for transfected lines, new selective agents at regular intervals. Flasks and plates of parasite cultures were grown under 90% N_2, 5% CO_2, and 5% O_2 atmosphere with media changes and infected culture dilutions occurring every ~48 hours to keep parasitemia below 5%. Use of cultures desired to be at high parasitemia was typically assisted by changing the media every 24 hours for a full life cycle in order to maximize nutrients available to the parasites. Red blood cells were prepared via a two stage wash/centrifugation in RPMI and the white buffy coat of white blood cells was removed after each centrifugation step to ensure only red blood cells were being introduced. Such prepared red blood cells were viable for up to a month without significant growth abnormalities in the

parasites infecting the red blood cells. A knobbed appearance to the membrane could be noticed when red blood cells were of sufficient age to inhibit parasite replication appreciably.

Western Blotting

Sample Preparation

Parasite pellets were prepared using traditional Saponin lysis treatment and then resuspended in parasite lysis buffer (typically around 0.1 mL for each T25 flask). The parasites mostly dissolved in the lysis buffer with mechanical agitation using a pipet tip or they benefitted from a -80 °C freeze-thaw step. The appropriate amount of lysate was diluted with 2x Laemmli buffer and boiled for 5 minutes, cooled to room temperature, and then spun at 10,000 x g for 2 minutes to prevent introduction of insoluble components.

Electrophoresis and Transfer

The SDS-PAGE gels were run according to standard methods, released from the cassette, fringes from the top of the comb removed, washed individually in trays of about 50 mL of water, and then soaked in Bio-Rad wet transfer solution for at least 10 minutes on a rocking platform. The Mini Protean immersive transfer tank was then setup with a stir bar at the bottom, most of the liquid added, and a pre-chilled cold pack and a station with a stir plate and power supply prepared in the cold room. The gel was loaded into the plastic transfer cassette with care that the black half was negative and

proteins would be directed to the positive/red/clear side of our apparatus. Assembly of the transfer sandwich was done in an oversized tray that was filled with wet transfer buffer. Another tray was used to expose PVDF membrane to methanol for a few minutes before assembly. The plastic cassette was put into the transfer buffer tray followed by the two reusable sponges in order to hydrate and remove air bubbles. The top sponge was lifted away and a layer of filter paper was placed on top of the lower sponge, followed by the gel, followed by the methanol treated PVDF membrane, followed by another layer of filter paper, followed by the second reusable sponge while avoiding any air bubbles or mis-aligned pieces. The cassettes were loaded into the wet transfer apparatus and the tank topped off to avoid any components not being immersed and drying out. Transfer was performed for approximately 14 hours using the overnight method at 30 volts and 80 milliamps if only one transfer box was used, 120 milliamps if two. After the overnight transfer, the cassettes were opened and the PVDF membrane transferred to a tray containing transfer buffer and the edges of the membrane were trimmed with scissors to reduce the size of the membrane down to more appropriately match the size of the gel (prestained ladders in the outer lanes made this straightforward). The top corner corresponding to lane 1 of the gel was "nicked" to help provide a consistent orientation to the blots.

Antibody Probing

The blots were generally blocked with 5% BioRad blocking buffer (non-fat milk of fine grind) in TBST at room temperature for a minimum of two hours. After blocking,

the primary antibody (1:5,000 dilution as a starting point) was applied in a solution of 4% milk in TBST. Best performance was typically achieved by overnight exposure to the primary antibody in this solution at 4 °C on a rocker in the cold room. The following morning the antibody solution was removed and the blot washed with 4% milk in TBST at least twice for 15 minutes, followed by additional TBST washes as desired. The secondary antibody was generally applied in 4% milk TBST solution at room temperature (1:50,000 Santa Cruz HRP conjugated secondary antibody dilution as a starting point) for approximately 3 hours. Afterwards, the blot was washed at room temperature with 4% milk in TBST at least twice for between 5 and 10 minutes each, followed by at least 3 TBST washes of similar length. Imaging was performed with Amersham ECL Prime and Lumi-Film Chemiluminescence Detection Film in a dark room with appropriate Kodak GBX fixer/developer solutions.

Digitonin Permeabilization Method

A non-microscopy method to examine localization was employed using digitonin to separate out the contents of each membrane-bound component of the parasite. Digitonin is a non-ionic detergent that may be used to permeabilize cell membranes. Digitonin complexes with sterols, with cholesterol as the primary partner in eukaryote cells, and causes rupture of the membrane. The different membranes of cells often have their properties fine-tuned by having a varied composition, including different ratios of cholesterol. The various ratios of cholesterol provide an opportunity to selectively permeabilize the different membranes by incubating them with varied

concentrations of digitonin. Differential susceptibility to digitonin permeabilization has been used to achieve rupture of the cytosolic contents versus the organellar contents for the recovery and assay of native enzymes from many different cell types[189], including more recent usage to assay asexual bloods stage malaria parasites [190-192]. The level of control of selective membrane permeabilization is limited, but others have used it to support the comparison of cytosolic localization to a specific organelle with some success. In malaria parasites, the trends are for mitochondrial fractions to release in the range of low, single millimolar concentrations rather sharply while cytosolic components are lysed more gradually, centered around the lower hundreds of micromolar range.

Bulusu *et al* performed experiments using malaria parasites and digitonin permeabilization at concentrations of 7, 3.5, 0.7, 0.35, 0.17, 0.08 and 0 mM digitonin, finding that the mitochondrial protein was released between 3.5 mM - 0.7 mM while the cytosolic protein had a more gradual release between 0.7, 0.35, and 0.17 mM concentrations of digitonin [190]. Hodges *et al* performed similar experiments at the concentrations of 10, 2.5, 0.5, 0.3, 0.1, and 0 mM digitonin, with the mitochondrial protein being released between 2.5 - 0.5 mM [192]. Hodges also observed cytosolic content release as even more spread out than observed by Bulusu, but the 50% point was between 0.5 - 0.3 mM. In all, mitochondrial membranes appear about 50% permeabilized near 1 mM with what may be a sharper release than cytosolic proteins, which appear centered about 0.3 mM.

To perform digitonin assays, parasites were prepared by first growing three 10 mL cultures of 2% hematocrit and approximately 4% parasitemia or greater. The excess media was removed and infected red blood cells were resuspended in 20 mL of ice cold PBS. The infected red blood cells were pelleted at 1,000 x g for 5 minutes in a 4 °C swinging bucket centrifuge. The supernatant was removed and replaced with 10 mL of fresh wash solution. Saponin from 12% w/v stock was added to lyse the RBCs at 0.03% w/v on ice for 2 minutes. When the red blood cells were lysed additional cold wash solution was added of equal volume. The freed parasites were then spun at 4,000 x g for 6 minutes to pellet. The supernatant was removed and the pellet was gently resuspended in approximately 5 mL of ice cold wash buffer. The pellet was then spun at 4,000 x g for 3 minutes. The supernatant was again removed from the pellet and the pellet was resuspended in 3 mL of ice cold wash buffer for this final wash. The pellet was then spun at 4,000 x g for 3 minutes, the supernatant removed, and a final aliquot of approximately 200 µL of ice cold wash buffer was added to the pellet. The color of supernatants removed from the parasites quickly faded from red to faint tan color by the last wash. More forceful shaking was used to resuspend the parasites in the buffer to make a parasite suspension that would be used for further experiments.

A total parasite lysate sample of 50 µL was made from 25 µL of the parasite suspension combined with 25 µL of 2x Laemmli buffer. Prior to harvesting the parasites, microcentrifuge tubes were prepared with 5 µL of the PBS wash buffer or digitonin from 35 and 3.5 mM intermediate stocks such that concentration of digitonin in each sample

after adding 20 µL of parasite suspension would be 7, 1.4, 0.7, 0.35, 0.18, and 0 mM digitonin. The digitonin aliquot tubes were chilled and 20 µL of the parasite suspension was added to the wall of the tube while on ice. The parasite suspension was "flicked" down into the digitonin, the mixture quickly mixed, and a water bath at 37 °C was then used to incubate the mixture for two minutes. After two minutes, the samples were removed back to an ice bath and then placed in a 4°C chilled fixed angle centrifuge and the samples spun at 20,000 x g for two minutes to separate the components present in the supernatant from what was still in the pellet. The supernatant was carefully removed to a new microcentrifuge tube that had been prepared with 25 µL of 2x Laemmli buffer. To the pellet samples, 20 µL of PBS was added followed by 25 µL of 2x Laemmli buffer. The samples were then mixed forcefully to help solubilize the pellet and the samples incubated at 95 °C for 6 minutes. The samples were then quickly frozen at -80°C until time permitted to run the Western blots.

The proteins present in the digitonin-treated samples were separated using 15 well SDS-PAGE gels of a 4-15% gradient. A total of 10 µL of each sample was loaded per lane, relative to 7.5 µL of Precision Plus WesternC prestained protein ladder (Bio-Rad 161-0376) and 10 µL of Precision Plus Dual Color prestained protein ladder loaded in the outside lanes. The gel contents were transferred and probed as described in the Western blot protocol. To mark the release of different organelle contents, several antibodies to proteins of known location were used including the malaria parasite aldolase (Abcam ab38905), GFP as part of a protein-fusion tag (Santa Cruz sc9995), and

the antibodies to malaria parasite DHFR-TS that were generated with GenScript's service. Primary antibodies were generally applied in a 5% milk-TBST solution at a 1:5,000 fold dilution. The aldolase antibody was applied at 1:2 million via an intermediary stock solution. For a uniform clarity in figures, the data was reduced so that the supernatant bands of each appropriate protein were shown.

Bibliography

1. Hay, S.I., et al., *The global distribution and population at risk of malaria: past, present, and future.* Lancet Infect Dis, 2004. **4**(6): p. 327-36.
2. Snow, R.W., et al., *The global distribution of clinical episodes of Plasmodium falciparum malaria.* Nature, 2005. **434**(7030): p. 214-7.
3. World Health Organization., *World Malaria Report*, 2010, World Health Organization: Geneva, Switzerland. p. v.
4. Murray, C.J., et al., *Global malaria mortality between 1980 and 2010: a systematic analysis.* Lancet, 2012. **379**(9814): p. 413-31.
5. Sachs, J. and P. Malaney, *The economic and social burden of malaria.* Nature, 2002. **415**(6872): p. 680-5.
6. Perry, A., *Battling a scourge. Malaria has plagued us for centuries but a new model for global aid could change the game.* Time, 2010. **175**(24): p. 37, 39-40, 42.
7. Burrows, J.N., et al., *Antimalarial drug discovery - the path towards eradication.* Parasitology, 2014. **141**(1): p. 128-39.
8. Slutsker, L. and S.P. Kachur, *It is time to rethink tactics in the fight against malaria.* Malar J, 2013. **12**: p. 140.
9. Liu, W., et al., *Origin of the human malaria parasite Plasmodium falciparum in gorillas.* Nature, 2010. **467**(7314): p. 420-5.
10. Tan, S.Y. and A. Ahana, *Charles Laveran (1845-1922): Nobel laureate pioneer of malaria.* Singapore Med J, 2009. **50**(7): p. 657-8.
11. Bruce-Chwatt, L.J., *Alphonse Laveran's discovery 100 years ago and today's global fight against malaria.* J R Soc Med, 1981. **74**(7): p. 531-6.
12. Capanna, E., *Grassi versus Ross: who solved the riddle of malaria?* Int Microbiol, 2006. **9**(1): p. 69-74.
13. Cox-Singh, J., et al., *Plasmodium knowlesi malaria in humans is widely distributed and potentially life threatening.* Clin Infect Dis, 2008. **46**(2): p. 165-71.
14. Miller, L.H., et al., *The pathogenic basis of malaria.* Nature, 2002. **415**(6872): p. 673-9.
15. Jongwutiwes, S., et al., *Naturally acquired Plasmodium knowlesi malaria in human, Thailand.* Emerg Infect Dis, 2004. **10**(12): p. 2211-3.
16. Collins, W.E. and G.M. Jeffery, *Plasmodium ovale: parasite and disease.* Clinical microbiology reviews, 2005. **18**(3): p. 570-81.
17. Collins, W.E. and G.M. Jeffery, *Plasmodium malariae: parasite and disease.* Clinical microbiology reviews, 2007. **20**(4): p. 579-92.
18. Collins, W.E., *Plasmodium knowlesi: a malaria parasite of monkeys and humans.* Annu Rev Entomol, 2012. **57**: p. 107-21.
19. Sherman, I.W. and A.S.f. Microbiology., *The power of plagues*2006, Washington, D.C.: ASM Press.

20. Cowman, A.F., D. Berry, and J. Baum, *The cellular and molecular basis for malaria parasite invasion of the human red blood cell.* J Cell Biol, 2012. **198**(6): p. 961-71.
21. Su, X., K. Hayton, and T.E. Wellems, *Genetic linkage and association analyses for trait mapping in Plasmodium falciparum.* Nat Rev Genet, 2007. **8**(7): p. 497-506.
22. Hekmat-Nejad, M. and P.K. Rathod, *Plasmodium falciparum:Kinetic Interactions of WR99210 with Pyrimethamine-Sensitive and Pyrimethamine-Resistant Dihydrofolate Reductase.* Experimental Parasitology, 1997. **87**(3): p. 222-228.
23. Cowman, A.F. and B.S. Crabb, *Invasion of red blood cells by malaria parasites.* Cell, 2006. **124**(4): p. 755-66.
24. Reyes, P., et al., *Enzymes of purine and pyrimidine metabolism from the human malaria parasite, Plasmodium falciparum.* Mol Biochem Parasitol, 1982. **5**(5): p. 275-90.
25. Bungener, W. and G. Nielsen, *[Nucleic acid metabolism in experimental malaria. 1. Studies on the incorporation of thymidine, uridine, and adenosine in the malaria parasite (Plasmodium berghei and Plasmodium vinckei)].* Z Tropenmed Parasitol, 1967. **18**(4): p. 456-62.
26. Sherman, I.W., *Biochemistry of Plasmodium (malarial parasites).* Microbiol Rev, 1979. **43**(4): p. 453-95.
27. Mitchell, H.K., E.E. Snell, and R.J. Williams, *THE CONCENTRATION OF "FOLIC ACID".* Journal of the American Chemical Society, 1941. **63**(8): p. 2284-2284.
28. Farber, S., et al., *The action of pteroylglutamic conjugates on man.* Science, 1947. **106**(2764): p. 619-621.
29. Farber, S., et al., *Temporary Remissions in Acute Leukemia in Children Produced by Folic Acid Antagonist, 4-Aminopteroyl-Glutamic Acid (Aminopterin).* New England Journal of Medicine, 1948. **238**(23): p. 787-793.
30. Sirawaraporn, W., et al., *The dihydrofolate reductase domain of Plasmodium falciparum thymidylate synthase-dihydrofolate reductase. Gene synthesis, expression, and anti-folate-resistant mutants.* J Biol Chem, 1993. **268**(29): p. 21637-44.
31. McGuire, J.J., *Anticancer antifolates: current status and future directions.* Curr Pharm Des, 2003. **9**(31): p. 2593-613.
32. Maegraith, B.G., A.R. Adams, and et al., *Studies on synthetic antimalarial drugs; results of a preliminary investigation of the therapeutic action of 4888 (paludrine) on acute attacks of malignant tertian malaria.* Ann Trop Med Parasitol, 1945. **39**: p. 232-6.
33. Curd, F.H., D.G. Davey, and F.L. Rose, *Studies on synthetic antimalarial drugs; some biguanide derivatives as new types of antimalarial substances with both therapeutic and causal prophylactic activity.* Annals of tropical medicine and parasitology, 1945. **39**: p. 208-16.
34. Peterson, D.S., W.K. Milhous, and T.E. Wellems, *Molecular basis of differential resistance to cycloguanil and pyrimethamine in Plasmodium falciparum malaria.* Proc Natl Acad Sci U S A, 1990. **87**(8): p. 3018-22.

35. Nzila, A., *The past, present and future of antifolates in the treatment of Plasmodium falciparum infection.* J Antimicrob Chemother, 2006. **57**(6): p. 1043-54.
36. Abeles, R.H., P.A. Frey, and W.P. Jencks, *Biochemistry*1992, Boston: Jones and Bartlett. xxii, 884 p.
37. Hyde, J.E., *Drug-resistant malaria - an insight.* FEBS J, 2007. **274**(18): p. 4688-98.
38. Chaudhary, K. and D.S. Roos, *Protozoan genomics for drug discovery.* Nat Biotechnol, 2005. **23**(9): p. 1089-91.
39. Gardner, M.J., et al., *Genome sequence of the human malaria parasite Plasmodium falciparum.* Nature, 2002. **419**(6906): p. 498-511.
40. Zhang, K. and P.K. Rathod, *Divergent regulation of dihydrofolate reductase between malaria parasite and human host.* Science, 2002. **296**(5567): p. 545-547.
41. Falco, E.A., et al., *2:4-diaminopyrimidines- a new series of antimalarials.* British journal of pharmacology and chemotherapy, 1951. **6**(2): p. 185-200.
42. McKie, J.H., et al., *Rational drug design approach for overcoming drug resistance: application to pyrimethamine resistance in malaria.* J Med Chem, 1998. **41**(9): p. 1367-70.
43. Sirawaraporn, W., *Dihydrofolate reductase and antifolate resistance in malaria.* Drug Resist Updat, 1998. **1**(6): p. 397-406.
44. McCutchan, T.F., et al., *Mechanism of pyrimethamine resistance in recent isolates of Plasmodium falciparum.* Antimicrobial Agents and Chemotherapy, 1984. **26**(5): p. 656-9.
45. Auliff, A., et al., *Amino acid mutations in Plasmodium vivax DHFR and DHPS from several geographical regions and susceptibility to antifolate drugs.* Am J Trop Med Hyg, 2006. **75**(4): p. 617-21.
46. Gregson, A. and C.V. Plowe, *Mechanisms of resistance of malaria parasites to antifolates.* Pharmacol Rev, 2005. **57**(1): p. 117-45.
47. Wang, P., et al., *Sulfadoxine resistance in the human malaria parasite Plasmodium falciparum is determined by mutations in dihydropteroate synthetase and an additional factor associated with folate utilization.* Mol Microbiol, 1997. **23**(5): p. 979-86.
48. Davies, C.S., et al., *The causal prophylactic activity of the novel hydroxynaphthoquinone 566C80 against Plasmodium berghei infections in rats.* Acta Leidensia, 1989. **58**(2): p. 115-28.
49. Olszewski, K.L., et al., *Branched tricarboxylic acid metabolism in Plasmodium falciparum.* Nature, 2010. **466**(7307): p. 774-8.
50. van Dooren, G.G., L.M. Stimmler, and G.I. McFadden, *Metabolic maps and functions of the Plasmodium mitochondrion.* FEMS Microbiol Rev, 2006. **30**(4): p. 596-630.
51. Gutteridge, W.E., D. Dave, and W.H. Richards, *Conversion of dihydroorotate to orotate in parasitic protozoa.* Biochimica et biophysica acta, 1979. **582**(3): p. 390-401.

52. Painter, H.J., et al., *Specific role of mitochondrial electron transport in blood-stage Plasmodium falciparum.* Nature, 2007. **446**(7131): p. 88-91.
53. Chiodini, P.L., et al., *Evaluation of atovaquone in the treatment of patients with uncomplicated Plasmodium falciparum malaria.* J Antimicrob Chemother, 1995. **36**(6): p. 1073-8.
54. Looareesuwan, S., et al., *Clinical studies of atovaquone, alone or in combination with other antimalarial drugs, for treatment of acute uncomplicated malaria in Thailand.* Am J Trop Med Hyg, 1996. **54**(1): p. 62-6.
55. Shapiro, T.A., et al., *Prophylactic activity of atovaquone against Plasmodium falciparum in humans.* Am J Trop Med Hyg, 1999. **60**(5): p. 831-6.
56. Cushion, M.T. and P.D. Walzer, *Preclinical drug discovery for new anti-pneumocystis compounds.* Curr Med Chem, 2009. **16**(20): p. 2514-30.
57. Meneceur, P., et al., *In vitro susceptibility of various genotypic strains of Toxoplasma gondii to pyrimethamine, sulfadiazine, and atovaquone.* Antimicrob Agents Chemother, 2008. **52**(4): p. 1269-77.
58. Vannier, E. and P.J. Krause, *Update on babesiosis.* Interdiscip Perspect Infect Dis, 2009. **2009**: p. 984568.
59. Canfield, C.J., M. Pudney, and W.E. Gutteridge, *Interactions of atovaquone with other antimalarial drugs against Plasmodium falciparum in vitro.* Exp Parasitol, 1995. **80**(3): p. 373-81.
60. Kelly, J.X., et al., *Discovery of dual function acridones as a new antimalarial chemotype.* Nature, 2009. **459**(7244): p. 270-273.
61. Winter, R.W., et al., *Evaluation and lead optimization of anti-malarial acridones.* Experimental Parasitology, 2006. **114**(1): p. 47-56.
62. Winter, R.W., et al., *Antimalarial quinolones: synthesis, potency, and mechanistic studies.* Exp Parasitol, 2008. **118**(4): p. 487-97.
63. Dong, C.K., et al., *Type II NADH dehydrogenase of the respiratory chain of Plasmodium falciparum and its inhibitors.* Bioorg Med Chem Lett, 2009. **19**(3): p. 972-5.
64. Ridley, R.G., et al., *Haematin (haem) polymerization and its inhibition by quinoline antimalarials.* Ann Trop Med Parasitol, 1997. **91**(5): p. 559-66.
65. Slater, A.F. and A. Cerami, *Inhibition by chloroquine of a novel haem polymerase enzyme activity in malaria trophozoites.* Nature, 1992. **355**(6356): p. 167-9.
66. Egan, T.J., D.C. Ross, and P.A. Adams, *Quinoline anti-malarial drugs inhibit spontaneous formation of beta-haematin (malaria pigment).* FEBS Lett, 1994. **352**(1): p. 54-7.
67. Combrinck, J.M., et al., *Insights into the role of heme in the mechanism of action of antimalarials.* ACS Chem Biol, 2013. **8**(1): p. 133-7.
68. Wellems, T.E. and C.V. Plowe, *Chloroquine-Resistant Malaria.* Journal of Infectious Diseases, 2001. **184**(6): p. 770-776.
69. Sidhu, A.B., D. Verdier-Pinard, and D.A. Fidock, *Chloroquine resistance in Plasmodium falciparum malaria parasites conferred by pfcrt mutations.* Science, 2002. **298**(5591): p. 210-3.

70. Haynes, R.K., et al., *Considerations on the mechanism of action of artemisinin antimalarials: part 1--the 'carbon radical' and 'heme' hypotheses.* Infect Disord Drug Targets, 2013. **13**(4): p. 217-77.
71. Antoine, T., et al., *Rapid kill of malaria parasites by artemisinin and semi-synthetic endoperoxides involves ROS-dependent depolarization of the membrane potential.* J Antimicrob Chemother, 2014. **69**(4): p. 1005-16.
72. Pandey, A.V., et al., *Artemisinin, an endoperoxide antimalarial, disrupts the hemoglobin catabolism and heme detoxification systems in malarial parasite.* J Biol Chem, 1999. **274**(27): p. 19383-8.
73. Hong, Y.L., Y.Z. Yang, and S.R. Meshnick, *The interaction of artemisinin with malarial hemozoin.* Mol Biochem Parasitol, 1994. **63**(1): p. 121-8.
74. Nosten, F. and N.J. White, *Artemisinin-based combination treatment of falciparum malaria.* Am J Trop Med Hyg, 2007. **77**(6 Suppl): p. 181-92.
75. Dondorp, A.M., et al., *Artemisinin resistance in Plasmodium falciparum malaria.* N Engl J Med, 2009. **361**(5): p. 455-67.
76. Carrara, V.I., et al., *Malaria burden and artemisinin resistance in the mobile and migrant population on the Thai-Myanmar border, 1999-2011: an observational study.* PLoS Med, 2013. **10**(3): p. e1001398.
77. Foster, K.A., et al., *Optical and pharmacological tools to investigate the role of mitochondria during oxidative stress and neurodegeneration.* Prog Neurobiol, 2006. **79**(3): p. 136-71.
78. MacRae, J.I., et al., *Mitochondrial metabolism of sexual and asexual blood stages of the malaria parasite Plasmodium falciparum.* BMC Biol, 2013. **11**: p. 67.
79. Fry, M. and J.E. Beesley, *Mitochondria of mammalian Plasmodium spp.* Parasitology, 1991. **102 Pt 1**: p. 17-26.
80. Uyemura, S.A., et al., *Oxidative phosphorylation and rotenone-insensitive malate- and NADH-quinone oxidoreductases in Plasmodium yoelii yoelii mitochondria in situ.* J Biol Chem, 2004. **279**(1): p. 385-93.
81. Scheibel, L.W. and W.K. Pflaum, *Carbohydrate Metabolism in Plasmodium-Knowlesi.* Comparative Biochemistry and Physiology, 1970. **37**(4): p. 543-&.
82. Barbrook, A.C., et al., *Organization and expression of organellar genomes.* Philos Trans R Soc Lond B Biol Sci, 2010. **365**(1541): p. 785-97.
83. Verma, R., G.C. Varshney, and G.P. Raghava, *Prediction of mitochondrial proteins of malaria parasite using split amino acid composition and PSSM profile.* Amino Acids, 2010. **39**(1): p. 101-10.
84. Bender, A., et al., *Properties and prediction of mitochondrial transit peptides from Plasmodium falciparum.* Mol Biochem Parasitol, 2003. **132**(2): p. 59-66.
85. Torrentino-Madamet, M., et al., *Microaerophilic respiratory metabolism of Plasmodium falciparum mitochondrion as a drug target.* Curr Mol Med, 2010. **10**(1): p. 29-46.
86. Pfanner, N. and A. Geissler, *Versatility of the mitochondrial protein import machinery.* Nat Rev Mol Cell Biol, 2001. **2**(5): p. 339-49.

87. Allary, M., et al., *Scavenging of the cofactor lipoate is essential for the survival of the malaria parasite Plasmodium falciparum.* Mol Microbiol, 2007. **63**(5): p. 1331-44.
88. Claros, M.G. and P. Vincens, *Computational method to predict mitochondrially imported proteins and their targeting sequences.* Eur J Biochem, 1996. **241**(3): p. 779-86.
89. Emanuelsson, O., et al., *Predicting subcellular localization of proteins based on their N-terminal amino acid sequence.* J Mol Biol, 2000. **300**(4): p. 1005-16.
90. Emanuelsson, O., et al., *Locating proteins in the cell using TargetP, SignalP and related tools.* Nat Protoc, 2007. **2**(4): p. 953-71.
91. Read, M., et al., *Dynamic subcellular localization of isoforms of the folate pathway enzyme serine hydroxymethyltransferase (SHMT) through the erythrocytic cycle of Plasmodium falciparum.* Malar J, 2010. **9**: p. 351.
92. Pornthanakasem, W., et al., *Plasmodium serine hydroxymethyltransferase: indispensability and display of distinct localization.* Malaria journal, 2012. **11**: p. 387.
93. Okinaka, O. and K. Iwai, *The biosynthesis of folic acid compounds in plants. 3. Distribution of the dihydropteroate-synthesizing enzyme in plants.* J Vitaminol (Kyoto), 1970. **16**(3): p. 196-200.
94. Neuburger, M., et al., *Mitochondria are a major site for folate and thymidylate synthesis in plants.* J Biol Chem, 1996. **271**(16): p. 9466-72.
95. Pribat, A., et al., *Nonflowering plants possess a unique folate-dependent phenylalanine hydroxylase that is localized in chloroplasts.* Plant Cell, 2010. **22**(10): p. 3410-22.
96. Toth, I., G. Lazar, and H.M. Goodman, *Purification and immunochemical characterization of a dihydrofolate reductase-thymidylate synthase enzyme complex from wild-carrot cells.* EMBO J, 1987. **6**(7): p. 1853-8.
97. Luo, M., et al., *Molecular cloning and analysis of a cDNA coding for the bifunctional dihydrofolate reductase-thymidylate synthase of Daucus carota.* Plant Mol Biol, 1993. **22**(3): p. 427-35.
98. Lazar, G., H. Zhang, and H.M. Goodman, *The origin of the bifunctional dihydrofolate reductase-thymidylate synthase isogenes of Arabidopsis thaliana.* Plant J, 1993. **3**(5): p. 657-68.
99. Wang, M., S. Ratnam, and J.H. Freisheim, *Cloning, nucleotide sequence and expression of the bifunctional dihydrofolate reductase-thymidylate synthase from Glycine max.* Biochimica et biophysica acta, 1995. **1261**(3): p. 325-36.
100. Cox, K., D. Robertson, and R. Fites, *Mapping and expression of a bifunctional thymidylate synthase, dihydrofolate reductase gene from maize.* Plant Mol Biol, 1999. **41**(6): p. 733-9.
101. Gueiros-Filho, F.J. and S.M. Beverley, *Selection against the dihydrofolate reductase-thymidylate synthase (DHFR-TS) locus as a probe of genetic alterations in Leishmania major.* Mol Cell Biol, 1996. **16**(10): p. 5655-63.

102. O'Neil, R.H., et al., *Phylogenetic Classification of Protozoa Based on the Structure of the Linker Domain in the Bifunctional Enzyme, Dihydrofolate Reductase-Thymidylate Synthase.* Journal of Biological Chemistry, 2003. **278**(52): p. 52980-52987.
103. Spalding, M.D., et al., *Validation of a modified method for Bxb1 mycobacteriophage integrase-mediated recombination in Plasmodium falciparum by localization of the H-protein of the glycine cleavage complex to the mitochondrion.* Mol Biochem Parasitol, 2010. **172**(2): p. 156-60.
104. Diaz, D.S., et al., *Role of specific cytochrome P450 isoforms in the conversion of phenoxypropoxybiguanide analogs in human liver microsomes to potent antimalarial dihydrotriazines.* Drug Metab Dispos, 2008. **36**(2): p. 380-5.
105. Jones, K. and S.A. Ward, *Biguanide-atovaquone synergy against Plasmodium falciparum in vitro.* Antimicrob Agents Chemother, 2002. **46**(8): p. 2700-3.
106. Bertilsson, L., *Geographical/interracial differences in polymorphic drug oxidation. Current state of knowledge of cytochromes P450 (CYP) 2D6 and 2C19.* Clin Pharmacokinet, 1995. **29**(3): p. 192-209.
107. Kaneko, A., et al., *Intrinsic efficacy of proguanil against falciparum and vivax malaria independent of the metabolite cycloguanil.* J Infect Dis, 1999. **179**(4): p. 974-9.
108. Ward, S.A., et al., *Inter-subject variability in the metabolism of proguanil to the active metabolite cycloguanil in man.* Br J Clin Pharmacol, 1989. **27**(6): p. 781-7.
109. Schmidt, L.H., et al., *Antimalarial activities of triazine metabolites of chlorguanide and dichlorguanide.* Proc Soc Exp Biol Med, 1952. **80**(2): p. 367-70.
110. Smith, C.C., J. Ihrig, and R. Menne, *Antimalarial Activity and Metabolism of Biguanides: I. Metabolism of Chlorguanide and Chlorguanide Triazine in Rhesus Monkeys and Man.* The American Journal of Tropical Medicine and Hygiene, 1961. **10**(5): p. 694-703.
111. Fidock, D.A. and T.E. Wellems, *Transformation with human dihydrofolate reductase renders malaria parasites insensitive to WR99210 but does not affect the intrinsic activity of proguanil.* Proc Natl Acad Sci U S A, 1997. **94**(20): p. 10931-6.
112. Fidock, D.A., T. Nomura, and T.E. Wellems, *Cycloguanil and its parent compound proguanil demonstrate distinct activities against Plasmodium falciparum malaria parasites transformed with human dihydrofolate reductase.* Mol Pharmacol, 1998. **54**(6): p. 1140-7.
113. Foote, S.J., D. Galatis, and A.F. Cowman, *Amino acids in the dihydrofolate reductase-thymidylate synthase gene of Plasmodium falciparum involved in cycloguanil resistance differ from those involved in pyrimethamine resistance.* Proceedings of the National Academy of Sciences of the United States of America, 1990. **87**(8): p. 3014-7.
114. Basco, L.K., et al., *Point mutations in the dihydrofolate reductase-thymidylate synthase gene and pyrimethamine and cycloguanil resistance in Plasmodium falciparum.* Molecular and biochemical parasitology, 1995. **69**(1): p. 135-8.

115. Sucharit, F., et al., *In vitro studies on the sensitivities of Plasmodium falciparum in Thailand to pyrimethamine and proguanil.* Annals of tropical medicine and parasitology, 1985. **79**(4): p. 375-7.
116. Looareesuwan, S., et al., *Malarone (atovaquone and proguanil hydrochloride): a review of its clinical development for treatment of malaria. Malarone Clinical Trials Study Group.* The American Journal of Tropical Medicine and Hygiene, 1999. **60**(4): p. 533-41.
117. Fivelman, Q.L., et al., *Malarone treatment failure and in vitro confirmation of resistance of Plasmodium falciparum isolate from Lagos, Nigeria.* Malar J, 2002. **1**: p. 1.
118. Korsinczky, M., et al., *Mutations in Plasmodium falciparum cytochrome b that are associated with atovaquone resistance are located at a putative drug-binding site.* Antimicrob Agents Chemother, 2000. **44**(8): p. 2100-8.
119. Vaidya, A.B. and M.W. Mather, *Atovaquone resistance in malaria parasites.* Drug Resist Updat, 2000. **3**(5): p. 283-287.
120. Hudson, A.T., et al., *566C80: a potent broad spectrum anti-infective agent with activity against malaria and opportunistic infections in AIDS patients.* Drugs Exp Clin Res, 1991. **17**(9): p. 427-35.
121. Vinetz, J.M., et al., eds. *Chapter 49. Chemotherapy of Malaria*. 12 ed. Goodman & Gilman's The Pharmacological Basis of Therapeutics, ed. L.L. Brunton, B.A. Chabner, and B.C. Knollmann2011, McGraw-Hill: New York.
122. Canfield, C.J., et al., *PS-15: a potent, orally active antimalarial from a new class of folic acid antagonists.* Am J Trop Med Hyg, 1993. **49**(1): p. 121-6.
123. Hussein, Z., et al., *Population pharmacokinetics of proguanil in patients with acute P. falciparum malaria after combined therapy with atovaquone.* Br J Clin Pharmacol, 1996. **42**(5): p. 589-97.
124. Srivastava, I.K. and A.B. Vaidya, *A mechanism for the synergistic antimalarial action of atovaquone and proguanil.* Antimicrob Agents Chemother, 1999. **43**(6): p. 1334-9.
125. Kar, S., *Control of malaria.* Nat Rev Drug Discov, 2010. **9**(7): p. 511-2.
126. Thapar, M.M., et al., *Time-dependent pharmacokinetics and drug metabolism of atovaquone plus proguanil (Malarone) when taken as chemoprophylaxis.* European journal of clinical pharmacology, 2002. **58**(1): p. 19-27.
127. Thapar, M.M., et al., *Pharmacodynamic interactions among atovaquone, proguanil and cycloguanil against Plasmodium falciparum in vitro.* Transactions of the Royal Society of Tropical Medicine and Hygiene, 2003. **97**(3): p. 331-7.
128. Edstein, M.D., et al., *Pharmacokinetics of proguanil in malaria patients treated with proguanil plus atovaquone.* The Southeast Asian journal of tropical medicine and public health, 1996. **27**(2): p. 216-20.
129. Edstein, M.D., et al., *Lengthy Antimalarial Activity of Atovaquone in Human Plasma following Atovaquone-Proguanil Administration.* Antimicrobial Agents and Chemotherapy, 2005. **49**(10): p. 4421-4422.

130. Huang, X.Q. and W. Miller, *A Time-Efficient, Linear-Space Local Similarity Algorithm.* Advances in Applied Mathematics, 1991. **12**(3): p. 337-357.
131. Kapuscinski, J., *DAPI: a DNA-specific fluorescent probe.* Biotech Histochem, 1995. **70**(5): p. 220-33.
132. Morikawa, K. and M. Yanagida, *Visualization of individual DNA molecules in solution by light microscopy: DAPI staining method.* J Biochem, 1981. **89**(2): p. 693-6.
133. Bazhulina, N.P., et al., *Binding of Hoechst 33258 and its derivatives to DNA.* J Biomol Struct Dyn, 2009. **26**(6): p. 701-18.
134. Chazotte, B., *Labeling mitochondria with MitoTracker dyes.* Cold Spring Harb Protoc, 2011. **2011**(8): p. 990-2.
135. Christensen, K.E. and R.E. MacKenzie, *Mitochondrial one-carbon metabolism is adapted to the specific needs of yeast, plants and mammals.* Bioessays, 2006. **28**(6): p. 595-605.
136. Malmquist, N.A., J. Baldwin, and M.A. Phillips, *Detergent-dependent kinetics of truncated Plasmodium falciparum dihydroorotate dehydrogenase.* J Biol Chem, 2007. **282**(17): p. 12678-86.
137. Baldwin, J., et al., *Malarial dihydroorotate dehydrogenase. Substrate and inhibitor specificity.* The Journal of biological chemistry, 2002. **277**(44): p. 41827-34.
138. Waller, R.F., et al., *Protein trafficking to the plastid of Plasmodium falciparum is via the secretory pathway.* EMBO J, 2000. **19**(8): p. 1794-802.
139. Rohrbach, P., et al., *Quantitative calcium measurements in subcellular compartments of Plasmodium falciparum-infected erythrocytes.* J Biol Chem, 2005. **280**(30): p. 27960-9.
140. Uhlemann, A.C., et al., *Mechanism of antimalarial action of the synthetic trioxolane RBX11160 (OZ277).* Antimicrob Agents Chemother, 2007. **51**(2): p. 667-72.
141. Tomlins, A.M., et al., *Plasmodium falciparum ATG8 implicated in both autophagy and apicoplast formation.* Autophagy, 2013. **9**(10): p. 1540-52.
142. Deponte, M., et al., *Wherever I may roam: protein and membrane trafficking in P. falciparum-infected red blood cells.* Mol Biochem Parasitol, 2012. **186**(2): p. 95-116.
143. Hain, A.U. and J. Bosch, *Autophagy in , a multifunctional pathway?* Comput Struct Biotechnol J, 2013. **8**: p. e201308002.
144. Schindelin, J., et al., *Fiji: an open-source platform for biological-image analysis.* Nat Meth, 2012. **9**(7): p. 676-682.
145. Pearson, K., *Note on Regression and Inheritance in the Case of Two Parents.* Proceedings of the Royal Society of London, 1895. **58**(347-352): p. 240-242.
146. Manders, E.M.M., F.J. Verbeek, and J.A. Aten, *Measurement of co-localization of objects in dual-colour confocal images.* Journal of Microscopy, 1993. **169**(3): p. 375-382.

147. Nkrumah, L.J., et al., *Efficient site-specific integration in Plasmodium falciparum chromosomes mediated by mycobacteriophage Bxb1 integrase.* Nature methods, 2006. **3**(8): p. 615-21.
148. Nirmalan, N., et al., *Transcriptional analysis of genes encoding enzymes of the folate pathway in the human malaria parasite Plasmodium falciparum.* Molecular microbiology, 2002. **46**(1): p. 179-190.
149. Nirmalan, N., P.F. Sims, and J.E. Hyde, *Translational up-regulation of antifolate drug targets in the human malaria parasite< i> Plasmodium falciparum</i> upon challenge with inhibitors.* Molecular and biochemical parasitology, 2004. **136**(1): p. 63-70.
150. Auliff, A.M., et al., *Functional analysis of Plasmodium vivax dihydrofolate reductase-thymidylate synthase genes through stable transformation of Plasmodium falciparum.* PLoS One, 2012. **7**(7): p. e40416.
151. Alifrangis, M., et al., *Homology building as a means to define antigenic epitopes on dihydrofolate reductase (DHFR) from Plasmodium falciparum.* Malar J, 2004. **3**: p. 16.
152. Modest, E.J., *Chemical and Biological Studies on 1,2-Dihydro-S-Triazines .2. 3-Component Synthesis.* Journal of Organic Chemistry, 1956. **21**(1): p. 1-13.
153. Yuthavong, Y., et al., *Development of a lead inhibitor for the A16V+S108T mutant of dihydrofolate reductase from the cycloguanil-resistant strain (T9/94) of Plasmodium falciparum.* J Med Chem, 2000. **43**(14): p. 2738-44.
154. O'Neil, M.T., et al., *A novel Plasmodium falciparum expression system for assessing antifolate resistance caused by mutant P. vivax dihydrofolate reductase-thymidylate synthase.* J Infect Dis, 2007. **196**(3): p. 467-74.
155. El Bissati, K., et al., *The plasma membrane permease PfNT1 is essential for purine salvage in the human malaria parasite Plasmodium falciparum.* Proc Natl Acad Sci U S A, 2006. **103**(24): p. 9286-91.
156. Sullivan, J.S., et al., *Adaptation of the AMRU-1 strain of Plasmodium vivax to Aotus and Saimiri monkeys and to four species of anopheline mosquitoes.* J Parasitol, 1999. **85**(4): p. 672-7.
157. O'Donnell, R.A., et al., *A genetic screen for improved plasmid segregation reveals a role for Rep20 in the interaction of Plasmodium falciparum chromosomes.* EMBO J, 2002. **21**(5): p. 1231-9.
158. Deitsch, K., C. Driskill, and T. Wellems, *Transformation of malaria parasites by the spontaneous uptake and expression of DNA from human erythrocytes.* Nucleic Acids Res, 2001. **29**(3): p. 850-3.
159. Hasenkamp, S., K.T. Russell, and P. Horrocks, *Comparison of the absolute and relative efficiencies of electroporation-based transfection protocols for Plasmodium falciparum.* Malar J, 2012. **11**: p. 210.
160. Wu, Y., et al., *Transfection of Plasmodium falciparum within human red blood cells.* Proc Natl Acad Sci U S A, 1995. **92**(4): p. 973-7.

161. Desjardins, R.E., et al., *Quantitative assessment of antimalarial activity in vitro by a semiautomated microdilution technique.* Antimicrob Agents Chemother, 1979. **16**(6): p. 710-8.
162. Smilkstein, M.J., et al., *A drug-selected Plasmodium falciparum lacking the need for conventional electron transport.* Mol Biochem Parasitol, 2008. **159**(1): p. 64-8.
163. Helsby, N.A., et al., *The pharmacokinetics and activation of proguanil in man: consequences of variability in drug metabolism.* Br J Clin Pharmacol, 1990. **30**(4): p. 593-8.
164. Cowman, A.F., et al., *Amino acid changes linked to pyrimethamine resistance in the dihydrofolate reductase-thymidylate synthase gene of Plasmodium falciparum.* Proc Natl Acad Sci U S A, 1988. **85**(23): p. 9109-13.
165. Wang, P., et al., *Resistance to antifolates in Plasmodium falciparum monitored by sequence analysis of dihydropteroate synthetase and dihydrofolate reductase alleles in a large number of field samples of diverse origins.* Mol Biochem Parasitol, 1997. **89**(2): p. 161-77.
166. Charles, L.J., et al., *The appearance of pyrimethamine resistance in Plasmodium falciparum following self-medication by a rural community in Ghana.* Bull World Health Organ, 1962. **26**: p. 103-8.
167. Chotivanich, K., et al., *The effects of serum lipids on the in vitro activity of lumefantrine and atovaquone against Plasmodium falciparum.* Malaria journal, 2012. **11**: p. 177.
168. Fisher, N., et al., *Cytochrome b mutation Y268S conferring atovaquone resistance phenotype in malaria parasite results in reduced parasite bc1 catalytic turnover and protein expression.* J Biol Chem, 2012. **287**(13): p. 9731-41.
169. Wenz, T., et al., *Mutational analysis of cytochrome b at the ubiquinol oxidation site of yeast complex III.* J Biol Chem, 2007. **282**(6): p. 3977-88.
170. Vallieres, C., N. Fisher, and B. Meunier, *Reconstructing the Qo site of Plasmodium falciparum bc 1 complex in the yeast enzyme.* PLoS One, 2013. **8**(8): p. e71726.
171. Bailey, C.J. and C. Day, *Metformin: its botanical background.* Practical Diabetes International, 2004. **21**(3): p. 115-117.
172. *Synthalin and Insulin.* Science, 1927. **65**(1684): p. x.
173. Rabinowitch, I.M., *Observations on the Use of Synthalin in the Treatment of Diabetes Mellitus.* Can Med Assoc J, 1927. **17**(8): p. 901-4.
174. Thomson, A.P., R.J. Gittins, and G. Thomas, *Synthalin in the Treatment of Diabetes.* Br Med J, 1932. **1**(3711): p. 322-5.
175. Sands, M., M.A. Kron, and R.B. Brown, *Pentamidine: a review.* Rev Infect Dis, 1985. **7**(5): p. 625-34.
176. Ponnudurai, T., et al., *The production of mature gametocytes of Plasmodium falciparum in continuous cultures of different isolates infective to mosquitoes.* Transactions of the Royal Society of Tropical Medicine and Hygiene, 1982. **76**(2): p. 242-50.
177. Kafsack, B.F.C., et al., *A transcriptional switch underlies commitment to sexual development in malaria parasites.* Nature, 2014. **507**(7491): p. 248-252.

178. Vaidya, A.B., et al., *Unidirectional dominance of cytoplasmic inheritance in two genetic crosses of Plasmodium falciparum.* Molecular and cellular biology, 1993. **13**(12): p. 7349-57.
179. Furuya, T., et al., *Disruption of a Plasmodium falciparum gene linked to male sexual development causes early arrest in gametocytogenesis.* Proceedings of the National Academy of Sciences of the United States of America, 2005. **102**(46): p. 16813-16818.
180. Silvestrini, F., et al., *Genome-wide identification of genes upregulated at the onset of gametocytogenesis in Plasmodium falciparum.* Mol Biochem Parasitol, 2005. **143**(1): p. 100-10.
181. Udeinya, I.J., et al., *Plasmodium falciparum: effect of time in continuous culture on binding to human endothelial cells and amelanotic melanoma cells.* Exp Parasitol, 1983. **56**(2): p. 207-14.
182. Salcedo-Sora, J.E., et al., *The Molecular Basis of Folate Salvage in Plasmodium falciparum: CHARACTERIZATION OF TWO FOLATE TRANSPORTERS.* Journal of Biological Chemistry, 2011. **286**(52): p. 44659-44668.
183. Shallom, S., et al., *Essential protein-protein interactions between Plasmodium falciparum thymidylate synthase and dihydrofolate reductase domains.* J Biol Chem, 1999. **274**(53): p. 37781-6.
184. Rathod, P.K., T. McErlean, and P.C. Lee, *Variations in frequencies of drug resistance in Plasmodium falciparum.* Proc Natl Acad Sci U S A, 1997. **94**(17): p. 9389-93.
185. Watkins, W.M., et al., *Antagonism of sulfadoxine and pyrimethamine antimalarial activity in vitro by p-aminobenzoic acid, p-aminobenzoylglutamic acid and folic acid.* Mol Biochem Parasitol, 1985. **14**(1): p. 55-61.
186. Wang, P., et al., *Genetic and metabolic analysis of folate salvage in the human malaria parasite Plasmodium falciparum.* Mol Biochem Parasitol, 2004. **135**(1): p. 77-87.
187. Chen, G.X., et al., *Kinetic and molecular properties of the dihydrofolate reductase from pyrimethamine-sensitive and pyrimethamine-resistant clones of the human malaria parasite Plasmodium falciparum.* Mol Pharmacol, 1987. **31**(4): p. 430-7.
188. Trager, W. and J.B. Jensen, *Human malaria parasites in continuous culture.* Science, 1976. **193**(4254): p. 673-5.
189. Fiskum, G., et al., *The cytoskeleton of digitonin-treated rat hepatocytes.* Proceedings of the National Academy of Sciences of the United States of America, 1980. **77**(6): p. 3430-4.
190. Bulusu, V., V. Jayaraman, and H. Balaram, *Metabolic fate of fumarate, a side product of the purine salvage pathway in the intraerythrocytic stages of Plasmodium falciparum.* The Journal of biological chemistry, 2011. **286**(11): p. 9236-45.
191. Krungkrai, J., *Purification, characterization and localization of mitochondrial dihydroorotate dehydrogenase in Plasmodium falciparum, human malaria parasite.* Biochimica et biophysica acta, 1995. **1243**(3): p. 351-60.

192. Hodges, M., et al., *An iron regulatory-like protein expressed in Plasmodium falciparum displays aconitase activity.* Molecular and biochemical parasitology, 2005. **143**(1): p. 29-38.